

**Supporting Information for
Ab initio Based Kinetic Monte Carlo Analysis to Unravel the
Propagation Kinetics in Vinyl Acetate Pulsed Laser Polymerization**

Gilles B. Desmet,^{a,†} Yoshi W. Marien,^{a,†} Paul H.M. Van Steenberge,^a

Dagmar R. D'hooge,^{a,b} Marie-Françoise Reyniers,^{a*} Guy B. Marin^a

^a Laboratory for Chemical Technology, Ghent University, Technologiepark 914,
B-9052, Gent, Belgium.

^b Centre for Textiles Sciences and Engineering, Ghent University, Technologiepark 907,
B-9052 Gent, Belgium.

E-mail: *Marie-Françoise.Reyniers@ugent.be*

[†] These authors contributed equally.

Contents

Part I: Ab initio calculations.....	4
S1 The use of truncated oligomer models	4
S1.1 Dimer model	5
S1.1.1 Head-to-tail propagation	5
S1.1.2 Head-to-head propagation	7
S1.1.3 Tail-to-tail propagation	8
S1.1.4 Tail-to-head propagation	10
S1.2 Trimer model for 1,5 intramolecular chain transfer (backbiting)	12
S1.2.1 1,5 intramolecular chain transfer with a head radical (backbiting by head radical)	12
S1.2.2 1,5 intramolecular chain transfer (backbiting by tail)	13

S1.3	Extended trimer+methyl model	14
S2	Computational details.....	16
S3	Thermodynamic and kinetic values.....	18
S3.1	Thermodynamic and kinetic values of all stereospecific model reactions in gas phase	18
S3.2	Thermodynamics and kinetics of all stereospecific model reactions in vinyl acetate	
	19	
S3.3	Thermodynamic values of the global, stereo-aspecific model reactions	20
S4	Transition state structures for backbiting	21
	Part II: Kinetic Monte Carlo Modeling of PLP-SEC	23
S5	Calculation of the reaction probabilities shown in Figure 2	23
S6	Details on the kinetic Monte Carlo modeling of PLP	25
S7	Chain length dependent propagation	27
S8	Observed rate coefficients as a function of laser pulse frequency for the case in which backbiting by a head radical is not taken into account (case 5)	28
S9	Evaluation of the termination rate limit	29
S10	Effect of the degree of SEC broadening.....	35
S11	Laser pulse frequency dependence of observed propagation rate coefficients based on peak maxima	37
S12	Laser pulse frequency dependence of observed propagation rate coefficients in the value of the head-to-head propagation rate coefficient is reduced by a factor 2.....	38

S13	Evaluation of the average propagation rate coefficient $\langle k_p \rangle$ as defined on the polymerization rate.....	39
S13.1	Analytical derivation.....	39
S13.2	Comparison of $\langle k_p \rangle$ and k_p^{obs} both using the location of the inflection point and peak maximum	41
S14	Comparison of simulated and experimental data at 323 K	43
S15	Observed propagation rates coefficient based on inflection points at lower temperatures	44
S16	Observed propagation rates coefficient based on peak maxima at lower temperatures	
	45	
S17	Pulse frequency dependence of the activation energy of the observed propagation rate coefficient.....	46
S18	Profiles of macroradical concentrations and molar fractions as a function of time simulated using the ab initio rate coefficients (Case 4) under the conditions of the current work	47
S19	Profiles of macroradical concentrations and fractions as a function of time simulated using the ab initio rate coefficients (Case 4) under typical PLP-EPR conditions.....	52
S20	References	54
	Part III: Cartesian coordinates of the calculated structures	56
S21	Cartesian coordinates of all minimum energy conformations	56
S22	Cartesian coordinates and imaginary frequencies of all transition state structure	64

Part I: Ab initio calculations

S1 The use of truncated oligomer models

Ab initio studies on propagation typically employ truncated oligomer models,¹⁻⁸ such as shown in Figure S1. Noble and Coote⁹ recently provided an excellent overview of the different electronic structure techniques to obtain intrinsic rate coefficients in radical polymerization processes, including an assessment of their accuracy and reliability. These authors concluded that dimers, trimers or tetramers are, in general, suitable model molecules to retrieve gas phase thermodynamic and kinetic information on important reactions such as propagation and addition/fragmentation involving RAFT CTA species.

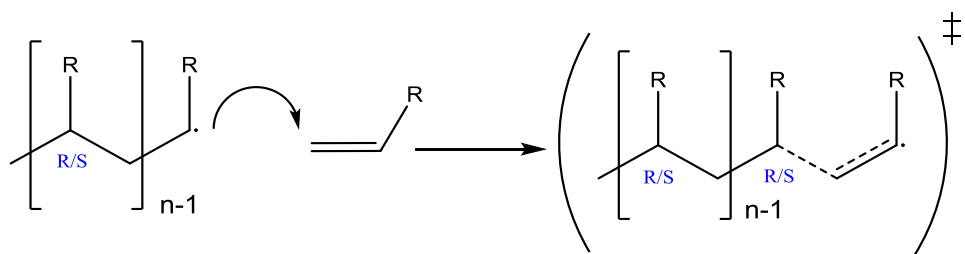


Figure S1. Truncated oligomer model reaction for head-to-tail propagation used for the ab initio calculation of the propagation rate coefficient (k_p) in radical polymerization of a vinylic monomer. R/S: configuration of the chiral center.

As already indicated in Figure S1, it is important to realize that a new chiral center is formed during each propagation step. Depending on the truncated oligomer that is used as a model compound, the rate coefficient might therefore depend on the stereochemistry. In most cases, one is interested in a overall, stereo-aspecific rate coefficient, since these are the ones that are used in a kinetic model. The relation between the stereo-aspecific rate coefficient and the stereospecific rate coefficients depends on the used truncated oligomer model and is explained in the following subsections for head-to-tail, head-to-head, tail-to-tail and tail-to-head propagation using the dimer model (S1.1), for backbiting by a head and by a tail radical using a trimer model (S1.2) and for propagation of a mid-chain radical using an extended trimer+methyl model (S1.3). A similar procedure is applicable for equilibrium coefficients.

S1.1 Dimer model

S1.1.1 Head-to-tail propagation

In case of a head-to-tail propagation of a vinylic monomer using a dimer model, two enantiomeric reactants are possible, leading to four stereoisomers as products, as shown explicitly in Figure S2.

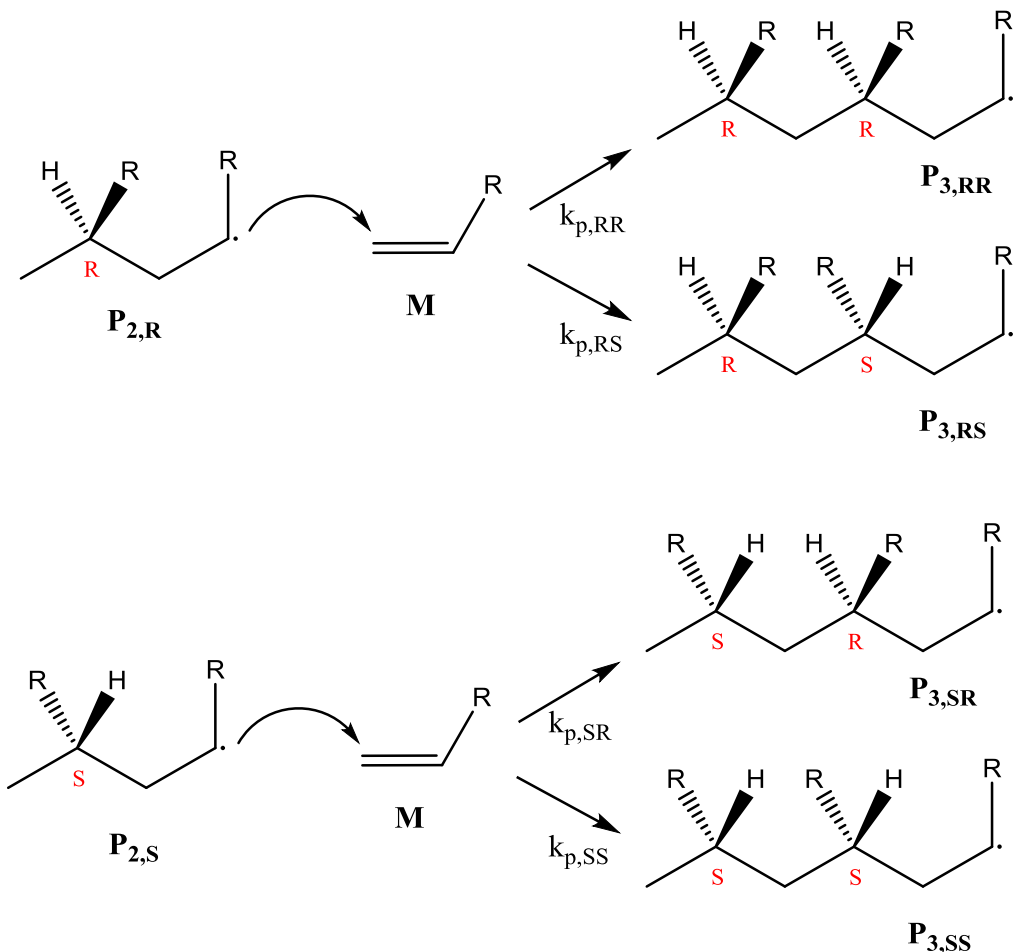


Figure S2. Dimer model for the propagation of a vinylic monomer.

In the case of vinyl acetate polymerization, this is shown in Figure S3.

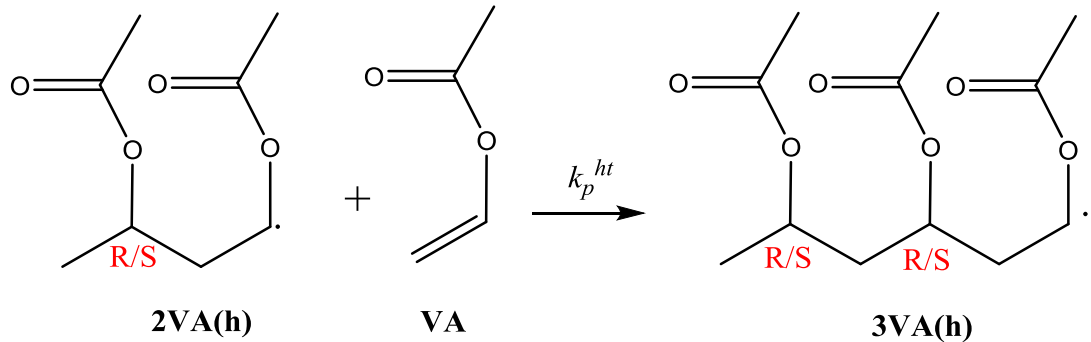


Figure S3. Dimer model reaction for a head-to-tail propagation.

The formation rate of $3VA(h)$ is the sum of the formation rate of the different stereoisomers:

$$R_{f,3VA(h)} = (k_{p,RR}^{ht} + k_{p,RS}^{ht})[2VA(h)_R][VA] + (k_{p,SR}^{ht} + k_{p,SS}^{ht})[2VA(h)_S][VA] \quad (S1)$$

Because of enantiomery: i) $k_{p,RR}^{ht} = k_{p,SS}^{ht}$ and $k_{p,RS}^{ht} = k_{p,SR}^{ht}$ and ii) $[2VA(h)_R] = [2VA(h)_S] = 0.5 [2VA(h)]$, and therefore:

$$\begin{aligned} R_{f,3VA(h)} &= 2(k_{p,RR}^{ht} + k_{p,RS}^{ht}) \frac{[2VA(h)]}{2} [VA] \\ &= (k_{p,RR}^{ht} + k_{p,RS}^{ht})[2VA(h)][VA] \end{aligned} \quad (S2)$$

Hence, the stereo-aspecific rate coefficient k_p is equal to the sum of the different diastereomeric rate coefficients:

$$k_p^{ht} = k_{p,RR}^{ht} + k_{p,RS}^{ht} \quad (S3)$$

S1.1.2 Head-to-head propagation

For head-to-head propagation of vinyl acetate (VA) using a dimer model, 2 new chiral centers are created upon radical addition as shown in Figure S4.

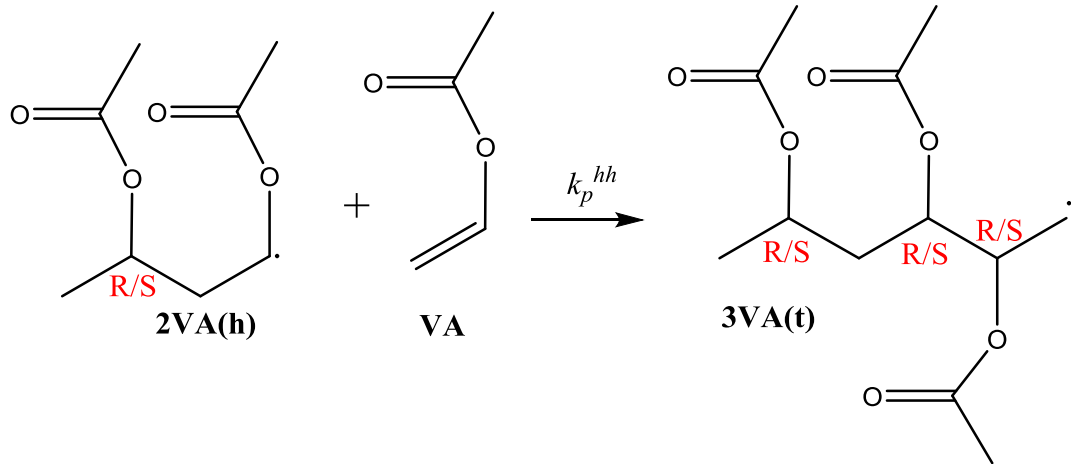


Figure S4. Dimer model reaction for a head-to-head propagation.

Using a similar reasoning as in Section (S1.1.1), the overall stereo-aspecific rate of formation of 3VA(t) is now equal to:

$$R_f,3VA(t) = (k_{p,RRR}^{hh} + k_{p,RRS}^{hh} + k_{p,RSR}^{hh} + k_{p,RSS}^{hh})[2VA(h)_R][VA] + (k_{p,SSS}^{hh} + k_{p,SSR}^{hh} + k_{p,SRS}^{hh} + k_{p,SRR}^{hh})[2VA(h)_S][VA] \quad (S4)$$

Which, taking into account enantiomery simplifies to:

$$R_f,3VA(t) = (k_{p,RRR}^{hh} + k_{p,RRS}^{hh} + k_{p,RSR}^{hh} + k_{p,RSS}^{hh})[2VA(h)][VA] \quad (S5)$$

And hence, the overall stereo-aspecific rate coefficient for head-to-head propagation is:

$$k_p^{hh} = k_{p,RRR}^{hh} + k_{p,RRS}^{hh} + k_{p,RSR}^{hh} + k_{p,RSS}^{hh} \quad (S6)$$

S1.1.3 Tail-to-tail propagation

The dimer model reaction for tail-to-tail propagation is shown in Figure S5.

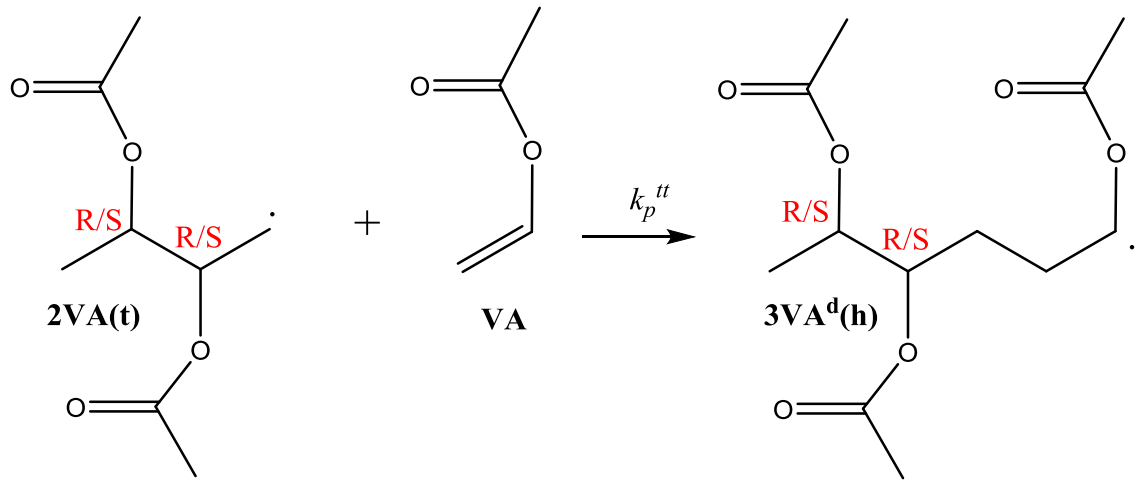


Figure S5. Dimer model reaction for a tail-to-tail propagation. Note that the notation $3VA^d(h)$ is used to distinguish it from the conventional $3VA(h)$ radical as obtained from head-to-tail propagation (Figure S3).

In case of a dimer tail radical, $2VA(t)$ there are four possible configurations of the stereocenters. For tail-to-tail propagation, this leads to the following expression for the overall stereo-aspecific rate of formation of $3VA^d(h)$:

$$R_{f,3VA^d(h)} = k_{p,RR}^{tt} [2VA(t)_{RR}][VA] + k_{p,RS}^{tt} [2VA(t)_{RS}][VA] \\ + k_{p,SR}^{tt} [2VA(t)_{SR}][VA] + k_{p,SS}^{tt} [2VA(t)_{SS}][VA] \quad (S7)$$

To further simplify this expression, the distribution of the population of the different stereoisomers of the tail radicals has to be known. The latter will be depending on the reactions leading to the tail radical, i.e. the head-to-head and tail-to-head propagations. In a first approximation we assume that the majority of the tail radicals will be formed via a head-to-head propagation, and hence:

$$\frac{[2VA(t)_{RR}]}{[2VA(t)]} = \frac{0.5(k_{p,RRR}^{hh} + k_{p,RSS}^{hh})}{k_{p,RRR}^{hh} + k_{p,RRS}^{hh} + k_{p,RSR}^{hh} + k_{p,RSS}^{hh}} = \frac{0.5(k_{p,RRR}^{hh} + k_{p,RSS}^{hh})}{k_p^{hh}} \quad (S8)$$

$$\frac{[2VA(t)_{RS}]}{[2VA(t)]} = \frac{0.5(k_{p,RRS}^{hh} + k_{p,RSR}^{hh})}{k_{p,RRR}^{hh} + k_{p,RRS}^{hh} + k_{p,RSR}^{hh} + k_{p,RSS}^{hh}} = \frac{0.5(k_{p,RRS}^{hh} + k_{p,RSR}^{hh})}{k_p^{hh}} \quad (S9)$$

$$\frac{[2VA(t)_{SR}]}{[2VA(t)]} = \frac{0.5(k_{p,RSR}^{hh} + k_{p,RRS}^{hh})}{k_{p,RRR}^{hh} + k_{p,RRS}^{hh} + k_{p,RSR}^{hh} + k_{p,RSS}^{hh}} = \frac{0.5(k_{p,RSR}^{hh} + k_{p,RRS}^{hh})}{k_p^{hh}} \quad (S10)$$

$$\frac{[2VA(t)_{SS}]}{[2VA(t)]} = \frac{0.5(k_{p,RSS}^{hh} + k_{p,RRR}^{hh})}{k_{p,RRR}^{hh} + k_{p,RRS}^{hh} + k_{p,RSR}^{hh} + k_{p,RSS}^{hh}} = \frac{0.5(k_{p,RSS}^{hh} + k_{p,RRR}^{hh})}{k_p^{hh}} \quad (S11)$$

Substituting these back into equation S7 leads to:

$$\begin{aligned} R_{f,3VA^d(h)} &= 0.5 k_{p,RR}^{tt} \left(\frac{k_{p,RRR}^{hh}}{k_p^{hh}} + \frac{k_{p,RSS}^{hh}}{k_p^{hh}} \right) [VA][2VA(t)] \\ &\quad + 0.5 k_{p,RS}^{tt} \left(\frac{k_{p,RRS}^{hh}}{k_p^{hh}} + \frac{k_{p,RSR}^{hh}}{k_p^{hh}} \right) [VA][2VA(t)] \\ &\quad + 0.5 k_{p,SR}^{tt} \left(\frac{k_{p,RSR}^{hh}}{k_p^{hh}} + \frac{k_{p,RRS}^{hh}}{k_p^{hh}} \right) [VA][2VA(t)] \\ &\quad + 0.5 k_{p,SS}^{tt} \left(\frac{k_{p,RSS}^{hh}}{k_p^{hh}} + \frac{k_{p,RRR}^{hh}}{k_p^{hh}} \right) [VA][2VA(t)] \end{aligned} \quad (S12)$$

Which, taking into account the enantiomer pairs, further simplifies to:

$$R_{f,3VA^d(h)} = \left(k_{p,RR}^{tt} \frac{k_{p,RRR}^{hh} + k_{p,RSS}^{hh}}{k_p^{hh}} + k_{p,RS}^{tt} \frac{k_{p,RRS}^{hh} + k_{p,RSR}^{hh}}{k_p^{hh}} \right) [2VA(t)][VA] \quad (S13)$$

and hence:

$$k_p^{tt} = k_{p,RR}^{tt} \frac{k_{p,RRR}^{hh} + k_{p,RSS}^{hh}}{k_p^{hh}} + k_{p,RS}^{tt} \frac{k_{p,RRS}^{hh} + k_{p,RSR}^{hh}}{k_p^{hh}} \quad (S14)$$

S1.1.4 Tail-to-head propagation

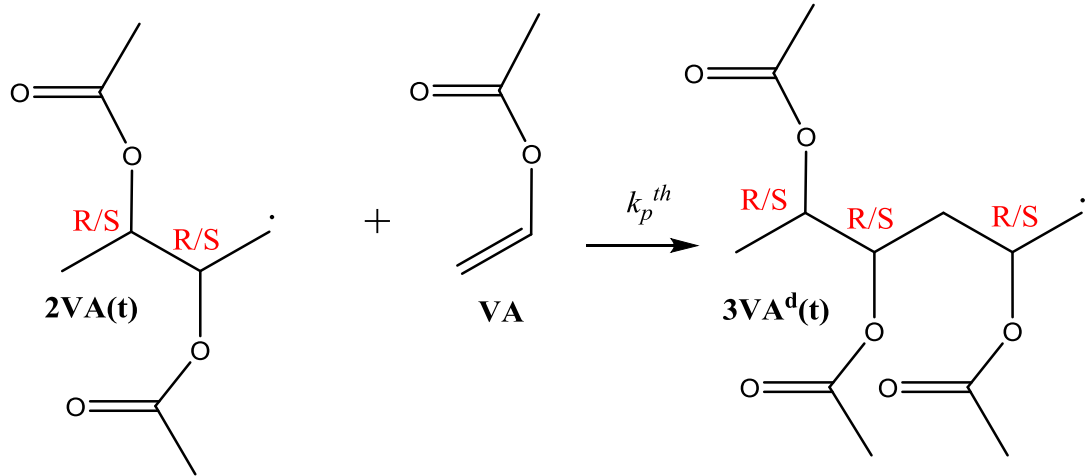


Figure S6. Dimer model reaction for a tail-to-head propagation. Note that the notation $3VA^d(t)$ is used to distinguish it from the conventional $3VA(t)$ tail radical as obtained from head-to-head propagation (Figure S4).

For tail-to-head propagation, the overall stereo-aspecific rate of formation of $3VA^d(t)$ is equal to:

$$\begin{aligned}
 R_{f,3VA^d(t)} = & k_{p,RRR}^{th} [2VA(t)_{RR}] [VA] + k_{p,RRS}^{th} [2VA(t)_{RR}] [VA] \\
 & + k_{p,RSR}^{th} [2VA(t)_{RS}] [VA] + k_{p,RSS}^{th} [2VA(t)_{RS}] [VA] \\
 & + k_{p,SRR}^{th} [2VA(t)_{SR}] [VA] + k_{p,SRS}^{th} [2VA(t)_{SR}] [VA] \\
 & + k_{p,SSR}^{th} [2VA(t)_{SS}] [VA] + k_{p,SSS}^{th} [2VA(t)_{SS}] [VA]
 \end{aligned} \tag{S15}$$

Substituting equations S8 to S11 in the above expression leads to:

$$\begin{aligned}
 R_{f,3VA^d(t)} = & 0.5 (k_{p,RRR}^{th} + k_{p,RRS}^{th}) \left(\frac{k_{p,RRR}^{hh}}{k_p^{hh}} + \frac{k_{p,RSS}^{hh}}{k_p^{hh}} \right) [2VA(t)] [VA] \\
 & + 0.5 (k_{p,RSR}^{th} + k_{p,RSS}^{th}) \left(\frac{k_{p,RRS}^{hh}}{k_p^{hh}} + \frac{k_{p,RSR}^{hh}}{k_p^{hh}} \right) [2VA(t)] [VA] \\
 & + 0.5 (k_{p,SRR}^{th} + k_{p,SRS}^{th}) \left(\frac{k_{p,RSR}^{hh}}{k_p^{hh}} + \frac{k_{p,RSS}^{hh}}{k_p^{hh}} \right) [2VA(t)] [VA] \\
 & + 0.5 (k_{p,SSR}^{th} + k_{p,SSS}^{th}) \left(\frac{k_{p,RSR}^{hh}}{k_p^{hh}} + \frac{k_{p,RRR}^{hh}}{k_p^{hh}} \right) [2VA(t)] [VA]
 \end{aligned} \tag{S16}$$

Which, taking into account the enantiomer pairs, further simplifies to:

$$R_{f,3VA^d(t)} = \left((k_{p,RRR}^{th} + k_{p,RRS}^{th}) \frac{k_{p,RRR}^{hh} + k_{p,RSS}^{hh}}{k_p^{hh}} + (k_{p,RSR}^{th} + k_{p,RSS}^{th}) \frac{k_{p,RRS}^{hh} + k_{p,RSR}^{hh}}{k_p^{hh}} \right) [2VA(t)][VA] \quad (\text{S17})$$

And hence:

$$k_p^{th} = (k_{p,RRR}^{th} + k_{p,RRS}^{th}) \frac{k_{p,RRR}^{hh} + k_{p,RSS}^{hh}}{k_p^{hh}} + (k_{p,RSR}^{th} + k_{p,RSS}^{th}) \frac{k_{p,RRS}^{hh} + k_{p,RSR}^{hh}}{k_p^{hh}} \quad (\text{S18})$$

S1.2 Trimer model for 1,5 intramolecular chain transfer (backbiting)

S1.2.1 1,5 intramolecular chain transfer with a head radical (backbiting by head radical)

Since a dimer model is not sufficiently long to model backbiting reactions, a trimer model has been used.

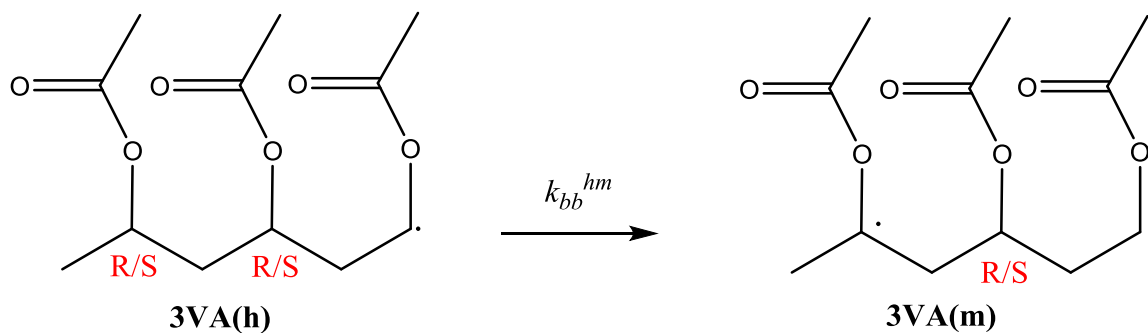


Figure S7. Trimer model reaction for 1,5 intramolecular chain transfer with a ‘head’ macroradical.

The rate of overall stereo-aspecific formation of the poly(vinyl acetate) tertiary mid-chain radical, 3VA(m), is equal to:

$$R_{f,3VA(m)} = k_{bb,RR}^h [3VA(h)_{RR}] + k_{bb,RS}^h [3VA(h)_{RS}] + k_{bb,SR}^h [3VA(h)_{SR}] + k_{bb,SS}^h [3VA(h)_{SS}] \quad (S19)$$

The population of the different 3VA(h) stereoisomers is depending on the reaction leading to these radicals, which is depending on the rate coefficients of head-to-tail propagation:

$$\frac{[3VA(h)_{RR}]}{[3VA(h)]} = \frac{0.5 k_{p,RR}^{ht}}{k_p^{ht}} \quad (S20)$$

$$\frac{[3VA(h)_{RS}]}{[3VA(h)]} = \frac{0.5 k_{p,RS}^{ht}}{k_p^{ht}} \quad (S21)$$

$$\frac{[3VA(h)_{SR}]}{[3VA(h)]} = \frac{0.5 k_{p,SR}^{ht}}{k_p^{ht}} \quad (S22)$$

$$\frac{[3VA(h)_{SS}]}{[3VA(h)]} = \frac{0.5 k_{p,SS}^{ht}}{k_p^{ht}} \quad (S23)$$

And hence, the overall stereo-aspecific rate coefficient for backbiting by a head radical is equal to:

$$k_{bb}^h = \sum_i k_{bb,Ri}^h \frac{k_{p,Ri}^{ht}}{k_p^{ht}} \text{ where } i = R, S \quad (\text{S24})$$

S1.2.2 1,5 intramolecular chain transfer (backbiting by tail)

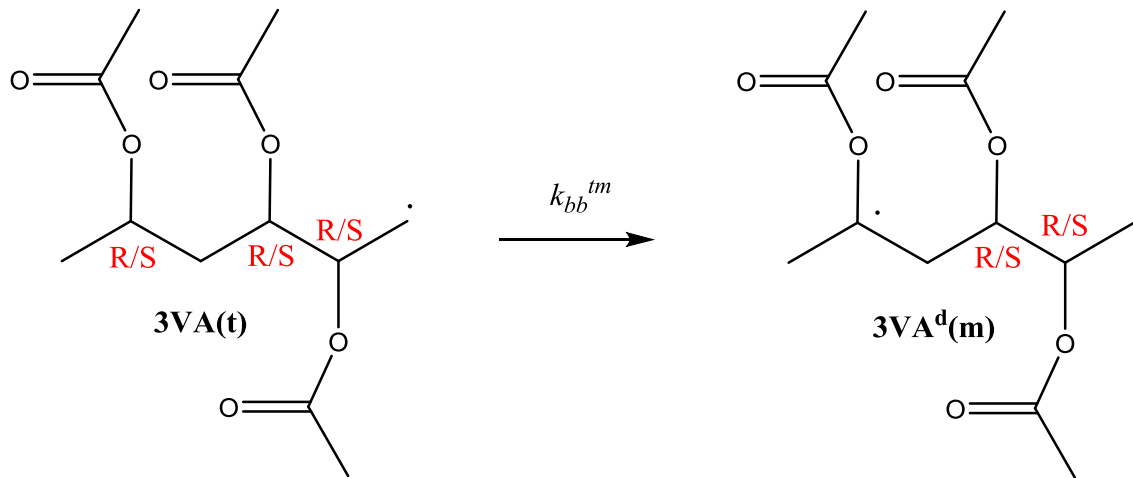


Figure S8. Trimer model reaction for 1,5 intramolecular chain transfer with a ‘tail’ macroradical.

Analogously as to backbiting with a head radical, the following expression for the overall stereo-aspecific rate coefficient for backbiting by a tail radical is found:

$$k_{bb}^t = \sum_{i,j} k_{bb,Rij}^t \frac{k_{p,Rij}^{hh}}{k_p^{hh}} \text{ where } i, j = R, S \quad (\text{S25})$$

S1.3 Extended trimer+methyl model

In order to reflect the steric effects surrounding the mid-chain radical as accurately as possible, a more extended trimer+methyl model was used as a model reaction for mid-chain propagation, as shown in Figure S9.

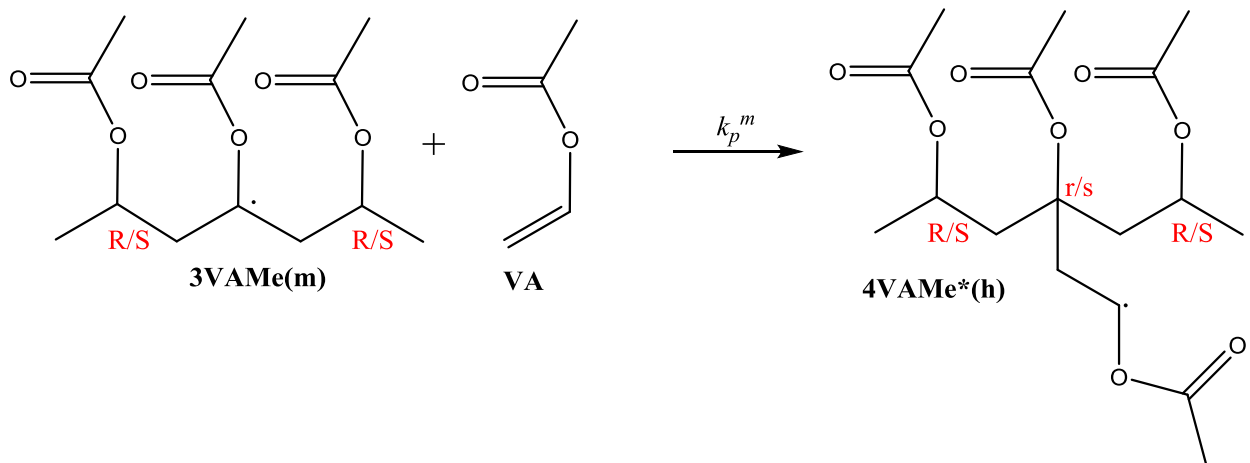


Figure S9. Extended trimer+methyl model reaction for tertiary radical addition using a trimer radical extended with a methyl group. Note that there are 2 chiral centers (R/S) and 1 pseudo chiral center (r/s) present in this reaction.

When using a trimer tertiary radical model, the rate of formation of the branched poly(vinyl acetate) head radical, 4VAMe*(h), is equal to:

$$\begin{aligned}
 R_f,4VAMe^*(h) = & k_{p,RrR}^m [3VAMe(m)_{RR}][VA] + k_{p,RsR}^m [3VAMe(m)_{RR}][VA] \\
 & + k_{p,Rrs}^m [3VAMe(m)_{RS}][VA] + k_{p,Rss}^m [3VAMe(m)_{RS}][VA] \\
 & + k_{p,SrR}^m [3VAMe(m)_{SR}][VA] + k_{p,SSR}^m [3VAMe(m)_{SR}][VA] \\
 & + k_{p,Srs}^m [3VAMe(m)_{SS}][VA] + k_{p,SSS}^m [3VAMe(m)_{SS}]
 \end{aligned} \tag{S26}$$

In order to find a stereo-aspecific rate coefficient for the reaction in Figure S9, the population of the diastereomers of 3VAMe(m) needs to be known. This is depending on the preceding backbiting reaction rate. In a first approximation, we can assume that the majority of tertiary radicals will be formed by backbiting reactions from a tail radical, which in turn are formed by a head-to-head propagation.

Since the monomer unit on the α -chain end has not been included in the backbiting model reactions of the tail radical (Figure S8), the distribution between the RX and SX diastereomers is unknown. However, in a first approximation we can assume them to be evenly distributed and hence:

$$\begin{aligned} [3VAMe(m)_{RR}] &= [3VAMe(m)_{SR}] = [3VAMe(m)_{RS}] = [3VAMe(m)_{SS}] \\ &= \frac{[3VAMe(m)]}{4} \end{aligned} \quad (\text{S27})$$

After substitution in S26, we find the following expression for the overall stereo-aspecific rate coefficient:

$$k_p^m = \frac{1}{4} \sum (k_{p,irj}^m + k_{p,isj}^m) \text{ where } i,j = R,S \quad (\text{S28})$$

S2 Computational details

All calculations were performed using the Gaussian 09 software.¹⁰ The following standard textbook equations where used to determine enthalpies, entropies and Gibbs free energies:¹¹

$$H^\circ_{gas} = E + RT^2 \left(\frac{\partial \ln q}{\partial T} \right)_V + PV \quad (S29)$$

$$S^\circ_{gas} = R + R \ln q + RT \left(\frac{\partial \ln q}{\partial T} \right)_V \quad (S30)$$

$$G^\circ_{gas} = H^\circ_{gas} - TS^\circ_{gas} \quad (S31)$$

Where E is the electronic energy calculated on the M06-2X/6-311+G(d,p) level of theory, P the pressure equal to 1 atmosphere, V the volume equal to 1 L, R the universal gas constant, T the temperature equal to 298 K and q the total molecular partition function including the contribution due to the zero-point energy vibration at the B3LYP/6-31G(d) level of theory, and defined as:

$$q_i = q_{el} q_{rot} q_{trans} q_{vib} \quad (S32)$$

where q_{el} is the partition function for electronic motion, and formally equal to the degeneracy, q_{rot} for external rotation, q_{trans} for translation. q_{vib} is the vibrational partition function including contributions from zero-point vibrations, in the harmonic oscillator approximation in which internal rotations are approximated as harmonic vibrations. Note that the number of optical isomers is not included in the partition function.

Standard enthalpies and entropies of solvation were calculated using the following thermodynamic functions:¹²

$$\Delta_{solv}H^\circ(T) = -T^2 \frac{\partial \left(\frac{\Delta_{solv}G^\circ(T)}{T} \right)}{\partial T} \approx -T^2 \left[\frac{\left(\frac{\Delta_{solv}G^\circ(T_2)}{T_2} \right) - \left(\frac{\Delta_{solv}G^\circ(T_1)}{T_1} \right)}{T_2 - T_1} \right] \quad (S33)$$

$$\Delta_{solv}S^\circ(T) = \frac{\Delta_{solv}H^\circ(T) - \Delta_{solv}G^\circ(T)}{T} \quad (S34)$$

Standards enthalpies, entropies and Gibbs free energies in the condensed phase were then calculated by adding the respective standard enthalpy, entropy or Gibbs free energy of solvation to the respective gas phase equivalent.

Subsequent application of classical transition state theory¹³ allows to calculate the rate coefficient k as follows:

$$k(T) = \kappa(T) \frac{k_B T}{h} (c^0)^{1-m} \exp\left(\frac{-\Delta G_0^\ddagger}{RT}\right) \quad (\text{S35})$$

in which $\kappa(T)$ is the quantum tunneling correction factor, k_B the Boltzmann constant ($1.381 \cdot 10^{-23}$ J mol⁻¹ K⁻¹), h the Planck constant ($6.626 \cdot 10^{-34}$ J s), c^0 the standard unit of concentration (mol L⁻¹) and m the molecularity of the reaction (1 for a unimolecular and 2 for a bimolecular reaction).

For hydrogen abstraction reactions, the quantum tunneling correction factor $\kappa(T)$ has been taken into account using the Eckart tunneling scheme¹⁴ at the B3LYP level of theory, since the thermal analysis has been done at that level of theory. Eckart quantum tunneling correction factors have proven their reliability before for reactions involving hydrogen radicals.^{15, 16} For other reactions, such as radical additions, tunneling contributions can be considered to be insignificant and $\kappa(T)$ has been chosen equal to 1.

Calculations of the rate coefficient $k(T)$ at two different temperatures, the activation energies E_a and pre-exponential factors A are obtained via regression of the Arrhenius equation:

$$E_a = -R \left(\frac{\ln k(T_2) - \ln k(T_1)}{\frac{1}{T_2} - \frac{1}{T_1}} \right) \quad (\text{S36})$$

$$\ln A = \ln k(T) + \frac{E_a}{RT} \quad (\text{S37})$$

S3 Thermodynamic and kinetic values

S3.1 *Thermodynamic and kinetic values of all stereospecific model reactions in gas phase*

Table S1. Standard reaction and activation enthalpy, entropy and Gibbs free energy (Δ_rH° , Δ_rS° , Δ_rG° and $\Delta^\ddagger H^\circ$, $\Delta^\ddagger S^\circ$, $\Delta^\ddagger G^\circ$, in respectively kJ mol^{-1} , $\text{J mol}^{-1} \text{K}^{-1}$, kJ mol^{-1}) at 298 K in the gas phase (reference state is 1 mol L^{-1}).

reaction	Δ_rH°	Δ_rS°	Δ_rG°	$\Delta^\ddagger H^\circ$	$\Delta^\ddagger S^\circ$	$\Delta^\ddagger G^\circ$	k (298 K)
$2\text{VA(h)} + \text{VA} \rightarrow 3\text{VA(h)}_{\text{RR}}$	-111.5	-180.0	-57.9	10.8	-167.1	60.6	1.5E+02
$2\text{VA(h)} + \text{VA} \rightarrow 3\text{VA(h)}_{\text{RS}}$	-117.6	-173.2	-65.9	7.2	-153.5	53.0	3.3E+03
$2\text{VA(h)} + \text{VA} \rightarrow 3\text{VA(t)}_{\text{RRR}}$	-91.5	-148.7	-47.2	13.6	-177.1	66.4	1.4E+01
$2\text{VA(h)} + \text{VA} \rightarrow 3\text{VA(t)}_{\text{RRS}}$	-103.6	-174.4	-51.6	10.4	-173.8	62.2	7.8E+01
$2\text{VA(h)} + \text{VA} \rightarrow 3\text{VA(t)}_{\text{RSR}}$	-106.9	-182.1	-52.6	10.5	-173.9	62.3	7.4E+01
$2\text{VA(h)} + \text{VA} \rightarrow 3\text{VA(t)}_{\text{RSS}}$	-102.5	-167.9	-52.4	12.5	-172.4	63.9	4.0E+01
$2\text{VA(t)} + \text{VA} \rightarrow 3\text{VA(tt)}_{\text{RR}}$	-111.2	-165.8	-61.8	20.1	-150.8	65.1	2.5E+01
$2\text{VA(t)} + \text{VA} \rightarrow 3\text{VA(tt)}_{\text{RS}}$	-116.7	-176.2	-64.2	19.1	-174.9	71.3	2.0E+00
$2\text{VA(t)} + \text{VA} \rightarrow 3\text{VA(th)}_{\text{RRR}}$	-107.7	-156.3	-61.1	27.6	-156.7	74.4	5.8E-01
$2\text{VA(t)} + \text{VA} \rightarrow 3\text{VA(th)}_{\text{RRS}}$	-109.0	-166.4	-59.4	14.3	-169.7	64.9	2.6E+01
$2\text{VA(t)} + \text{VA} \rightarrow 3\text{VA(th)}_{\text{RSR}}$	-118.9	-166.2	-69.3	7.8	-165.1	57.0	6.3E+02
$2\text{VA(t)} + \text{VA} \rightarrow 3\text{VA(th)}_{\text{RSS}}$	-118.7	-167.7	-68.7	8.2	-158.6	55.5	1.2E+03
$3\text{VA(h)}_{\text{RR}} \rightarrow 3\text{VA(m)}$	3.2	31.0	-6.1	83.2	7.1	81.1	4.5E+00
$3\text{VA(h)}_{\text{RS}} \rightarrow 3\text{VA(m)}$	9.2	25.3	1.6	100.3	5.6	98.6	6.9E-03
$3\text{VA(t)}_{\text{RRR}} \rightarrow 3\text{VA}^*(\text{m})_{\text{RR}}$	-29.9	-7.3	-27.7	48.9	-37.7	60.2	8.3E+03
$3\text{VA(t)}_{\text{RRS}} \rightarrow 3\text{VA}^*(\text{m})_{\text{RS}}$	-11.4	15.8	-16.1	72.0	7.8	69.7	2.1E+02
$3\text{VA(t)}_{\text{RSR}} \rightarrow 3\text{VA}^*(\text{m})_{\text{SR}}$	-14.5	20.0	-20.5	76.5	10.5	73.4	6.4E+01
$3\text{VA(t)}_{\text{RSS}} \rightarrow 3\text{VA}^*(\text{m})_{\text{SS}}$	-12.5	7.3	-14.7	70.4	-5.4	72.0	9.4E+01
$3\text{VAm(m)}_{\text{RR}} + \text{VA} \rightarrow 4\text{VAm}^*(\text{h})_{\text{RRR}}$	-106.9	-189.8	-50.3	9.7	-165.7	59.1	2.7E+02
$3\text{VAm(m)}_{\text{RR}} + \text{VA} \rightarrow 4\text{VAm}^*(\text{h})_{\text{RRS}}$	-97.5	-155.5	-51.1	12.4	-165.8	61.8	9.2E+01
$3\text{VAm(m)}_{\text{RS}} + \text{VA} \rightarrow 4\text{VAm}^*(\text{h})_{\text{RSR}}$	-86.8	-181.5	-32.7	33.1	-177.3	86.0	5.4E-03
$3\text{VAm(m)}_{\text{RS}} + \text{VA} \rightarrow 4\text{VAm}^*(\text{h})_{\text{RSS}}$	-86.8	-207.2	-25.0	26.9	-209.5	89.3	1.4E-03

S3.2 *Thermodynamics and kinetics of all stereospecific model reactions in vinyl acetate*

Table S2. Standard reaction and activation enthalpy, entropy and Gibbs free energy (Δ_rH° , Δ_rS° , Δ_rG° and $\Delta^\ddagger H^\circ$, $\Delta^\ddagger S^\circ$, $\Delta^\ddagger G^\circ$, in respectively kJ mol^{-1} , $\text{J mol}^{-1} \text{K}^{-1}$, kJ mol^{-1}) at 298 K in the bulk phase (vinyl acetate, reference state is 1 mol L⁻¹).

reaction	Δ_rH°	Δ_rS°	Δ_rG°	$\Delta^\ddagger H^\circ$	$\Delta^\ddagger S^\circ$	$\Delta^\ddagger G^\circ$	k (298 K)
2VA(h) + VA → 3VA(h) _{RR}	-101.2	-154.0	-55.2	20.8	-142.1	63.2	5.3E+01
2VA(h) + VA → 3VA(h) _{RS}	-110.2	-151.1	-65.1	13.9	-130.1	52.7	3.7E+03
2VA(h) + VA → 3VA(t) _{RRR}	-85.1	-126.6	-47.3	25.9	-151.1	71.0	2.3E+00
2VA(h) + VA → 3VA(t) _{RRS}	-95.5	-149.4	-50.9	19.8	-148.5	64.0	3.7E+01
2VA(h) + VA → 3VA(t) _{RSR}	-96.9	-157.0	-50.0	20.4	-149.2	64.9	2.6E+01
2VA(h) + VA → 3VA(t) _{RSS}	-95.6	-144.9	-52.4	22.7	-146.8	66.4	1.4E+01
2VA(t) + VA → 3VA(tt) _{RR}	-102.2	-141.5	-60.1	30.0	-125.4	67.4	9.8E+00
2VA(t) + VA → 3VA(tt) _{RS}	-106.7	-152.2	-61.3	29.6	-150.7	74.5	5.5E-01
2VA(t) + VA → 3VA(th) _{RRR}	-99.3	-133.0	-59.7	36.0	-133.0	75.6	3.5E-01
2VA(t) + VA → 3VA(th) _{RRS}	-101.4	-141.9	-59.1	25.0	-144.8	68.2	7.1E+00
2VA(t) + VA → 3VA(th) _{RSR}	-109.6	-140.8	-67.6	16.6	-139.7	58.2	3.9E+02
2VA(t) + VA → 3VA(th) _{RSS}	-110.0	-143.8	-67.1	16.5	-135.1	56.8	6.8E+02
3VA(h) _{RR} → 3VA(m)	0.4	27.4	-7.8	79.1	3.2	78.2	1.2E-01
3VA(h) _{RS} → 3VA(m)	7.4	22.3	0.8	95.4	4.3	94.1	2.0E-04
3VA(t) _{RRR} → 3VA*(m) _{RR}	-29.3	-6.4	-27.4	49.9	-36.3	60.7	1.4E+02
3VA(t) _{RRS} → 3VA*(m) _{RS}	-12.1	13.1	-16.0	68.4	2.4	67.7	8.7E+00
3VA(t) _{RSR} → 3VA*(m) _{SR}	-17.5	17.9	-22.9	68.1	6.2	66.2	1.5E+01
3VA(t) _{RSS} → 3VA*(m) _{SS}	-12.0	6.6	-14.0	67.8	-5.3	69.4	4.4E+00
3VAm(m) _{RR} + VA → 4VAm*(h) _{RRR}	-95.2	-164.4	-46.1	18.8	-141.0	60.8	1.4E+02
3VAm(m) _{RR} + VA → 4VAm*(h) _{RRS}	-90.3	-135.1	-50.0	21.6	-142.2	64.0	3.9E+01
3VAm(m) _{RS} + VA → 4VAm*(h) _{RSR}	-73.2	-157.1	-26.4	45.6	-151.7	90.8	7.6E-04
3VAm(m) _{RS} + VA → 4VAm*(h) _{RSS}	-68.9	-178.7	-15.7	45.6	-179.5	99.1	2.7E-05

S3.3 *Thermodynamic values of the global, stereo-aspecific model reactions*

Table S3. Ab initio calculated standard reaction enthalpy (Δ_rH°) and entropy (Δ_rS) for the elementary reactions shown in Figure 2 determined in the interval 298 – 333 K.

Reaction	Δ_rH°	Δ_rS°
	[kJ mol ⁻¹]	[J mol ⁻¹ K ⁻¹]
head-to-tail propagation (p, ht)	-106.4	-138.4
head-to-head propagation (p,hh)	-91.3	-124.6
tail-to-tail propagation (p, tt)	-100.7	-129.0
tail-to-head propagation (p,th)	-106.2	-130.7
backbiting by head radical (bb,h)	-8.5	-28.2
backbiting by tail radical (bb,t)	-31.6	-34.3
mid-chain propagation (p,m)	-87.4	-129.8

S4 Transition state structures for backbiting

The different diastereomers for the transition state structures for backbiting by head and tail radicals are shown in Figure S10. The values of the dihedral angles of the carbon atoms in the six-membered rings are given in Table S4.

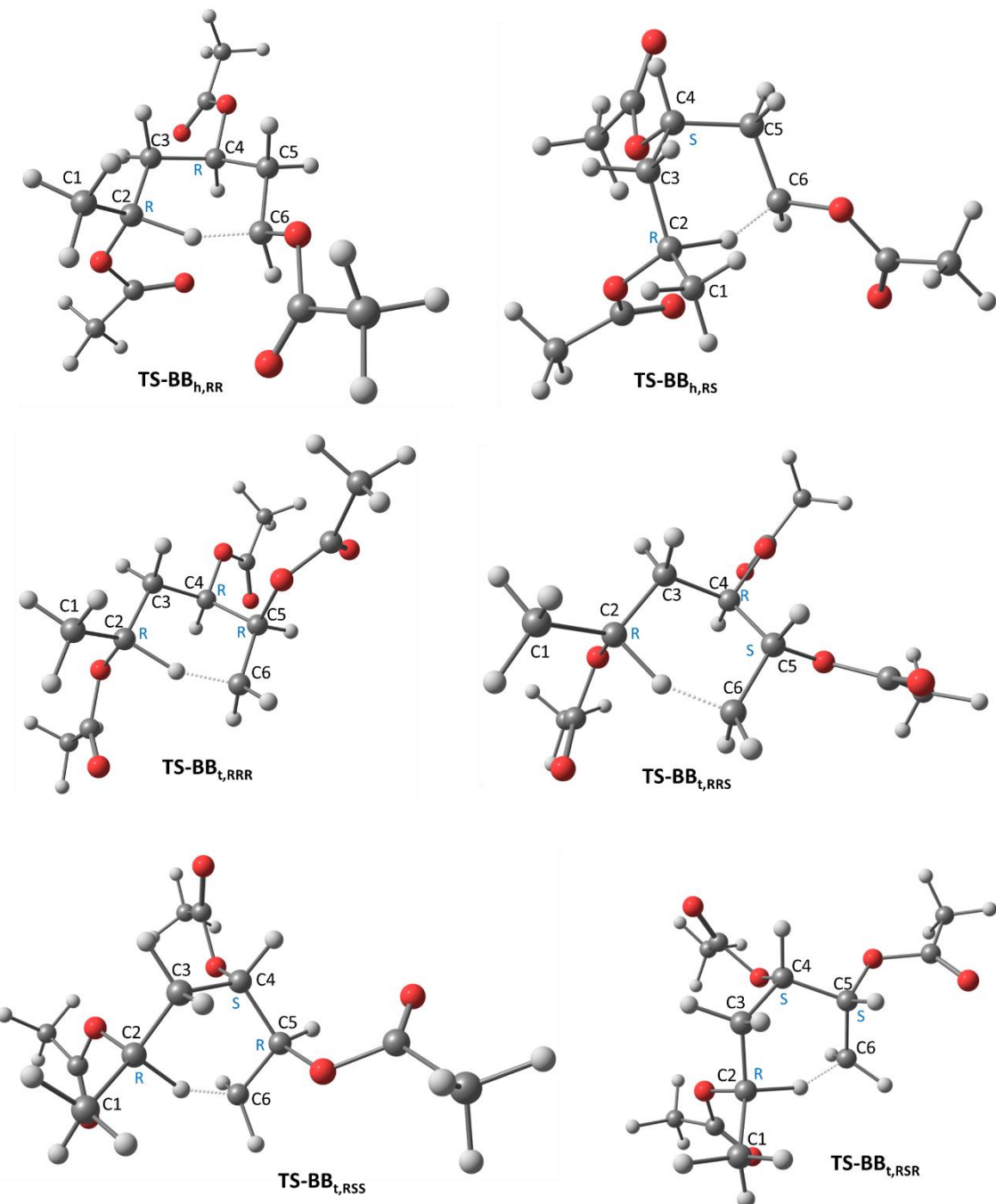


Figure S10. Molecular structures of the different diastereomers of the transition states for backbiting by head (TS-BB_h) and tail (TS-BB_t) radicals. The configuration of the chiral centers are shown (R/S in blue). The carbons from the 6-membered ring are numbered from C1 to C6.

Table S4. Dihedral angles of the carbon atoms of the six-membered ring of the transition states of backbiting by head and tail radicals (cf. Figure S10)

structures	dihedral angle (°)		
	C1-C2-C3-C4	C2-C3-C4-C5	C3-C4-C5-C6
TS-BB _{h,RR}	135.4	-50.6	58.3
TS-BB _{h,RS}	140.1	-56.9	53.5
TS-BB _{t,RRR}	155.2	-59.3	59.1
TS-BB _{t,RRS}	156.6	-59.8	57.3
TS-BB _{t,RSR}	146.5	-54.2	60.5
TS-BB _{t,RSS}	147.5	-52.5	55.7
ideal value	180	-60	60

For backbiting by tail radicals, the dihedral angles are significantly closer to the 'ideal' ones, rationalizing the lower activation energy for backbiting by tail radicals.

Part II: Kinetic Monte Carlo Modeling of PLP-SEC

S5 Calculation of the reaction probabilities shown in Figure 2

Table S5. Frequency and time scale at which a radical undergoes reaction, based on rate coefficients calculated using the pre-exponential factors and activation energies shown in Table 1 in the main manuscript.

Radical type	Reaction	Equation	Frequency			Time scale		
			50 °C [s ⁻¹]	30 °C [s ⁻¹]	10 °C [s ⁻¹]	50 °C [s ⁻¹]	30 °C [s ⁻¹]	10 °C [s ⁻¹]
head	head-to-tail propagation	$k_p^{ht} [M]_0$	7.0E+04	4.4E+04	2.6E+04	1.4E-05	2.3E-05	3.9E-05
head	head-to-head propagation	$k_p^{hh} [M]_0$	1.9E+03	1.0E+03	4.8E+02	5.2E-04	9.9E-04	2.1E-03
head	backbiting by head radical	k_{bb}^h	1.5E+00	3.6E-01	7.1E-02	6.6E-01	2.8E+00	1.4E+01
tail	tail-to-tail propagation	$k_p^{tt} [M]_0$	1.3E+04	7.7E+03	4.2E+03	7.7E-05	1.3E-04	2.4E-04
tail	tail-to-head propagation	$k_p^{th} [M]_0$	3.0E+02	1.3E+02	5.0E+01	3.3E-03	7.7E-03	2.0E-02
tail	backbiting by tail radical	k_{bb}^t	3.1E+03	1.1E+03	3.4E+02	3.2E-04	9.0E-04	2.9E-03
mid-chain	mid-chain radical propagation	$k_p^{mt} [M]_0$	2.0E+03	1.1E+03	5.5E+02	4.9E-04	9.0E-04	1.8E-03

The total frequency at which a head radical undergoes reaction is equal to the sum of the frequencies of head-to-tail propagation, head-to-head propagation and backbiting by a head radical.

The total frequency at which a tail radical undergoes reaction is equal to the sum of the frequencies of tail-to-tail propagation, tail-to-head propagation and backbiting by a tail radical.

The probability at which an individual reaction occurs is equal to the ratio of the frequency of the respective reaction to the total frequency of reaction for that radical type. Note that termination reactions are not considered.

S6 Details on the kinetic Monte Carlo modeling of PLP

Table S6. Reaction scheme used for the kinetic Monte Carlo modeling of PLP spectra.

Entry	Reaction	Equation	A [(L mol ⁻¹) s ⁻¹]	E _a [kJ mol ⁻¹]	k (50 °C) [(L mol ⁻¹) s ⁻¹]	ref
1	Photodissociation	$DMPA \xrightarrow{h\nu} R_0^I + R_0^{II}$	-	-	^a	-
2	Chain initiation ^b	$R_0^I + M \xrightarrow{k_p^{It}} R_{1,h}$			7.4E+04	^b
3		$R_0^I + M \xrightarrow{k_p^{lh}} R_{1,t}$			2.0E+03	^b
4	Propagation ^c	$R_{i,h} + M \xrightarrow{k_p^{ht}} R_{i+1,h}$	1.2E+07	20.1	6.8E+03	This work
5		$R_{i,h} + M \xrightarrow{k_p^{hh}} R_{i+1,t}$	4.6E+06	27.2	1.8E+02	This work
6		$R_{i,t} + M \xrightarrow{k_p^{tt}} R_{i+1,h}$	5.4E+06	22.5	1.2E+03	This work
7		$R_{i,t} + M \xrightarrow{k_p^{th}} R_{i+1,t}$	1.6E+07	35.5	2.9E+01	This work
8		$R_{i,m} + M \xrightarrow{k_p^m} R_{i+1,h}$	2.9E+06	25.8	2.0E+02	This work
9	Backbiting ^d	$R_{i,h} \xrightarrow{k_{bb}^h} R_{i,m}$	4.2E+09	58.4	1.5E+00	This work
10		$R_{i,t} \xrightarrow{k_{bb}^t} R_{i,m}$	2.0E+10	42.1	3.1E+03	This work
11	Termination ^e	$R_{i,h} + R_{j,h} \xrightarrow{k_{t,ee}^{app}(i,j)} P_i + P_j$	3.2E+10	9.0	2.2E+09	¹⁷
12		$R_{i,h} + R_{j,t} \xrightarrow{k_{t,ee}^{app}(i,j)} P_i + P_j$	3.2E+10	9.0	2.2E+09	¹⁷
13		$R_{i,t} + R_{j,t} \xrightarrow{k_{t,ee}^{app}(i,j)} P_i + P_j$	3.2E+10	9.0	2.2E+09	¹⁷
14		$R_{i,h} + R_{j,m} \xrightarrow{k_{t,em}^{app}(i,j)} P_i + P_j$			7.5E+08	^f
15		$R_{i,t} + R_{j,m} \xrightarrow{k_{t,em}^{app}(i,j)} P_i + P_j$			7.5E+08	^f
16		$R_{i,m} + R_{j,m} \xrightarrow{k_{t,mm}^{app}(i,j)} P_i + P_j$			4.7E+06	^f
17		$R_{0,e}^{I/II} + R_{0,e}^{I/II} \xrightarrow{k_{t,oo}^{app}} P_0$	3.2E+10	9.0	2.2E+09	^g
18		$R_{0,e}^{I/II} + R_{i,h} \xrightarrow{k_{t,ee}^{app}(1,i)} P_i + P_0$	3.2E+10	9.0	2.2E+09	^h
19		$R_{0,e}^{I/II} + R_{i,t} \xrightarrow{k_{t,ee}^{app}(1,i)} P_i + P_0$	3.2E+10	9.0	2.2E+09	^h
20		$R_{0,e}^{I/II} + R_{i,m} \xrightarrow{k_{t,em}^{app}(1,i)} P_i + P_0$			7.5E+08	^h

^a: Dissociation into a benzoyl ($R_{0,I}$) and dimethoxy benzyl ($R_{0,II}$) radical; $\Delta[R_0]$ is calculated as a function of time using Equation (S42).

^b: No propagation of $R_{0,II}$,¹⁸⁻²⁰ $k_p^{It} = 11 k_p^{ht}$ and $k_p^{lh} = 11 k_p^{hh}$, cf. Section S7.^{21,22}

^c: Chain length dependent propagation accounted for cf. Section S7.

^d: Always H-abstraction on C-X position.

^e: chain length dependent apparent termination rate coefficients are considered;²³ only $k_t^{app}(1,1)$ is reported here, taking into account a correction with a factor 2, as indicated by Derboven *et al.*²⁴ termination assumed to occur solely via disproportionation,¹⁷ except for termination between two initiator radicals, which occurs via recombination; no effect of radical type on termination reactivity assumed.

^f: $k_{t,em}(1,1) = k_{t,ee}(1,1)/3$, $k_{t,mm}(1,1) = k_{t,ee}(1,1)/480$; cf.²⁵

^g: assumed equal to $k_{t,ee}(1,1)$.

^h: assumed equal to $k_{t,ee/m}(1,i)$; $k_{t,ee/m}(1,1)$ is reported.

The concentration of photoinitiator radical fragments generated per pulse ($\Delta[R_0]$) is calculated for each pulse using Equation (S42) and considering typical experimental conditions, namely a laser pulse energy of 1.5 mJ, a laser wavelength of 351 nm, an initial DMPA concentration of 5 mmol L⁻¹, an optical path length of 0.5 cm and a sample volume of 0.2 mL; ε is taken equal to 280 L mol⁻¹ cm⁻¹ and $\Phi_{diss} = 0.42$ (cf. ref.²⁰).

Macroradicals are assumed to terminate exclusively via disproportionation.²⁶ The apparent termination reactivity is assumed to be independent of the type (head or tail) of the radicals involved and is described using a composite k_t model.²⁷ The geometric mean for the apparent short-long termination reactivity is used:

$$k_t^{app}(i, i) = k_t^{app}(1,1)i^{-\alpha_S} \quad i \leq i_c \quad (\text{S38})$$

$$k_t^{app}(i, i) = k_t^{app}(1,1)i_c^{-\alpha_S + \alpha_L}i^{-\alpha_L} \quad i > i_c \quad (\text{S39})$$

$$k_t^{app}(i, j) = [k_t^{app}(i, i)k_t^{app}(j, j)]^{0.5} \quad (\text{S40})$$

where $\alpha_S = 0.57$, $\alpha_L = 0.16$ and $i_c = 20$.²³

S7 Chain length dependent propagation

Chain length dependent propagation is formally accounted for via:²¹

$$k_p(i) = k_p \left[1 + C_1 \exp\left(-\frac{\ln(2)}{i_{1/2}} i\right) \right] \quad (\text{S41})$$

in which i refers to the chain length (0 for an initiator-derived radical).

The recently reported values for C_1 and $i_{1/2}$ by Haven et al.,²² namely $C_1 = 10$ and $i_{1/2} = 1$ have been used in this work for all propagations involving head and tail radicals. Note that for these values of C_1 and $i_{1/2}$ $k_p(i)$ converges after 5 propagation steps to the long chain limit; $k_p(i)$ for the chain initiation step and the first 5 propagation steps is listed below (Table S7).

Table S7. Chain length dependence of the first 5 propagation steps.

Reaction	Rate coefficient
$R_{0,e}^I + M \rightarrow R_{1,h/t}$	$11k_p^{ht/hh}$
$R_{1,h/t} + M \rightarrow R_{2,h/t}$	$6k_p^{ht/hh/tt/th}$
$R_{2,h/t} + M \rightarrow R_{3,h/t}$	$3.5k_p^{ht/hh/tt/th}$
$R_{3,h/t} + M \rightarrow R_{4,h/t}$	$2.3k_p^{ht/hh/tt/th}$
$R_{4,h/t} + M \rightarrow R_{5,h/t}$	$1.6k_p^{ht/hh/tt/th}$
$R_{5,h/t} + M \rightarrow R_{6,h/t}$	$1.3k_p^{ht/hh/tt/th}$

S8 Observed rate coefficients as a function of laser pulse frequency for the case in which backbiting by a head radical is not taken into account (case 5)

In order to demonstrate that the observed decrease in k_p^{obs} when shifting from case 3 to case 4 is mainly due to backbiting of tail radicals, an extra case in which only tail radicals are allowed to undergo backbiting is considered (case 5, i.e. case 4 in which $k_{bb}^h = 0 \text{ s}^{-1}$). The pulse frequency dependence of k_p^{obs} is shown for case 1-5 in Figure S11. The coinciding green triangles and purple crosses illustrate that backbiting of head radicals is indeed negligible.

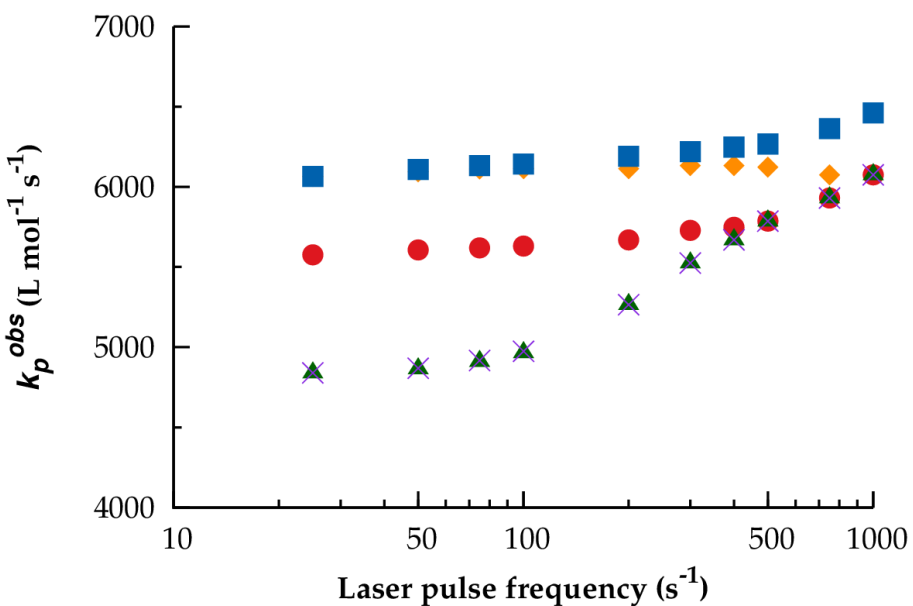


Figure S11. Illustration of the dominance of backbiting by tail radicals. Observed propagation rate coefficients k_p^{obs} calculated using Equation (2) with L_1 based on the first inflection point of the PLP-SEC traces simulated using the ab initio rate coefficients in Table 1 (main text) and the reaction scheme in Section S6 of the Supporting Information. Case 1 (\diamond): chain length independent head-to-tail propagation, Case 2 (\blacksquare): chain length dependent head-to-tail propagation, Case 3 (\bullet): chain length dependent head-to-tail, head-to-head, tail-to-tail and tail-to-head propagation, and Case 4 (\blacktriangle): case 3 with additional backbiting by head and tail radicals, and mid-chain propagation. Case 5 (\times): case 4 in which $k_{bb}^h = 0 \text{ s}^{-1}$. T = 323 K, $[\text{VAc}]_0 = 10.4 \text{ mol L}^{-1}$, $[\text{DMPA}]_0 = 5 \cdot 10^{-3} \text{ mol L}^{-1}$, $E_{\text{pulse}} = 1.5 \text{ mJ}$, $\lambda = 351 \text{ nm}$, $N_{\text{pulse}} = 500$, $V = 0.2 \text{ mL}$, $L = 0.5 \text{ cm}$.

S9 Evaluation of the termination rate limit

As highlighted in the main text, an important consideration that has to be made when applying Equation (2, main text), is whether a small ($\beta \ll 1$) or high ($\beta \rightarrow 1$) fraction of the radicals terminate during a dark period.²⁸ This is determined by the (apparent) chain length dependent termination kinetics and the concentration of radicals generated at the laser pulses, $\Delta[R_0]$.²⁹ The latter is determined by the laser pulse energy E_{pulse} , photoinitiator concentration $[I_2]$, optical path length L and sample volume V and can be calculated via:²⁵

$$\Delta[R_0] = 2\Phi_{diss} \frac{E_{pulse}\lambda}{hcN_A V} [1 - \exp(-2.303\varepsilon[I_2]L)] \quad (\text{S42})$$

in which Φ_{diss} is the photodissociation quantum yield, λ the laser wavelength, c the speed of light, h the Planck constant, N_A the Avogadro constant and ε the molar absorptivity of the photoinitiator.

The evolution of $\Delta[R_0]$ with increasing number of pulses is shown in Figure S12, considering DMPA as photoinitiator and typical experimental conditions, namely a laser pulse energy of 1.5 mJ, a laser wavelength of 351 nm, an initial DMPA concentration of 5 mmol L⁻¹, an optical path length of 0.5 cm and a sample volume of 0.2 mL; ε is taken equal to 280 L mol⁻¹ cm⁻¹ and $\Phi_{diss} = 0.42$ (cf. ref.²⁰). The number of pulses is limited to 500, so that monomer conversion is less than 5% (molar basis) for all pulse frequencies considered in Figure 5 (25 – 1000 s⁻¹). In addition to the evolution of $\Delta[R_0]$, the evolution of the DMPA concentration is shown in Figure S12. A strong decrease of [DMPA] is observed, explaining the strong decrease of $\Delta[R_0]$ (Equation S42).

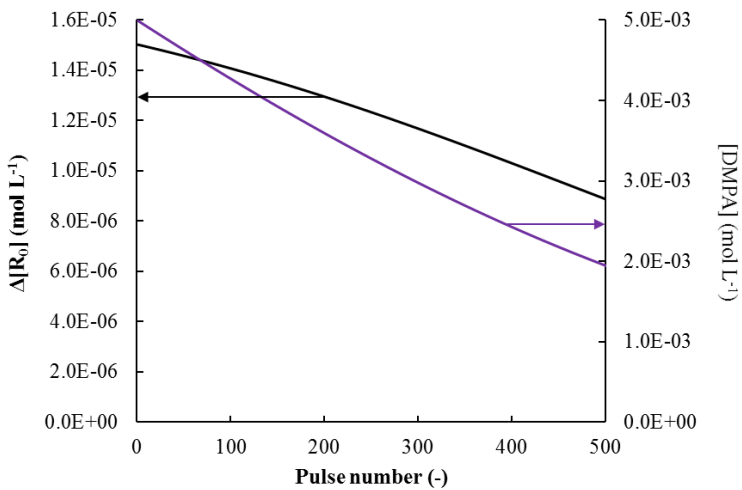


Figure S12. Evolution of $\Delta[R_0]$ and [DMPA] calculated using Equation S42 for typical experimental conditions, namely $E_{pulse} = 1.5 \text{ mJ}$, $\lambda = 351 \text{ nm}$, $[DMPA]_0 = 5 \text{ mmol L}^{-1}$, $L = 0.5 \text{ cm}$ and $V = 0.2 \text{ mL}$; ϵ is taken equal to $280 \text{ L mol}^{-1} \text{ cm}^{-1}$ and $\Phi_{diss} = 0.42$ (cf. ref.²⁰).

The strong decrease of [DMPA] and hence $\Delta[R_0]$ explains the overall decrease of the total radical concentration, as demonstrated in Figure S13 for a pulse frequency of 100 s^{-1} . As a result of the overall decreasing radical concentration, the value of β decreases from 0.98 in the beginning of the PLP experiment to 0.97 at the end of the experiment.

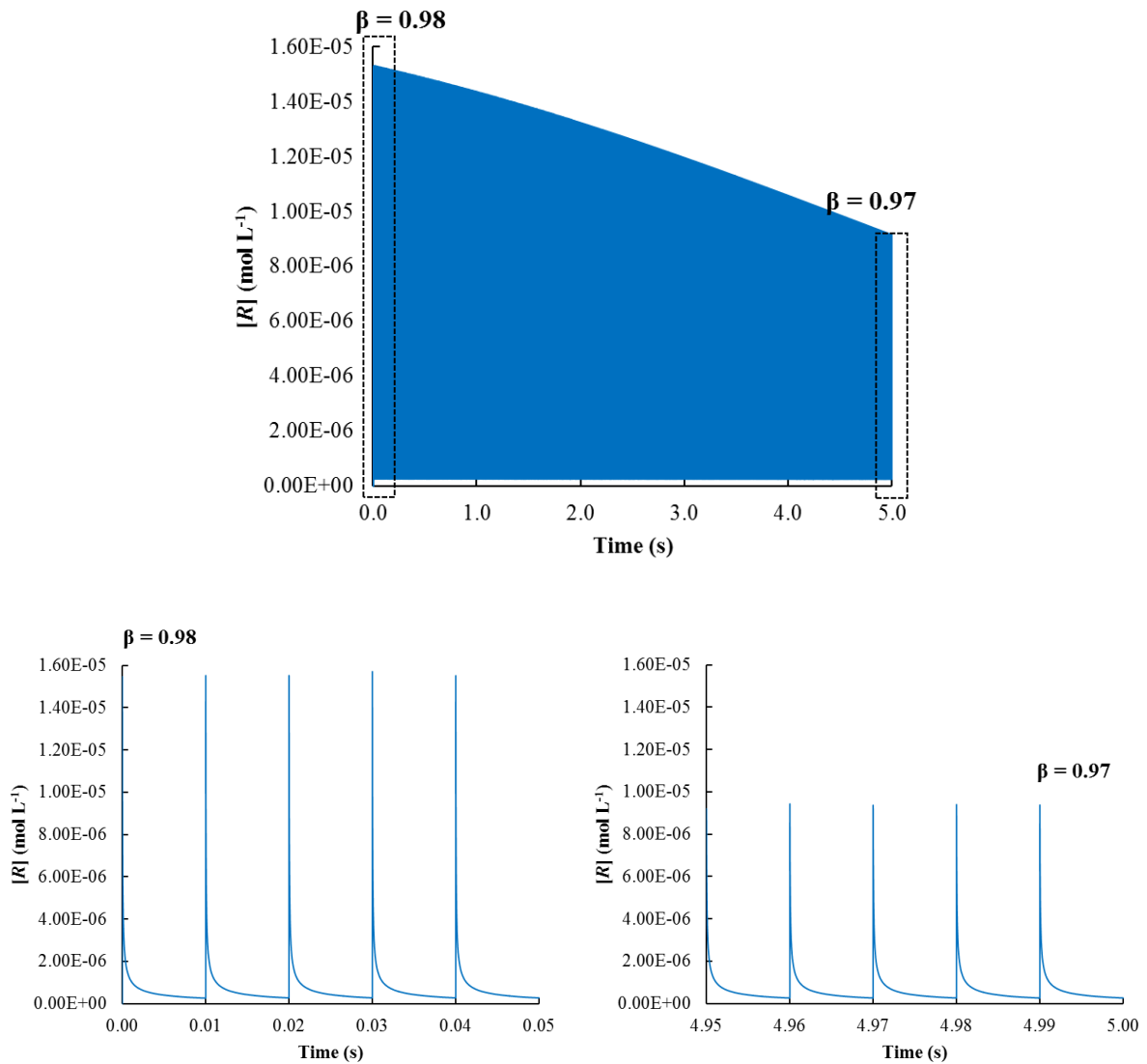


Figure S13. Top: Evolution of the total radical concentration for a pulse frequency of 100 s^{-1} ; $T = 323\text{ K}$, $[\text{VAc}]_0 = 10.4\text{ mol L}^{-1}$, $[\text{DMPA}]_0 = 5\text{ mmol L}^{-1}$, $E_{\text{pulse}} = 1.5\text{ mJ}$, $\lambda = 351\text{ nm}$, $V = 0.2\text{ mL}$, $L = 0.5\text{ cm}$, $N_{\text{pulse}} = 500$. Bottom: inset of top figure focusing on the first five dark periods (left) and the last five dark periods (right).

For a pulse frequency of 500 s^{-1} , the value of β remains rather high ($\beta = 0.95$ in the beginning and 0.92 at the end of the experiment) which means there is only a limited shift away from the HTRL and a shift away from the HTRL (hypothesis (i)) does not provide an adequate explanation for the experimentally observed pulse frequency dependency of k_p^{obs} as determined from the first inflection point when going from lower ($25\text{--}100\text{ s}^{-1}$) to higher ($300\text{--}500\text{ s}^{-1}$) pulse frequencies.

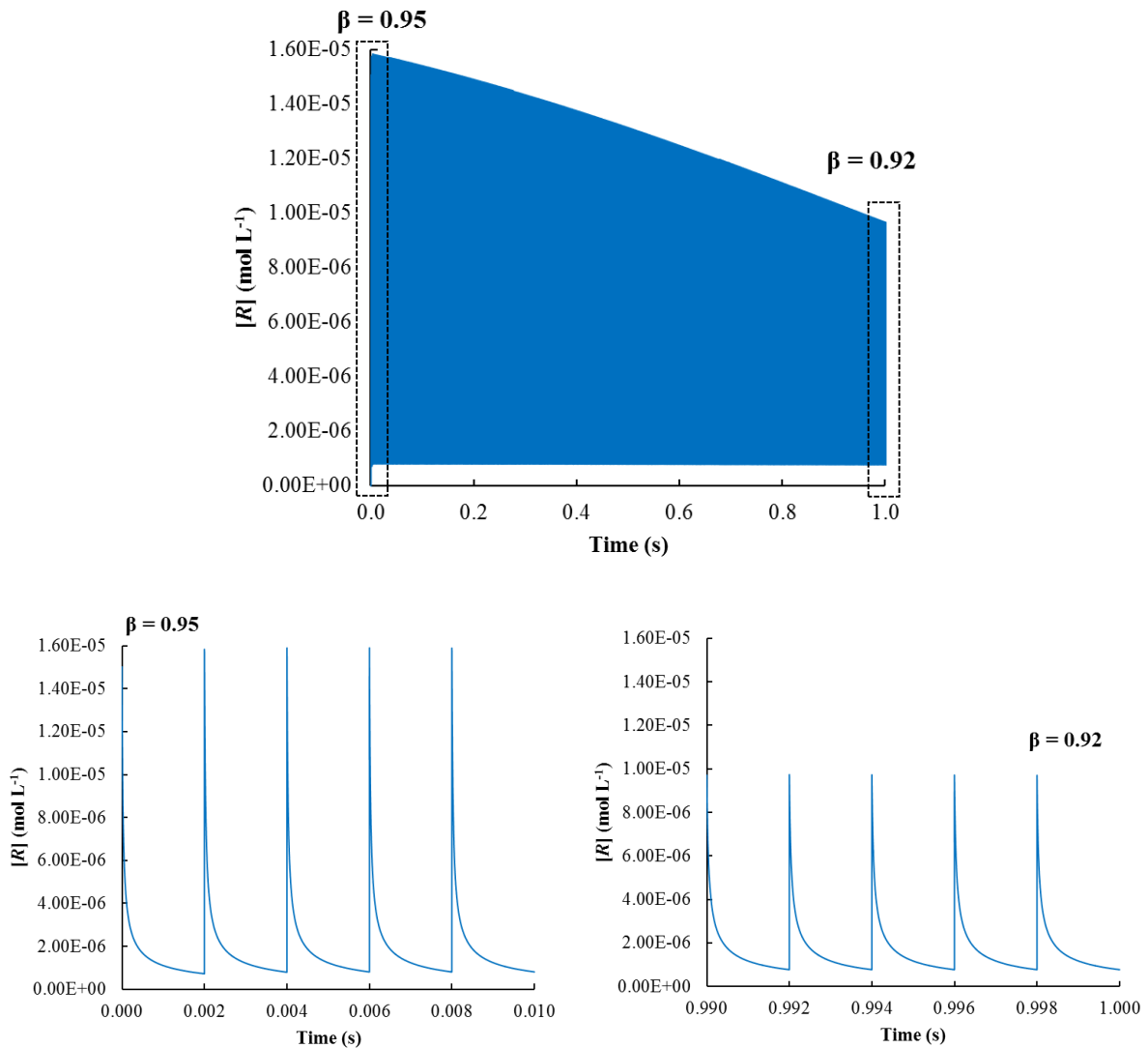


Figure S14. Top: Evolution of the total radical concentration for a pulse frequency of 500 s⁻¹; T = 323 K, [VAc]₀ = 10.4 mol L⁻¹, [DMPA]₀ = 5 mmol L⁻¹, E_{pulse} = 1.5 mJ, λ = 351 nm, V = 0.2 mL, L = 0.5 cm, N_{pulse} = 500. **Bottom:** inset of top figure focusing on the first five dark periods (left) and the last five dark periods.

The accuracy of using the location of the inflection point (or peak maximum) in Equation (2; main text) under these conditions can be evaluated *in silico* by considering case 1 (only head-to-tail addition, cf. main text). As shown in Figure S15, k_p^{obs} determined using the location of the peak maximum (unfilled symbols) corresponds best with the input value of k_p^{ht} (full green line); if the location of the inflection point is used (filled symbols), k_p^{obs} leads to an underestimation of ca. 10%.

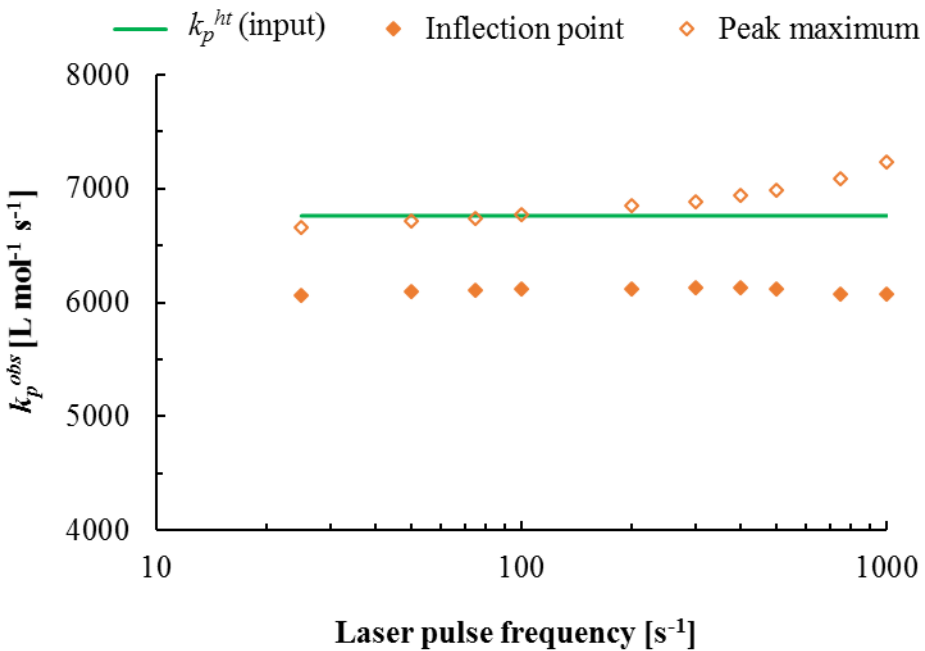


Figure S15. In silico evaluation of Equation (2) using the location of the inflection point (filled diamonds) and the location of the peak maximum (unfilled diamonds) for case 1 (only head-to-tail addition); T = 323 K, [VAc]₀ = 10.4 mol L⁻¹, [DMPA]₀ = 5 mmol L⁻¹, E_{pulse} = 1.5 mJ, λ = 351 nm, V = 0.2 mL, L = 0.5 cm, N_{pulse} = 500.

The preference of using the location of the peak maximum of the SEC trace for the determination of k_p^{obs} is illustrated further in Figure S16 in which the log-MMD of the radical species just before applying a new laser pulse at $t = 10\Delta t$ (full yellow line) is shown as well as the log-MMD of the polymer species P corrected for SEC broadening at the end of the PLP experiment ($t = 500\Delta t$; full black line) for case 1 (only head-to-tail propagation) and a pulse frequency of 500 s⁻¹ (top) and 100 s⁻¹ (bottom). In addition, the location of L_I based on the input value of k_p^{ht} (Equation 1) is indicated by the dashed green line and the location of the inflection point of the SEC broadened P log-MMD is indicated by the dotted red line. As expected,³⁰ the location of the peak maximum of the radical log-MMD corresponds to the input value of k_p^{ht} (dashed green line) Moreover, for both pulse frequencies, the location of the green dashed line corresponds better with the location of the peak maximum of the SEC trace compared to the location of its inflection point (dotted red line), thus confirming the preference of the using the location of the peak maximum of the SEC trace for the determination of k_p^{obs} .

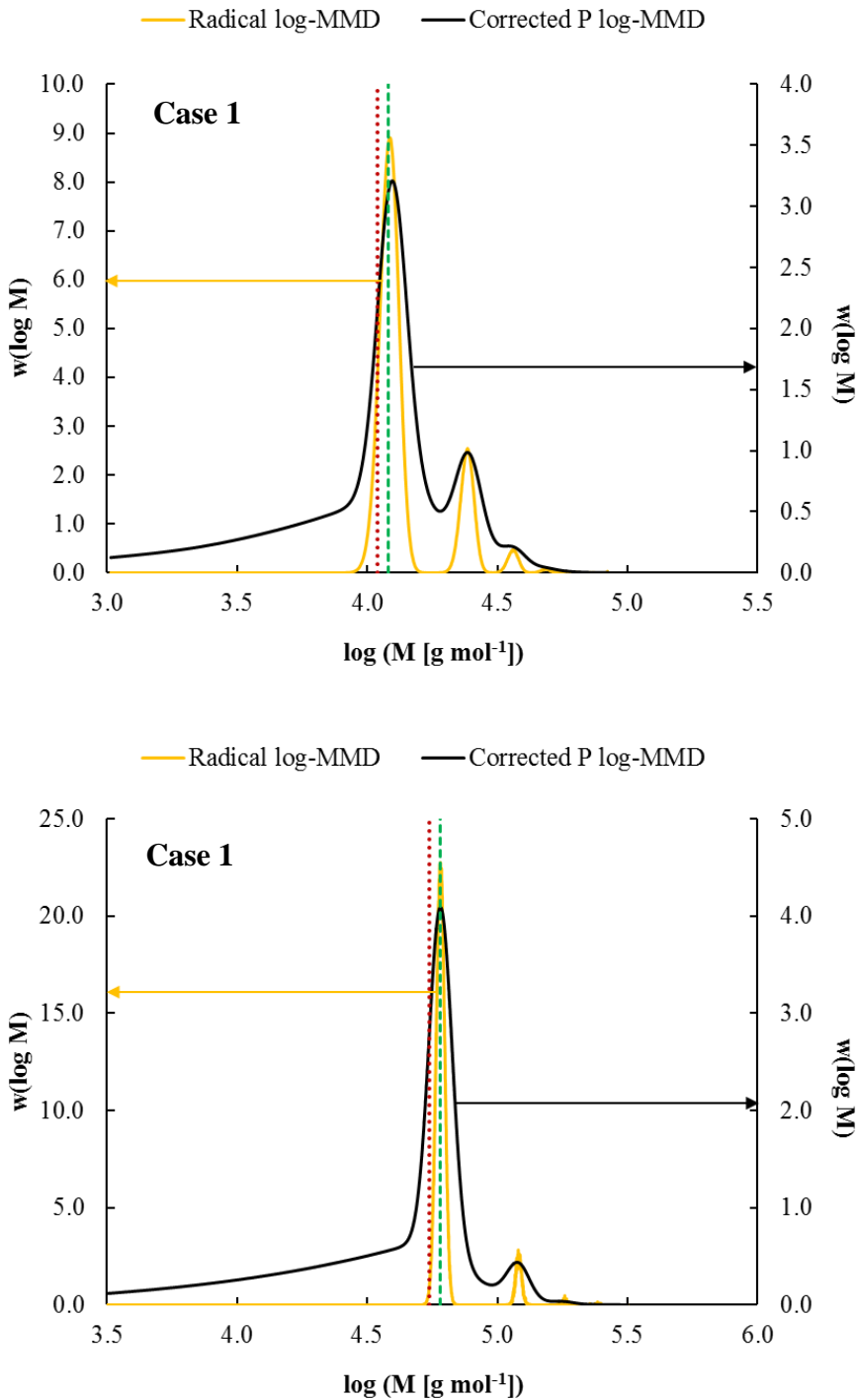


Figure S16. Log-MMD of the radical species just before applying a new pulse at $t = 10\Delta t$ (full yellow line) and log-MMD of the polymer species P at the end of the PLP experiment ($t = 500\Delta t$) corrected for SEC broadening (full black line) for Case 1 (only head-to-tail propagation) and a pulse frequency of 500 s^{-1} (top) and 100 s^{-1} (bottom). The location of L_1 based on the input value of k_p^{ht} (dashed green line) corresponds better with the location of the peak maximum of the SEC trace compared to the location of its inflection point (dotted red line). $T = 323 \text{ K}$, $[\text{VAc}]_0 = 10.4 \text{ mol L}^{-1}$, $[\text{DMPA}]_0 = 5 \text{ mmol L}^{-1}$, $E_{pulse} = 1.5 \text{ mJ}$, $\lambda = 351 \text{ nm}$, $L = 0.5 \text{ cm}$, $V = 0.2 \text{ mL}$.

S10 Effect of the degree of SEC broadening

As explained in the main text, SEC broadening is accounted for via an *a posteriori* correction of the simulated log-MMD (Equation (4)). It has been stated by Drawe and Buback²⁹ that for an optimized SEC system the SEC broadening parameter $\sigma_v b$ is in the range 0.01 to 0.06. In this work, all simulations are performed with a typical intermediate value ($\sigma_v b = 0.04$). In Figure S17, the effect of the degree of SEC broadening on the PLP-SEC trace simulated at 25, 100, 500 and 1000 s⁻¹ is shown. In Figure S18, the accuracy of k_p^{obs} determination using the location of the (first) inflection point/peak maximum is illustrated. In agreement with Figure S15, Case 1 (*i.e.* only head-to-tail propagation) is considered for this *in silico* evaluation.

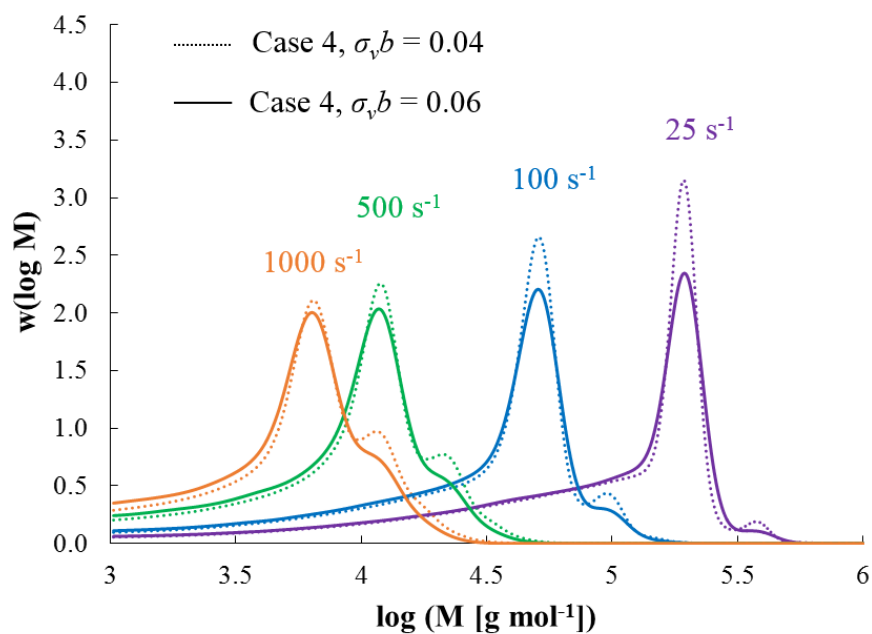


Figure S17. Illustration of the effect of SEC broadening on PLP-SEC traces. Model parameters: Table S6; T = 323 K, [VAc]₀ = 10.4 mol L⁻¹, [DMPA]₀ = 5 mmol L⁻¹, E_{pulse} = 1.5 mJ, λ = 351 nm, V = 0.2 mL, L = 0.5 cm, N_{pulse} = 500.

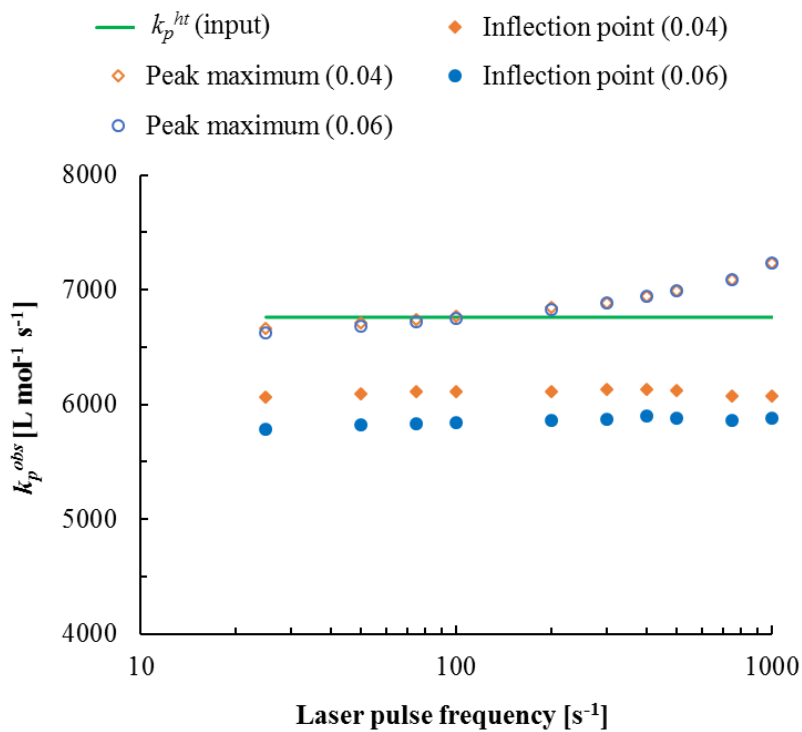


Figure S18. In silico evaluation of Equation (2) using the location of the inflection point (filled symbols) and the location of the peak maximum (unfilled symbols) for case 1 (only head-to-tail addition) and a SEC broadening parameter $\sigma_v b = 0.04$ (orange symbols; same as in Figure S15) and $\sigma_v b = 0.06$ (blue symbols); T = 323 K, [VAc]₀ = 10.4 mol L⁻¹, [DMPA]₀ = 5 mmol L⁻¹, E_{pulse} = 1.5 mJ, λ = 351 nm, V = 0.2 mL, L = 0.5 cm, N_{pulse} = 500.

From this Figure S18 it can be derived that under typical conditions for VAc PLP the underestimation of the k_p^{ht} is even more pronounced if the SEC broadening parameter is increased from 0.04 (orange symbols) to 0.06 (blue symbols) and L_I is based on the location of the inflection. The effect of the increased degree of SEC broadening is limited if the location of the peak maximum is used.

S11 Laser pulse frequency dependence of observed propagation rate coefficients based on peak maxima

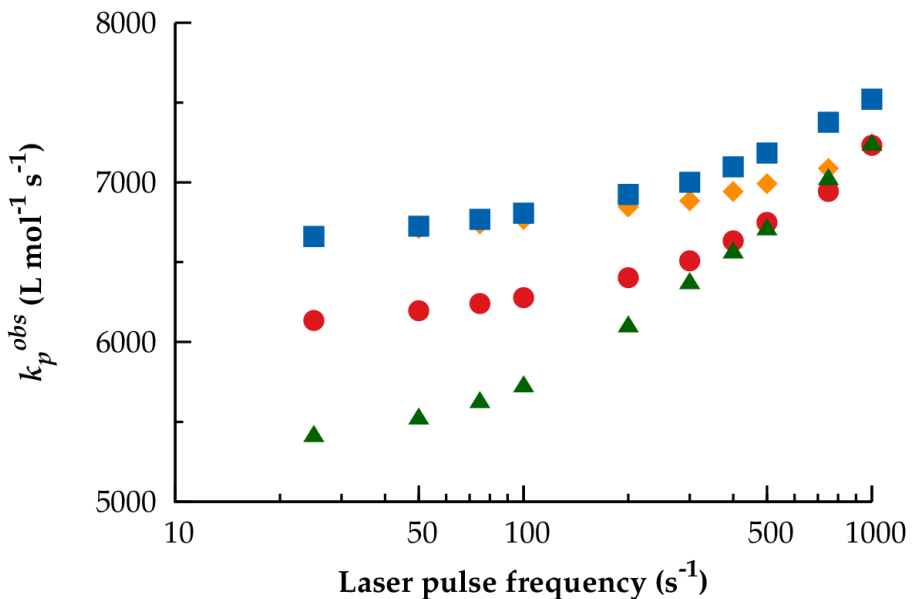


Figure S19. Frequency dependence of the observed propagation rate coefficients k_p^{obs} , see Equation (2) with L_1 based on the first peak maximum of the PLP-SEC traces simulated using the ab initio rate coefficients in Table 1 (main text) and the reaction scheme in Section S6 of the Supporting Information. Case 1 (♦): chain length independent head-to-tail propagation, Case 2 (■): chain length dependent head-to-tail propagation, Case 3 (●): chain length dependent head-to-tail, head-to-head, tail-to-tail, and tail-to-head propagation, and Case 4 (▲): Case 3 with additionally backbiting by head and tail radicals, and mid-chain propagation. A corresponding figure where k_p^{obs} is based on inflection points instead of peak maxima is shown in the main text. T = 323 K, [VAc]₀ = 10.4 mol L⁻¹, [DMPA]₀ = 5 10⁻³ mol L⁻¹, E_{pulse} = 1.5 mJ, λ = 351 nm, N_{pulse} = 500, V = 0.2 mL, L = 0.5 cm.

S12 Laser pulse frequency dependence of observed propagation rate coefficients in the value of the head-to-head propagation rate coefficient is reduced by a factor 2

In Figure S20, the pulse frequency dependence of k_p^{obs} at 323 K and based on inflection points is shown for Case 3 (unfilled red circles) and Case 4 (unfilled green triangles), however with a head-to-head propagation rate coefficient reduced by a factor 2 compared to the ab initio based head-to-head propagation rate coefficient reported in Table 1 (cf. Figure 5). For Case 1 and Case 2, k_p^{hh} remains 0 L mol⁻¹ s⁻¹. As a result of the reduced head-to-head propagation rate coefficient the difference between k_p^{obs} for Case 2 (filled blue squares) and Case 3 (unfilled red circles) and Case 2 (filled blue squares) and Case 4 (unfilled green triangles) is smaller. In addition, a less pronounced pulse frequency dependence is observed for Case 4 (a decrease of ca. 10% instead of 15% results from 500 to 100 s⁻¹).

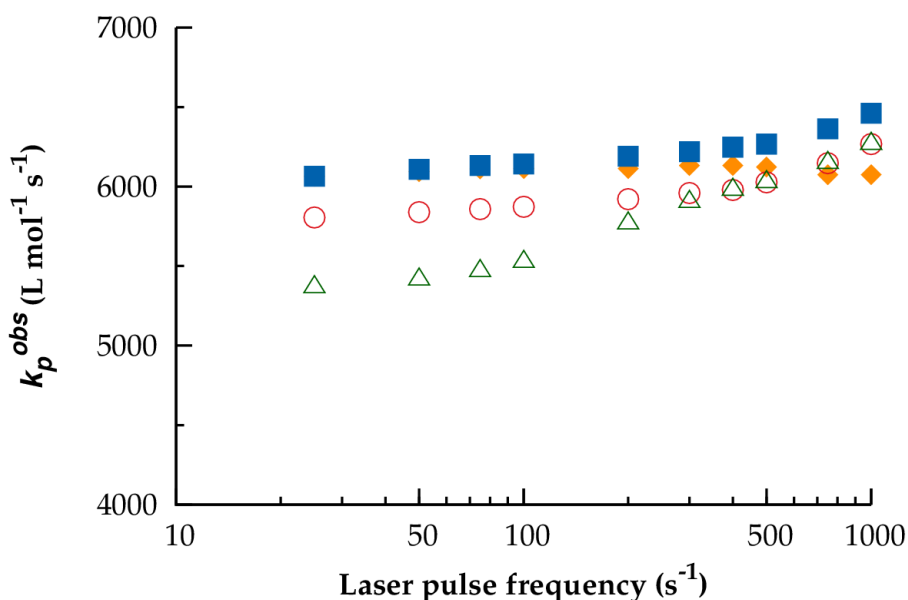


Figure S20. Frequency dependence of observed propagation rate coefficients based on inflection points. Case 1 (♦) and Case 2 (■) same as in Figure 5; Case 3 (○) and Case 4 (▲) same as in Figure 5, however with k_p^{hh} reduced by a factor 2. Model parameters: Table 1 and Table S6; T = 323 K, [VAc]₀ = 10.4 mol L⁻¹, [DMPA]₀ = 5 10⁻³ mol L⁻¹, E_{pulse} = 1.5 mJ, λ = 351 nm, N_{pulse} = 500, V = 0.2 mL, L = 0.5 cm.

S13 Evaluation of the average propagation rate coefficient $\langle k_p \rangle$ as defined on the polymerization rate

S13.1 Analytical derivation

Assuming a constant volume, the total propagation rate is equal to:

$$R_p = -\frac{d[M]}{dt} = k_p^{ht}[R_h][M] + k_p^{hh}[R_h][M] + k_p^{tt}[R_t][M] + k_p^{ht}[R_t][M] + k_p^m[R_m][M] \quad (\text{S43})$$

Which rearranges to:

$$R_p = ((k_p^{ht} + k_p^{hh})[R_h] + (k_p^{hh} + k_p^{tt})[R_t] + k_p^{ht}[R_t] + k_p^m[R_m])[M] \quad (\text{S44})$$

Applying the pseudo steady state approximation (PSSA) for the calculation of the concentrations of the different radical types, according to the scheme in Figure 2 in the main manuscript leads to the following expressions (backbiting by head radicals is ignored, cf. text and Table 1 in the main manuscript):

$$k_p^{hh}[R_h][M] = k_p^{tt}[R_t][M] + k_p^m[R_m][M] \quad (\text{S45})$$

$$k_p^m[R_m][M] = k_{bb}^t[R_t] \quad (\text{S46})$$

Substituting Equation (S46) in Equation (S45):

$$k_p^{hh}[R_h][M] = k_p^{tt}[R_t][M] + k_{bb}^t[R_t] \quad (\text{S47})$$

which can be rearranged to:

$$[R_t] = \frac{k_p^{hh}[M]}{k_p^{tt}[M] + k_{bb}^t} [R_h] \quad (\text{S48})$$

Inserting this in Equation (S46) leads to:

$$k_p^m[R_m] = \left(\frac{k_{bb}^t}{[M]} \frac{k_p^{hh}[M]}{k_p^{tt}[M] + k_{bb}^t} \right) [R_h] \quad (\text{S49})$$

Inserting Equation (S48) and (S49) into Equation (S44) leads to:

$$R_p = \left((k_p^{ht} + k_p^{hh}) + (k_p^{tt} + k_p^{th}) \frac{k_p^{hh}[M]}{k_p^{tt}[M] + k_{bb}^t} + \frac{k_{bb}^t}{[M]} \frac{k_p^{hh}[M]}{k_p^{tt}[M] + k_{bb}^t} \right) [R_h][M] \quad (\text{S50})$$

which rearranges to:

$$R_p = \left((k_p^{ht} + k_p^{hh}) + \left(k_p^{tt} + k_p^{th} + \frac{k_{bb}^t}{[M]} \right) \frac{k_p^{hh}[M]}{k_p^{tt} + \frac{k_{bb}^t}{[M]}} \right) [R_h][M] \quad (S51)$$

$$R_p = \left(\frac{k_p^{ht} \left(k_p^{tt} + \frac{k_{bb}^t}{[M]} \right) + 2k_p^{hh} \left(k_p^{tt} + \frac{k_{bb}^t}{[M]} \right) + k_p^{hh} k_p^{th}}{k_p^{tt} + \frac{k_{bb}^t}{[M]}} \right) [R_h][M] \quad (S52)$$

By definition, the total propagation rate can also be expressed as follows:

$$R_p = \langle k_p \rangle [R][M] \quad (S53)$$

$$R_p = \langle k_p \rangle ([R_h] + [R_t] + [R_m])[M] \quad (S54)$$

and hence:

$$\left(\frac{k_p^{ht} \left(k_p^{tt} + \frac{k_{bb}^t}{[M]} \right) + 2k_p^{hh} \left(k_p^{tt} + \frac{k_{bb}^t}{[M]} \right) + k_p^{hh} k_p^{th}}{k_p^{tt} + \frac{k_{bb}^t}{[M]}} \right) [R_h][M] = \quad (S55)$$

$$\langle k_p \rangle ([R_h] + [R_t] + [R_m])[M]$$

This leads to the following expression for the average rate coefficient:

$$\langle k_p \rangle = \left(\frac{k_p^{ht} \left(k_p^{tt} + \frac{k_{bb}^t}{[M]} \right) + 2k_p^{hh} \left(k_p^{tt} + \frac{k_{bb}^t}{[M]} \right) + k_p^{hh} k_p^{th}}{k_p^{tt} + \frac{k_{bb}^t}{[M]}} \right) \left(\frac{[R_h]}{[R_h] + [R_t] + [R_m]} \right) \quad (S56)$$

Substituting Equations (S45) and (S46) into the expression above leads to:

$$\begin{aligned} \langle k_p \rangle &= \left(\frac{k_p^{ht} \left(k_p^{tt} + \frac{k_{bb}^t}{[M]} \right) + 2k_p^{hh} \left(k_p^{tt} + \frac{k_{bb}^t}{[M]} \right) + k_p^{hh} k_p^{th}}{k_p^{tt} + \frac{k_{bb}^t}{[M]}} \right) \cdot \\ &\quad \left(\frac{1}{1 + \frac{k_p^{hh}}{k_p^{tt} + \frac{k_{bb}^t}{[M]}} + \frac{k_{bb}^t}{k_p^m[M]} \frac{k_p^{hh}}{k_p^{tt} + \frac{k_{bb}^t}{[M]}}} \right) \end{aligned} \quad (S57)$$

$$\langle k_p \rangle = \frac{k_p^{ht} \left(k_p^{tt} + \frac{k_{bb}^t}{[M]} \right) + 2k_p^{hh} \left(k_p^{tt} + \frac{k_{bb}^t}{[M]} \right) + k_p^{hh} k_p^{th}}{k_p^{tt} + \frac{k_{bb}^t}{[M]} + k_p^{hh} + \frac{k_{bb}^t}{k_p^m} k_p^{hh}} \quad (\text{S58})$$

$$\langle k_p \rangle = \frac{k_p^{ht} \left(k_p^{tt} + \frac{k_{bb}^t}{[M]} \right) + 2 \left(k_p^{hh} k_p^{tt} + k_p^{hh} \frac{k_{bb}^t}{[M]} \right) + k_p^{hh} k_p^{th}}{(k_p^{hh} + k_p^{tt}) + \left(1 + \frac{k_p^{hh}}{k_p^m} \right) \frac{k_{bb}^t}{[M]}} \quad (\text{S59})$$

which can also be rearranged to (Equation (5) in the main text):

$$\langle k_p \rangle = \frac{k_p^{ht} k_p^{tt} + 2k_p^{hh} k_p^{tt} + k_p^{hh} k_p^{th} + \frac{k_{bb}^t}{[M]} (k_p^{ht} + 2k_p^{hh})}{(k_p^{hh} + k_p^{tt}) + \frac{k_{bb}^t}{[M]} \left(1 + \frac{k_p^{hh}}{k_p^m} \right)} \quad (\text{S60})$$

Note that, in the theoretical case that k_{bb}^t is equal to 0 s^{-1} , this is identical to the formula earlier derived by Monyatsi et al.¹⁷ Moreover, under PLP conditions the monomer concentration can be replaced by the initial one.

S13.2 Comparison of $\langle k_p \rangle$ and k_p^{obs} both using the location of the inflection point and peak maximum

In Figure 6 (main text), a comparison between $\langle k_p \rangle$ (Equation (S60); lines) and k_p^{obs} (Equation (2) using the location of the inflection points (filled symbols) and peak maxima (unfilled symbols) is shown for case 4. In Figure S21 a comparison between $\langle k_p \rangle$ and k_p^{obs} for case 3 (i.e. case 4 with $k_{bb}^t = k_{bb}^h = 0 \text{ s}^{-1}$) is shown.

Note that for case 3 $\langle k_p \rangle$ Equation (S60) is identical to the formula earlier derived by Monyatsi et al.¹⁷ As for case 4, at low pulse frequencies, k_p^{obs} can be used to assess $\langle k_p \rangle$ in case the location of the peak maxima are used.

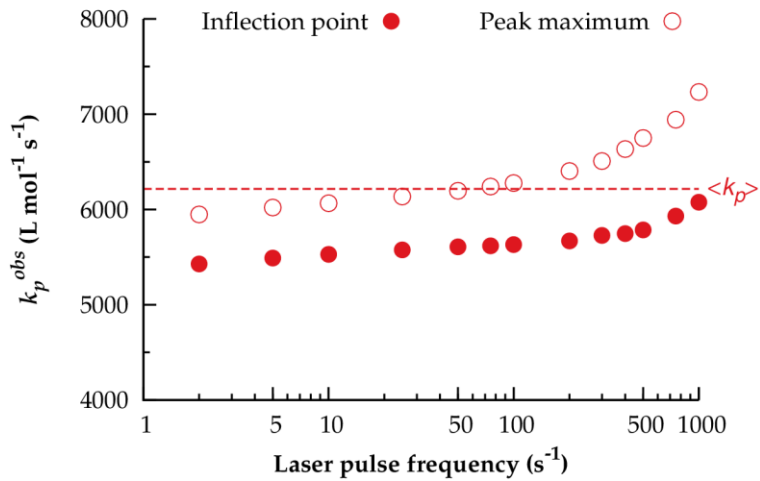


Figure S21. Comparison of $\langle k_p \rangle$ (Equation (S60); full line) and k_p^{obs} (Equation (2) based on the location of the peak maxima (unfilled symbols) and the location of the inflection points (filled symbols)) for case 3; the corresponding figure for case 4 is shown in the main text; $T = 323 \text{ K}$, $[\text{Vac}]_0 = 10.4 \text{ mol L}^{-1}$, $[\text{DMPA}]_0 = 5 \cdot 10^{-3} \text{ mol L}^{-1}$, $E_{\text{pulse}} = 1.5 \text{ mJ}$, $\lambda = 351 \text{ nm}$, $N_{\text{pulse}} = 500$, $V = 0.2 \text{ mL}$, $L = 0.5 \text{ cm}$.

S14 Comparison of simulated and experimental data at 323 K

A comparison between inflection point based k_p^{obs} data simulated with the full kinetic model (Case 4; Table 1 in the main text) and experimental data reported in the recent IUPAC contribution of Barner-Kowollik *et al.*³¹ is made in Figure S22. Note that in the current study, DMPA is selected as the photoinitiator, see Table S6. Hence, only experimental data corresponding to DMPA-based PLP experiments are considered in Figure S22 (black symbols). These data originate from the recent work of Monyatsi *et al.*¹⁷ Note that the experimental error indicated in Figure S22 (10%) is a lower bound of the experimental uncertainty.^{32, 33} The IUPAC recommended value of k_p at 323 K is also indicated in Figure S22 (full black line). Although a slight underestimation of the experimental data is observed, a good description of the evolution of k_p^{obs} with pulse frequency is observed.

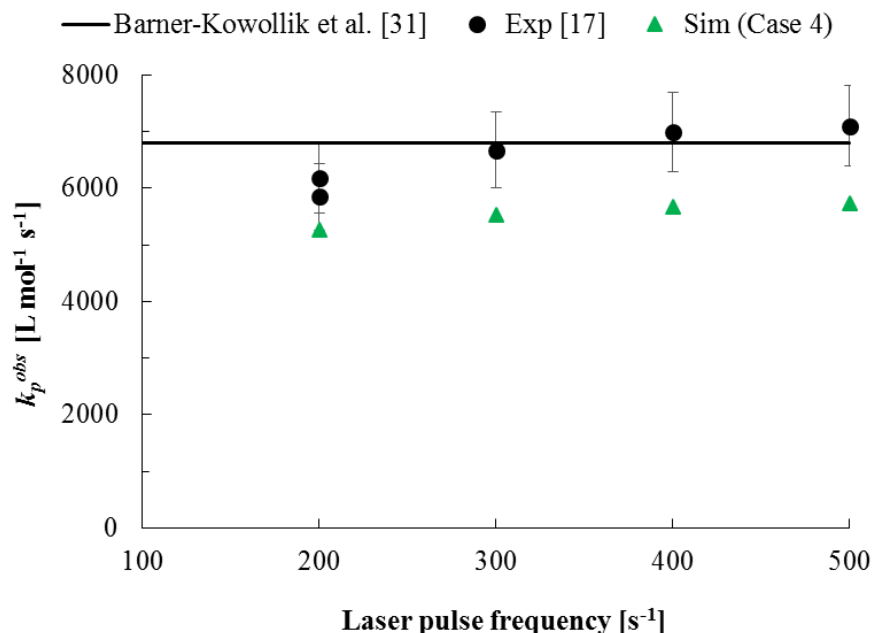


Figure S22. Comparison of inflection point based k_p^{obs} data obtained via experiment¹⁷ and simulation (Case 4; Table 1 in the main text). T = 323 K, $[DMPA]_0 = 5 \cdot 10^{-3}$ mol L⁻¹, $E_{\text{pulse}} = 3.7$ mJ. The sample volume and optical path length are unknown and set equal to V = 0.2 mL and L = 0.52 cm. Number of pulses simulated as reported in the Supporting Information of the work of Monyatsi *et al.*¹⁷

S15 Observed propagation rates coefficient based on inflection points at lower temperatures

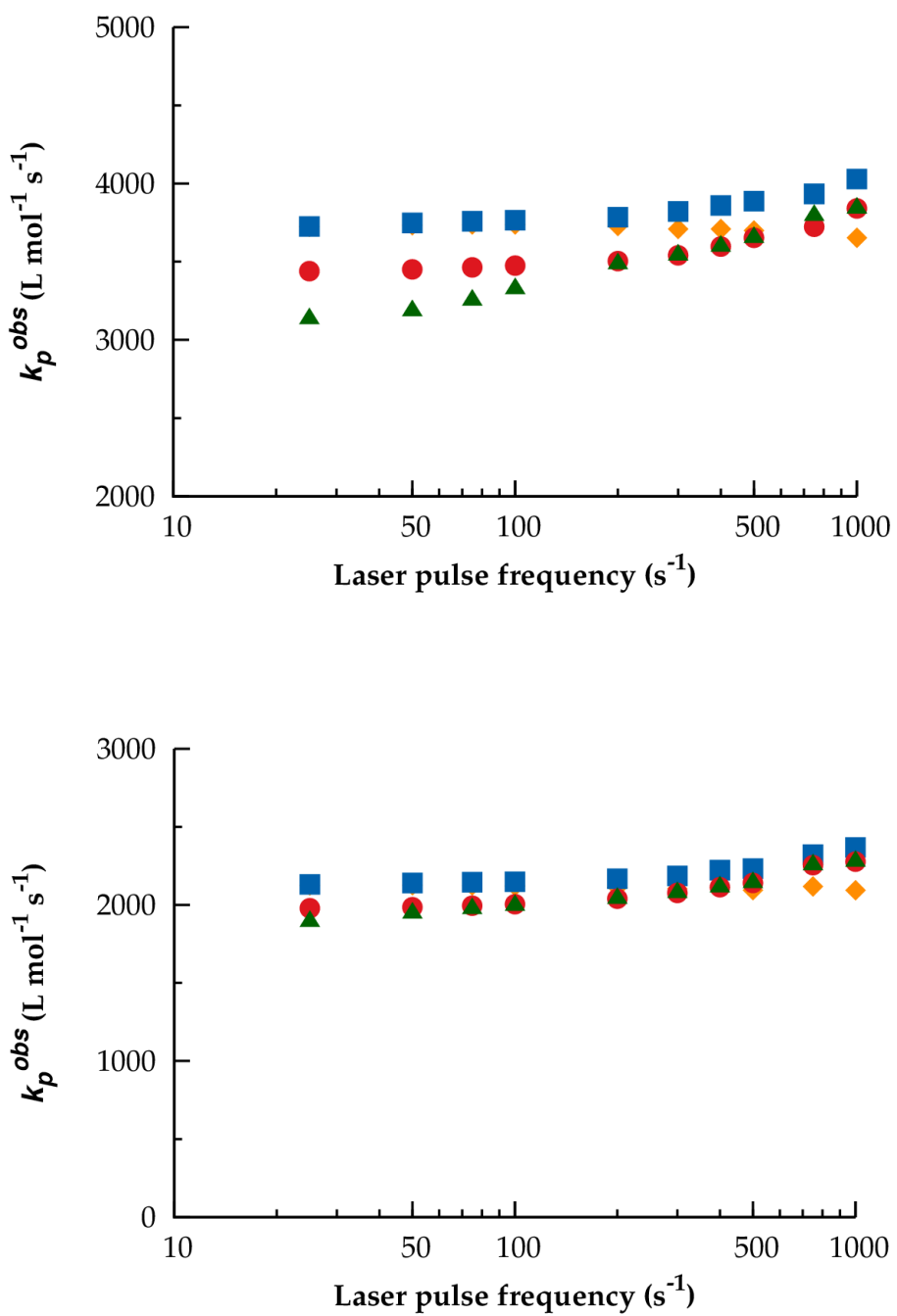


Figure S23. Observed propagation rate coefficients determined from the location of the inflection points of PLP-SEC traces simulated using the ab initio rate coefficients in Table 1 (main text) at 303 K (top; $[\text{VAc}]_0 = 10.7 \text{ mol L}^{-1}$) and 283 K (bottom; $[\text{VAc}]_0 = 11.0 \text{ mol L}^{-1}$); other conditions: $[\text{DMPA}]_0 = 5 \text{ mmol L}^{-1}$, $E_{\text{pulse}} = 1.5 \text{ mJ}$, $\lambda = 351 \text{ nm}$, $V = 0.2 \text{ mL}$, $L = 0.5 \text{ cm}$, $N_{\text{pulse}} = 500$.

S16 Observed propagation rates coefficient based on peak maxima at lower temperatures

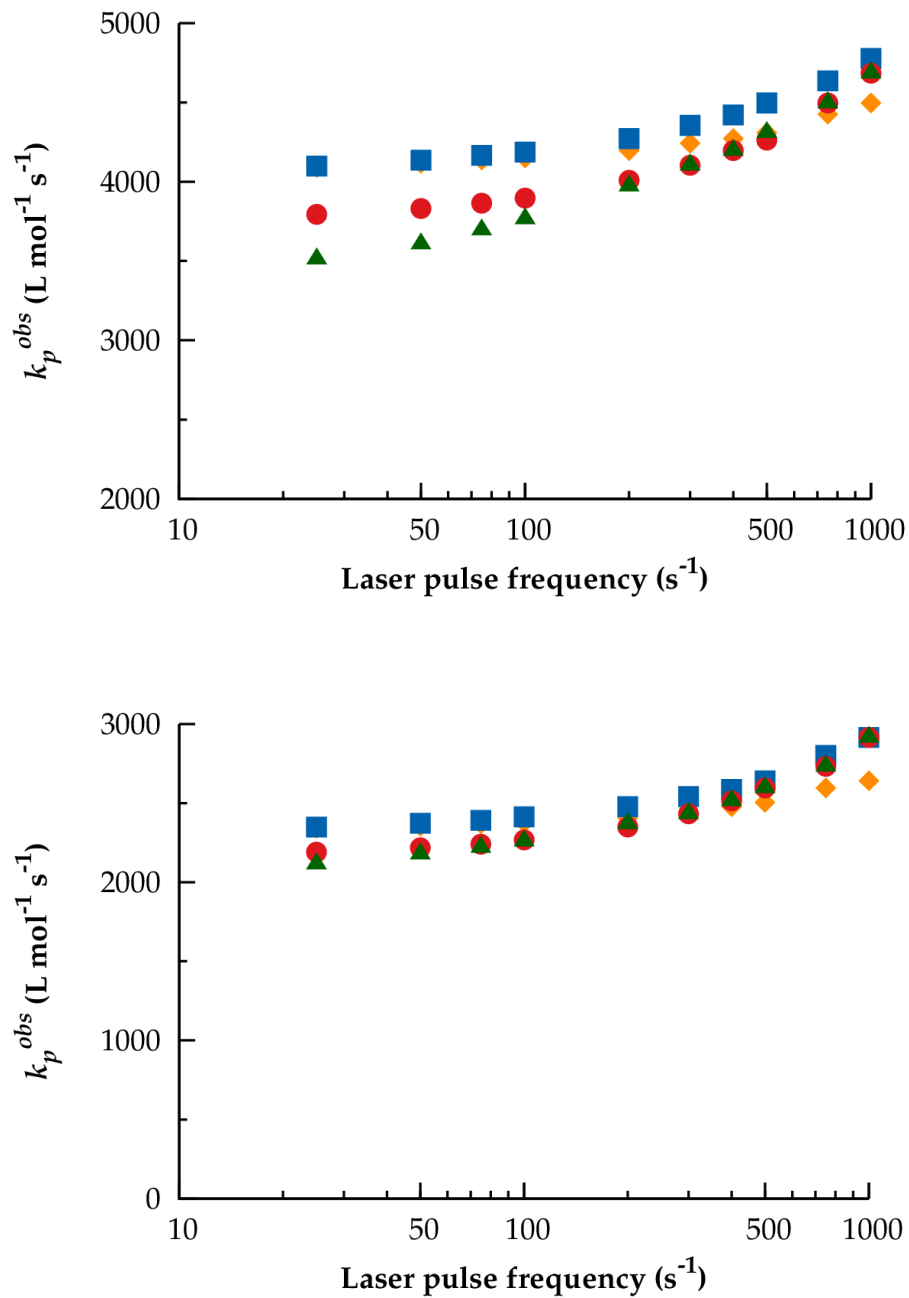


Figure S24. Observed propagation rate coefficients determined from the location of the peak maxima of PLP-SEC traces simulated using the ab initio rate coefficients in Table 1 (main text) at 303 K (top; $[\text{VAc}]_0 = 10.7 \text{ mol L}^{-1}$) and 283 K (bottom; $[\text{VAc}]_0 = 11.0 \text{ mol L}^{-1}$); other conditions: $[\text{DMPA}]_0 = 5 \text{ mmol L}^{-1}$, $E_{\text{pulse}} = 1.5 \text{ mJ}$, $\lambda = 351 \text{ nm}$, $V = 0.2 \text{ mL}$, $L = 0.5 \text{ cm}$, $N_{\text{pulse}} = 500$.

S17 Pulse frequency dependence of the activation energy of the observed propagation rate coefficient

Monyatsi *et al.*¹⁷ have reported a pulse frequency dependence for the (apparent) activation energy of k_p^{obs} , with this activation energy determined via regression of the Arrhenius equation to k_p^{obs} data at 500 s⁻¹ being higher than the activation energy determined via regression to 100 s⁻¹ data. As demonstrated in Figure S25, such an increase is also observed via kinetic Monte Carlo simulations using the ab initio based rate coefficients reported in Table 1. The activation energy determined from 500 s⁻¹ data in the temperature range 283 – 323 K is equal to 19.0 kJ mol⁻¹, while the activation energy determined from 100 s⁻¹ data is equal to 17.3 kJ mol⁻¹.

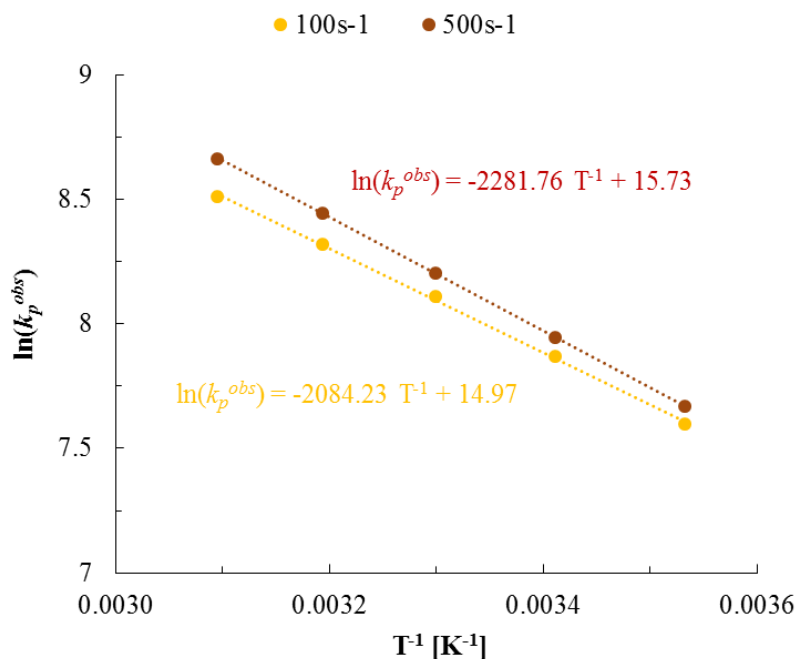


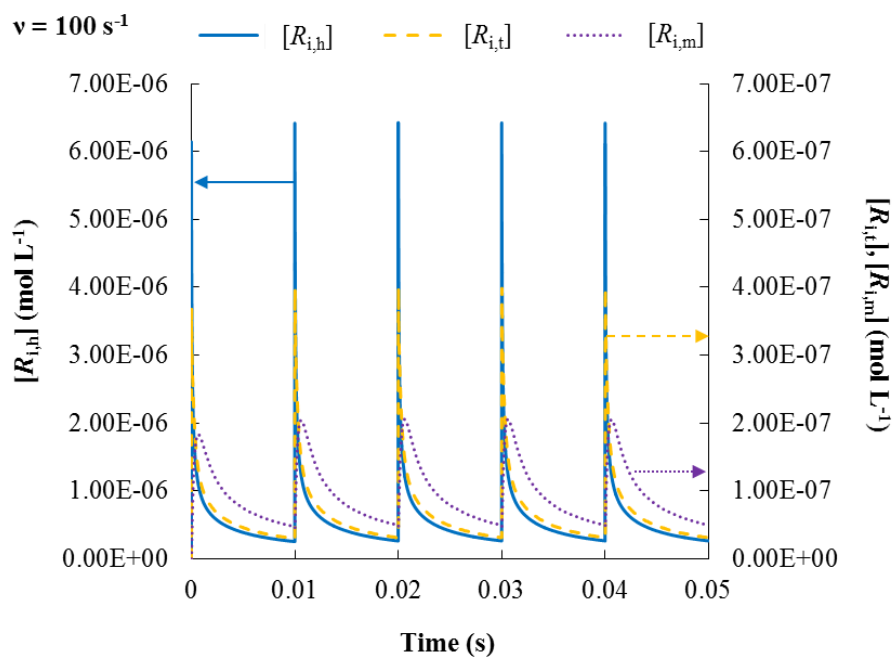
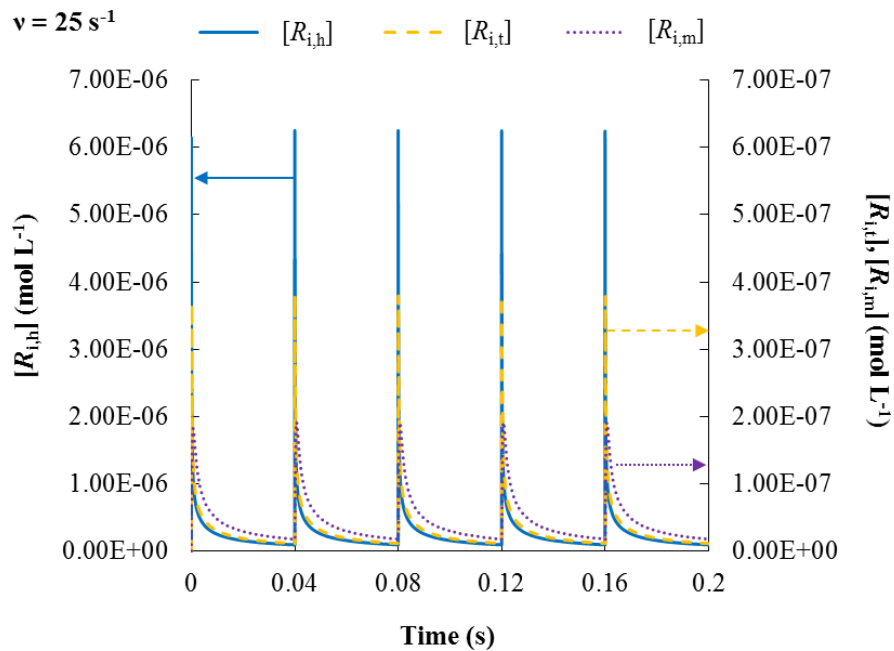
Figure S25. Arrhenius fit to simulated k_p^{obs} data at 100 s⁻¹ (dashed yellow line) and 500 s⁻¹ data (dashed red line); k_p^{obs} is calculated using the location of the first inflection point; model parameters: Table 1 and Table S6; T = 283 - 323 K, $[\text{VAc}]_0 = 10.4$ (323 K) - 11.0 mol L⁻¹ (283 K), $[\text{DMPA}]_0 = 5 \cdot 10^{-3}$ mol L⁻¹, $E_{\text{pulse}} = 1.5$ mJ, $\lambda = 351$ nm, $N_{\text{pulse}} = 500$, V = 0.2 mL, L = 0.5 cm.

S18 Profiles of macroradical concentrations and molar fractions as a function of time simulated using the ab initio rate coefficients (Case 4) under the conditions of the current work

In Figure S26 the radical concentration profiles of head, tail, and mid-chain macroradicals simulated using the ab initio rate coefficients corresponding to Case 4 (Table 1; main text) under the conditions corresponding to Figure 5 (main text) are shown for the first five dark periods. The concentrations of head, tail and mid-chain macroradicals averaged over the first five dark periods are listed in Table S8, as well as the corresponding molar fractions, also see Figure S27.

Table S8. Average radical concentrations during the first five dark periods and the corresponding fractions determined from the simulated radical concentration traces in Figure S26, *i.e.* simulated using the ab initio rate coefficients corresponding to Case 4 (Table 1; main text) under the conditions corresponding to Figure 5 (main text), namely: $T = 323\text{ K}$, $[VAc]_0 = 10.4\text{ mol L}^{-1}$, $[DMPA]_0 = 5\text{ mmol L}^{-1}$, $E_{pulse} = 1.5\text{ mJ}$, $\lambda = 351\text{ nm}$, $V = 0.2\text{ mL}$, $L = 0.5\text{ cm}$.

v (s^{-1})	$\overline{[R_{i,h}]}$ (mol L^{-1})	$\overline{[R_{i,t}]}$ (mol L^{-1})	$\overline{[R_{i,m}]}$ (mol L^{-1})	x_h (-)	x_t (-)	x_m (-)
25	$2.5 \cdot 10^{-7}$	$2.9 \cdot 10^{-8}$	$4.3 \cdot 10^{-8}$	0.77	0.09	0.14
100	$5.6 \cdot 10^{-7}$	$6.5 \cdot 10^{-8}$	$9.4 \cdot 10^{-8}$	0.78	0.09	0.13
500	$1.3 \cdot 10^{-6}$	$1.5 \cdot 10^{-7}$	$1.9 \cdot 10^{-7}$	0.80	0.09	0.11
1000	$1.9 \cdot 10^{-6}$	$2.1 \cdot 10^{-7}$	$2.3 \cdot 10^{-7}$	0.81	0.09	0.10



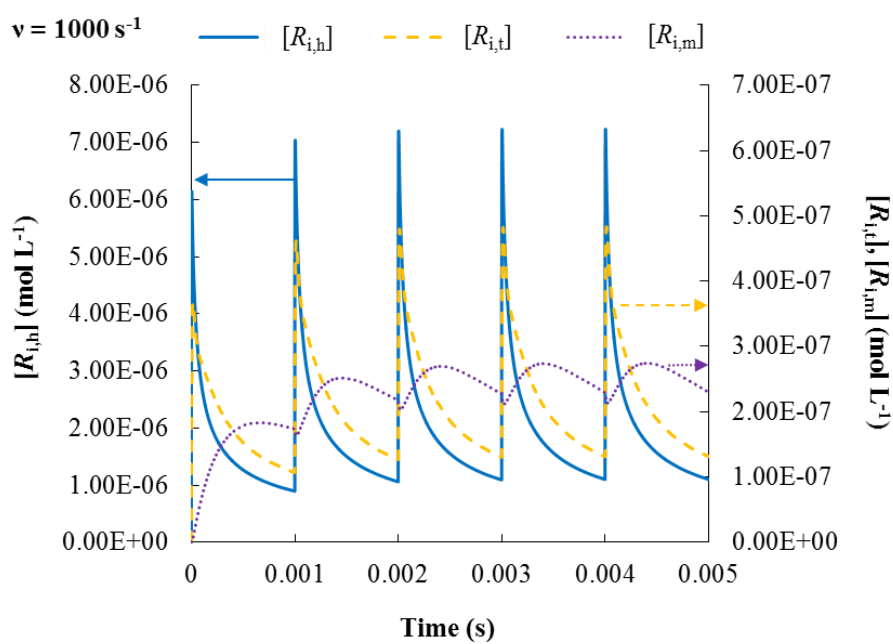
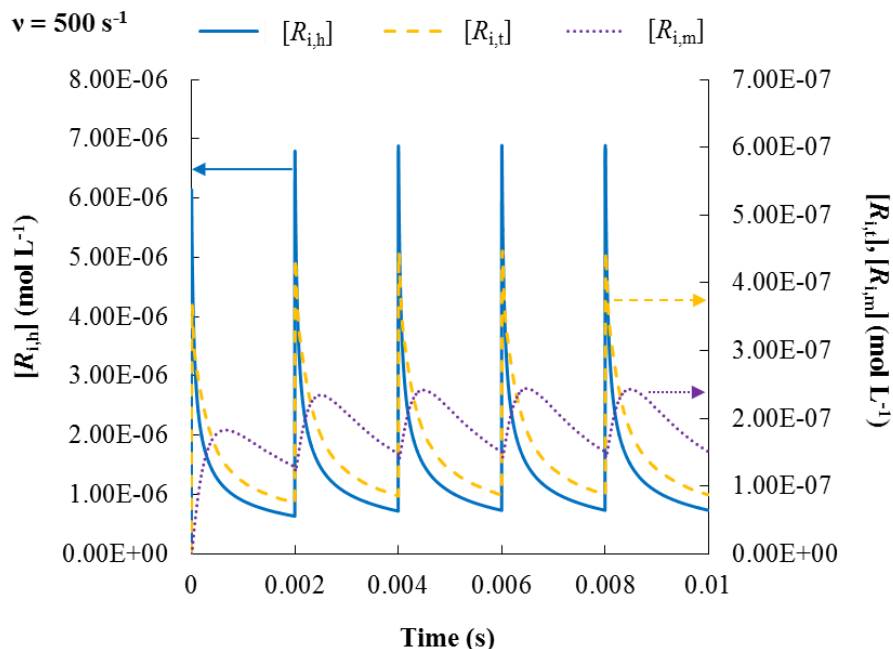
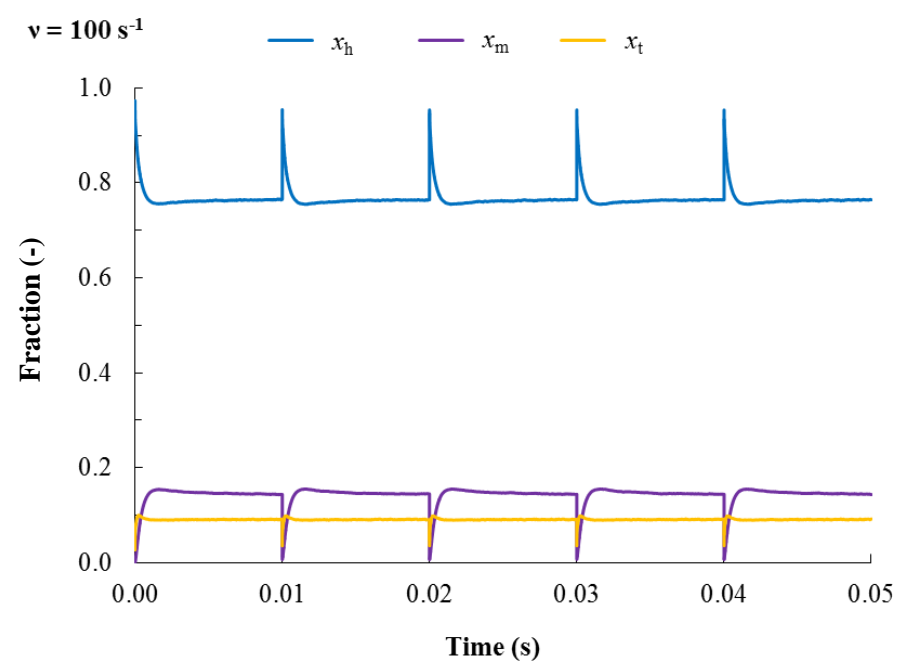
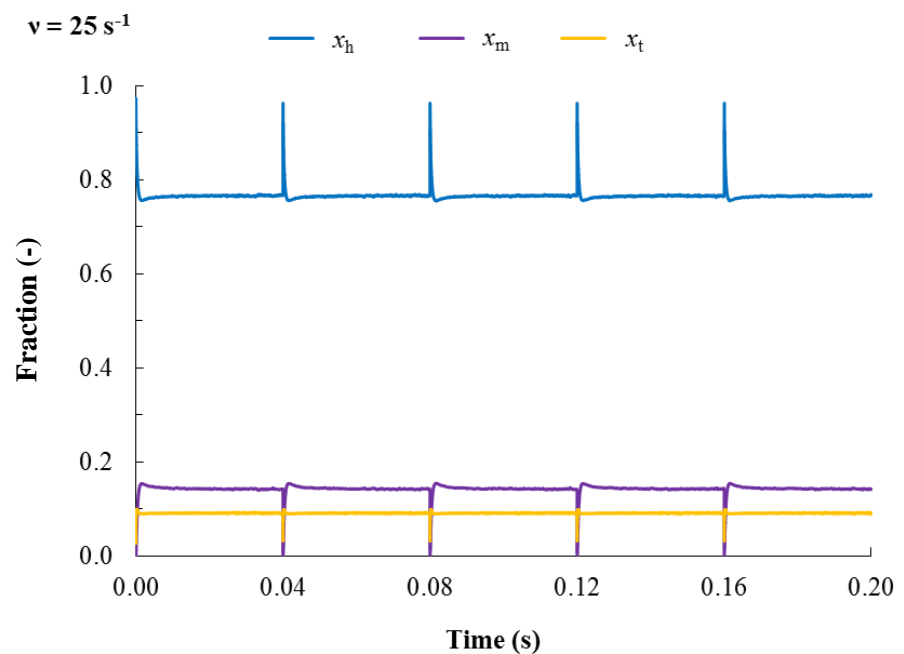


Figure S26. Radical concentration traces simulated using the ab initio based rate coefficients corresponding to Case 4 (Table 1; main text) focusing on the first five dark periods and a pulse frequency of 25, 100, 500 and 1000 s^{-1} . Model parameters: Table S6; $T = 323 \text{ K}$, $[\text{VAc}]_0 = 10.4 \text{ mol L}^{-1}$, $[\text{DMPA}]_0 = 5 \text{ mmol L}^{-1}$, $E_{\text{pulse}} = 1.5 \text{ mJ}$, $\lambda = 351 \text{ nm}$, $V = 0.2 \text{ mL}$, $L = 0.5 \text{ cm}$.



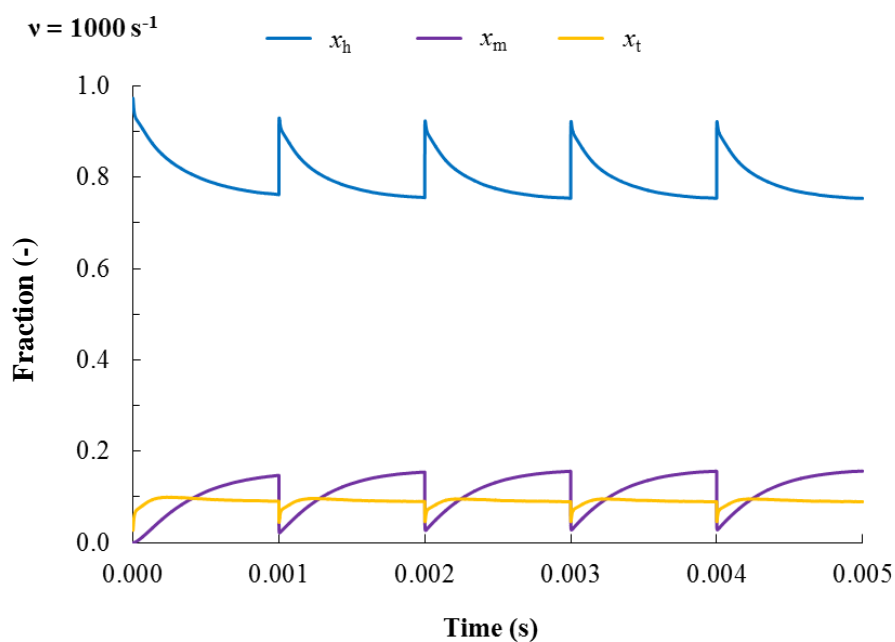
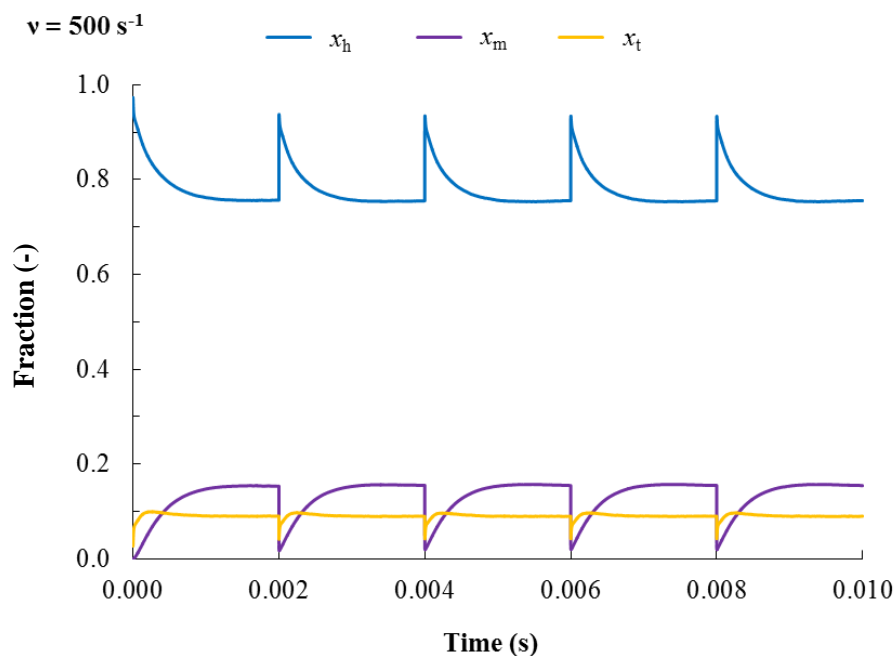


Figure S27. Profiles of macroradical fraction as a function of time simulated for Case 4 focusing on the first five dark periods and a pulse frequency of 25, 100, 500 and 1000 s^{-1} . Model parameters: Table S6; $T = 323 \text{ K}$, $[\text{VAc}]_0 = 10.4 \text{ mol L}^{-1}$, $[\text{DMPA}]_0 = 5 \text{ mmol L}^{-1}$, $E_{\text{pulse}} = 1.5 \text{ mJ}$, $\lambda = 351 \text{ nm}$, $V = 0.2 \text{ mL}$, $L = 0.5 \text{ cm}$.

S19 Profiles of macroradical concentrations and fractions as a function of time simulated using the ab initio rate coefficients (Case 4) under typical PLP-EPR conditions

In Figure S28, the radical concentration profiles of head, tail, and mid-chain macroradicals simulated using the ab initio rate coefficients corresponding to Case 4 (Table 1; main text) under typical conditions of the EPR study of Kattner and Buback,²³ namely $T = 333\text{ K}$, $v = 25\text{ s}^{-1}$ and $[\text{dicumyl peroxide}] = 9 \cdot 10^{-2}\text{ mol L}^{-1}$, are shown for the first five dark periods.

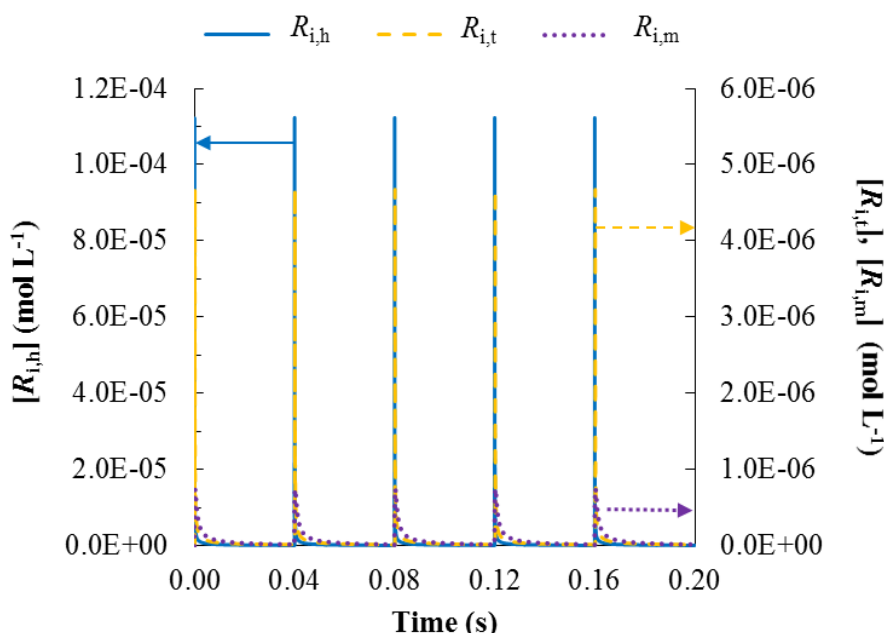


Figure S28. Radical concentration traces simulated using the ab initio rate coefficients corresponding to Case 4 (Table 1; main text) under typical conditions considered in the work of Kattner and Buback²³, namely $T = 333\text{ K}$, $v = 25\text{ s}^{-1}$ and $[\text{DCP}] = 9 \cdot 10^{-2}\text{ mol L}^{-1}$. In contrast to all other simulations in this work, in which DMPA is the photoinitiator, a constant $\Delta[R_0] = 3.2 \cdot 10^{-4}\text{ mol L}^{-1}$ is considered here, with both initiator radical fragments leading to chain initiation (Entry 1 in Table S6 is replaced by $\text{DCP} \xrightarrow{h\nu} 2R_0^I$).

A constant $\Delta[R_0]$ is considered in the simulation here for simplicity, with both initiator radical fragments having the same reactivity toward chain initiation, in contrast to all other simulations in the current work, in which DMPA is the photoinitiator and in which $\Delta[R_0]$ is explicitly calculated for each pulse using Equation (S42) in agreement with earlier work.^{18, 20} $\Delta[R_0]$ is taken equal to $3.2 \cdot 10^{-4}\text{ mol L}^{-1}$, the initial concentration of head radicals observed via

EPR. Note that this value slightly underestimates $\Delta[R_0]$, as this value does not take into account the fraction of initiator radicals which terminate before undergoing chain initiation. The simulated concentration of head, tail, and mid-chain macroradicals averaged over the first five dark periods is equal to $4.0 \cdot 10^{-7} \text{ mol L}^{-1}$, $4.5 \cdot 10^{-8} \text{ mol L}^{-1}$ and $7.7 \cdot 10^{-8} \text{ mol L}^{-1}$, which corresponds to a fraction of 0.765, 0.087 and 0.148, also see Figure S29 for the profiles of macroradical fractions. The simulated average concentration of head radicals is close to the experimentally determined concentration of $5 \cdot 10^{-7} \text{ mol L}^{-1}$. The slight underestimation can be attributed to the underestimation of $\Delta[R_0]$, as explained previously. The concentration of tail radicals and MCRs are in line with the ones obtained via simulation at the same pulse frequency (25 s^{-1}) and under the conditions of the current work ($T = 323 \text{ K}$, $[DMPA]_0 = 5 \cdot 10^{-3} \text{ mol L}^{-1}$, $E_{\text{pulse}} = 1.5 \text{ mJ}$, $\lambda = 351 \text{ nm}$, $V = 0.2 \text{ mL}$, $L = 0.5 \text{ cm}$; see Figure S26).

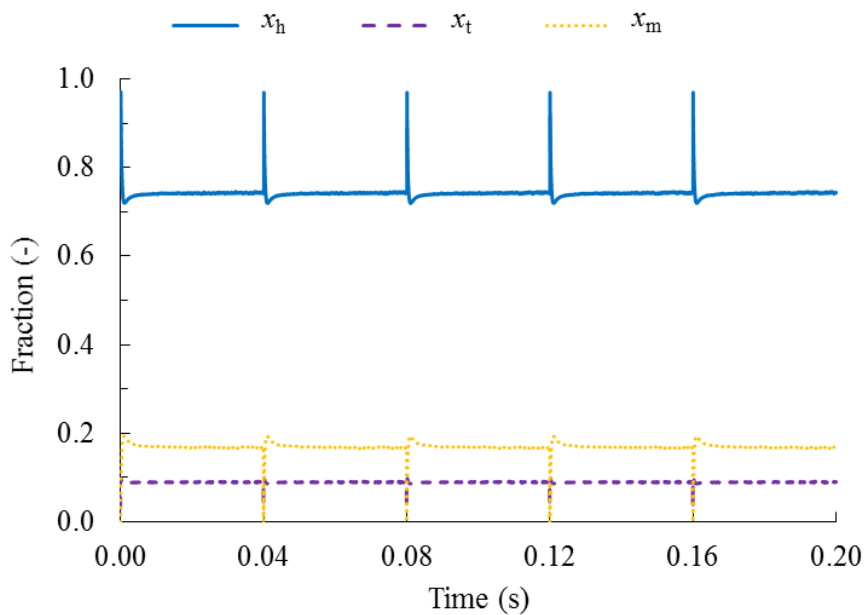


Figure S29. Profiles of macroradical fraction as a function of time simulated using the ab initio rate coefficients corresponding to Case 4 (Table 1; main text) under typical conditions considered in the work of Kattner and Buback²³, namely $T = 333 \text{ K}$, $v = 25 \text{ s}^{-1}$ and $[DCP] = 9 \cdot 10^{-2} \text{ mol L}^{-1}$. In contrast to all other simulations in this work, in which DMPA is the photoinitiator, a constant $\Delta[R_0] = 3.2 \cdot 10^{-4} \text{ mol L}^{-1}$ is considered here, with both initiator radical fragments leading to chain initiation (Entry 1 in Table S6 is replaced by $DCP \xrightarrow{h\nu} 2R_0^I$).

S20 References

1. D. Moscatelli, M. Dossi, C. Cavallotti and G. Storti, *J. Phys. Chem. A*, 2011, **115**, 52-62.
2. K. Van Cauter, B. J. Van Den Bossche, V. Van Speybroeck and M. Waroquier, *Macromolecules*, 2007, **40**, 1321-1331.
3. C. Y. Lin, E. I. Izgorodina and M. L. Coote, *Macromolecules*, 2010, **43**, 553-560.
4. X. Yu, J. Pfaendtner and L. J. Broadbelt, *J. Phys. Chem. A*, 2008, **112**, 6772-6782.
5. E. Mavroudakis, K. Liang, D. Moscatelli and R. A. Hutchinson, *Macromol. Chem. Phys.*, 2012, **213**, 1706-1716.
6. K. Liang, M. Dossi, D. Moscatelli and R. A. Hutchinson, *Macromolecules*, 2009, **42**, 7736-7744.
7. I. Degirmenci, D. Avci, V. Aviyente, K. Van Cauter, V. Van Speybroeck and M. Waroquier, *Macromolecules*, 2007, **40**, 9590-9602.
8. B. Dogan, S. Catak, V. Van Speybroeck, M. Waroquier and V. Aviyente, *Polymer*, 2012, **53**, 3211-3219.
9. B. B. Noble and M. L. Coote, *Int. Rev. Phys. Chem.*, 2013, **32**, 467-513.
10. M. J. Frisch, G. W. Trucks, H. B. Schlegel, G. E. Scuseria, M. A. Robb, J. R. Cheeseman, G. Scalmani, V. Barone, B. Mennucci, G. A. Petersson, H. Nakatsuji, M. Caricato, X. Li, H. P. Hratchian, A. F. Izmaylov, J. Bloino, G. Zheng, J. L. Sonnenberg, M. Hada, M. Ehara, K. Toyota, R. Fukuda, J. Hasegawa, M. Ishida, T. Nakajima, Y. Honda, O. Kitao, H. Nakai, T. Vreven, J. A. Montgomery, J. E. Peralta, F. Ogliaro, M. Bearpark, J. J. Heyd, E. Brothers, K. N. Kudin, V. N. Staroverov, R. Kobayashi, J. Normand, K. Raghavachari, A. Rendell, J. C. Burant, S. S. Iyengar, J. Tomasi, M. Cossi, N. Rega, J. M. Millam, M. Klene, J. E. Knox, J. B. Cross, V. Bakken, C. Adamo, J. Jaramillo, R. Gomperts, R. E. Stratmann, O. Yazyev, A. J. Austin, R. Cammi, C. Pomelli, J. W. Ochterski, R. L. Martin, K. Morokuma, V. G. Zakrzewski, G. A. Voth, P. Salvador, J. J. Dannenberg, S. Dapprich, A. D. Daniels, Farkas, J. B. Foresman, J. V. Ortiz, J. Cioslowski and D. J. Fox, Wallingford CT, 2009.
11. D. A. McQuarrie and J. D. Simon, *Physical chemistry: a molecular approach*, Sterling Publishing Company, 1997.
12. P. Deglmann, I. Müller, F. Becker, A. Schäfer, K.-D. Hungenberg and H. Weiß, *Macromol React Eng*, 2009, **3**, 496-515.
13. F. Jensen, *Introduction to Computational Chemistry*, John Wiley & Sons Inc, New York, 2007.
14. C. Eckart, *Phys Rev*, 1930, **35**, 1303-1309.
15. A. G. Vandeputte, M. K. Sabbe, M.-F. Reyniers, V. Van Speybroeck, M. Waroquier and G. B. Marin, *J Phys Chem A*, 2007, **111**, 11771-11786.
16. M. K. Sabbe, M.-F. Reyniers, M. Waroquier and G. B. Marin, *ChemPhysChem*, 2010, **11**, 195-210.
17. O. Monyatsi, A. N. Nikitin and R. A. Hutchinson, *Macromolecules*, 2014, **47**, 8145-8153.
18. Y. W. Marien, P. H. M. Van Steenberge, C. Barner-Kowollik, M. F. Reyniers, G. B. Marin and D. R. D'hooge, *Macromolecules*, 2017, **50**, 1371-1385.
19. M. Buback, M. Busch and C. Kowollik, *Macromol. Theory Simul.*, 2000, **9**, 442-452.
20. Y. W. Marien, P. H. M. Van Steenberge, K. B. Kockler, C. Barner-Kowollik, M.-F. Reyniers, G. B. Marin and D. R. D'hooge, *Polym. Chem.*, 2017, **8**, 3124-3128.
21. J. P. A. Heuts and G. T. Russell, *Eur. Polym. J.*, 2006, **42**, 3-20.

22. J. J. Haven, J. Vandenberghe, R. Kurita, J. Gruber and T. Junkers, *Polym. Chem.*, 2015, **6**, 5752-5765.
23. H. Kattner and M. Buback, *Macromol. Chem. Phys.*, 2014, **215**, 1180-1191.
24. P. Derboven, D. R. D'hooge, M.-F. Reyniers, G. B. Marin and C. Barner-Kowollik, *Macromolecules*, 2015, **48**, 492-501.
25. Y. W. Marien, P. H. M. Van Steenberge, K. B. Kockler, C. Barner-Kowollik, M.-F. Reyniers, D. R. D'hooge and G. B. Marin, *Polym. Chem.*, 2016, **7**, 6521-6528.
26. A. K. Chaudhuri and S. R. Palit, *J. Polym. Sci. A-1 Polym. Chem.*, 1968, **6**, 2196.
27. G. B. Smith, G. T. Russell and J. P. A. Heuts, *Macromol. Theory Simul.*, 2003, **12**, 299-314.
28. S. Beuermann, D. A. Paquet, J. H. McMinn and R. A. Hutchinson, *Macromolecules*, 1996, **29**, 4206-4215.
29. P. Drawe and M. Buback, *Macromol. Theory Simul.*, 2016, **25**, 74-84.
30. B. Wenn and T. Junkers, *Macromol Rapid Commun.*, 2016, **37**, 781-787.
31. C. Barner-Kowollik, S. Beuermann, M. Buback, R. A. Hutchinson, T. Junkers, H. Kattner, B. Manders, A. N. Nikitin, G. T. Russell and A. M. van Herk, *Macromol. Chem. Phys.*, 2017, **218**.
32. S. Beuermann, M. Buback, T. P. Davis, R. G. Gilbert, R. A. Hutchinson, O. F. Olaj, G. T. Russell, J. Schweer and A. M. vanHerk, *Macromol. Chem. Phys.*, 1997, **198**, 1545-1560.
33. M. Buback, R. G. Gilbert, R. A. Hutchinson, B. Klumperman, F.-D. Kuchta, B. G. Manders, K. F. O'Driscoll, G. T. Russell and J. Schweer, *Macromol. Chem. Phys.*, 1995, **196**, 3267-3280.

Part III: Cartesian coordinates of the calculated structures

S21 Cartesian coordinates of all minimum energy conformations

VA	C -0.946158 0.170838 0.000004 O -1.058146 1.372987 0.000041 C -2.074847 -0.828020 -0.000079 H -3.027527 -0.297886 -0.000724 H -2.006294 -1.472856 0.882292 H -2.005504 -1.473711 -0.881755 O 0.258798 -0.483887 0.000124 C 1.414101 0.280599 0.000029 C 2.603635 -0.310368 -0.000093 H 1.242703 1.350638 -0.000462 H 2.707165 -1.390472 0.000112 H 3.503848 0.293194 0.000053	H -3.565201 -2.493637 -0.197935 H -1.878540 -2.700372 -0.758438 H -2.996598 -1.722718 -1.709579 H 0.915351 0.970601 -1.217756 H 1.168854 2.611288 1.402904 H -2.551909 2.191993 -0.159869 H -1.097569 3.178328 0.081718 H -1.356686 2.351481 -1.469248 H 2.375154 2.561304 -0.018788 H 1.970839 -2.705865 0.586425 H 3.004129 -1.769783 1.666716 H 3.674224 -2.394997 0.130801 H -0.928586 0.930663 1.225906
2VA-h	C -1.317270 2.726350 -0.589370 C -1.039522 1.468737 0.200164 O -0.250252 1.386444 1.117593 O -1.780861 0.436686 -0.272554 C -1.590108 -0.875392 0.323253 C -0.804469 -1.759549 -0.673848 C 0.529239 -1.215506 -1.044052 O 1.402787 -1.085935 0.011348 C 2.423851 -0.169352 -0.090108 O 2.641357 0.467319 -1.092970 C -2.970949 -1.430126 0.644599 C 3.164592 -0.071146 1.215588 H -0.961503 3.592430 -0.029695 H -2.382813 2.822871 -0.813425 H -0.777948 2.676194 -1.542439 H 0.704825 -0.554786 -1.883829 H -1.398512 -1.888417 -1.586424 H -3.582464 -1.506265 -0.261431 H -2.885209 -2.428422 1.087823 H -3.490921 -0.782018 1.357189 H -0.699349 -2.751589 -0.209659 H 3.356543 -1.063073 1.634164 H 2.538074 0.478837 1.927412 H 4.100643 0.468094 1.064747 H -0.997801 -0.744068 1.230872	2VA-t-RS C -2.552402 -1.739295 0.374581 C -2.081685 -0.389498 -0.102319 O -1.148810 0.121666 0.745967 C -0.490126 1.340546 0.332429 C -0.006387 2.029548 1.599105 O -2.448910 0.171403 -1.111286 C 0.637207 0.984065 -0.671289 O 1.630758 0.170845 0.002748 C 1.572995 -1.173609 -0.166267 C 2.665709 -1.848222 0.629363 C 1.319121 2.178592 -1.231700 O 0.759812 -1.746300 -0.858117 H -3.474534 -2.009131 -0.141883 H -2.701079 -1.745813 1.457829 H -1.774323 -2.472847 0.134464 H 0.181508 0.381477 -1.465357 H 2.340377 2.410822 -0.955705 H 0.705659 1.397579 2.137160 H 0.486844 2.974278 1.348634 H -0.853313 2.241843 2.258299 H 0.776886 2.850289 -1.887718 H 2.482011 -1.708450 1.700289 H 3.637381 -1.399199 0.402323 H 2.679149 -2.913592 0.397150 H -1.215945 1.959079 -0.203397
2VA-t-RR	C -2.722119 -2.005844 -0.688165 C -2.319963 -0.781651 0.100963 O -2.839549 -0.407417 1.129238 O -1.286328 -0.146832 -0.503471 C -0.760964 1.034983 0.150434 C 0.739300 1.045425 -0.141686 C 1.447877 2.222437 0.427910 C -1.484260 2.266662 -0.384515 O 1.263790 -0.188572 0.468128 C 2.382011 -0.706076 -0.092746 O 2.967125 -0.205699 -1.028564 C 2.789157 -1.979288 0.613554	3VA-ht-RR C -2.396762 1.931555 1.725264 C -1.736866 1.896973 0.368350 O -0.393825 2.013099 0.463852 C 0.379982 1.941507 -0.772954 C 1.685778 2.670144 -0.487260 O -2.328732 1.750957 -0.684246 C 0.519075 0.476721 -1.208136 C 1.234649 -0.440819 -0.212652 O 2.650375 -0.408723 -0.557297 C 3.537060 -0.681963 0.431275 C 4.954231 -0.605619 -0.088405 C 0.732321 -1.908656 -0.261476

C -0.630235 -2.084272 0.306499
 O -1.684083 -1.832432 -0.545840
 C -2.918151 -1.551888 -0.006115
 O -3.116031 -1.503401 1.186931
 C -3.923244 -1.269062 -1.087801
 O 3.221845 -0.945640 1.571422
 H -3.340282 2.477651 1.651242
 H -1.750025 2.383261 2.479487
 H -2.629206 0.901658 2.020879
 H 1.132727 -0.074519 0.811760
 H 1.054750 0.439943 -2.164806
 H 2.226592 2.208757 0.344394
 H 2.329877 2.645909 -1.372401
 H 1.489153 3.715079 -0.227677
 H -0.486042 0.093971 -1.397979
 H 5.158704 0.396139 -0.480528
 H 5.091622 -1.312494 -0.913226
 H 5.649822 -0.836820 0.718929
 H -0.190502 2.469862 -1.542590
 H 0.765564 -2.265967 -1.298685
 H 1.428795 -2.513615 0.329169
 H -0.855719 -2.032278 1.364492
 H -3.721463 -1.857290 -1.985856
 H -3.850528 -0.205073 -1.343670
 H -4.927252 -1.472788 -0.711060

3VA-ht-RS

C 3.851724 -1.232684 -1.635024
 C 3.723472 -0.247967 -0.504489
 O 2.771685 0.698399 -0.806148
 C 2.421537 1.608811 0.164162
 C 1.091859 2.242761 -0.041126
 C -0.088581 1.245567 -0.023237
 C -1.438895 1.930929 -0.239913
 C -2.642661 0.996635 -0.095500
 C -3.967531 1.665199 -0.442400
 O 4.327461 -0.266701 0.540690
 O -0.127280 0.585808 1.269778
 C 0.232294 -0.722633 1.328009
 O 0.640656 -1.360709 0.378934
 C 0.001196 -1.283711 2.707575
 O -2.439717 -0.123253 -1.003705
 C -2.576142 -1.375912 -0.500619
 O -2.913100 -1.619381 0.639414
 C -2.202314 -2.412805 -1.530138
 H -2.678883 0.592605 0.917113
 H 0.073234 0.479278 -0.781824
 H -1.560147 2.750743 0.480549
 H -4.138300 2.531922 0.206103
 H -3.973185 2.005848 -1.483741
 H -4.797048 0.965377 -0.301127
 H -1.436170 2.379405 -1.242161
 H -1.036349 -1.635374 2.754063
 H 0.145428 -0.524405 3.479301
 H 0.666616 -2.132949 2.871594
 H 1.061084 2.761896 -1.010950
 H 0.939275 2.999286 0.737790
 H 2.887624 1.470283 1.131619
 H 3.886665 -0.719294 -2.600121
 H 2.968960 -1.882487 -1.632383
 H 4.747834 -1.837754 -1.491785

H -2.699076 -3.355851 -1.295733
 H -2.453037 -2.083473 -2.541101
 H -1.117905 -2.563508 -1.472703

3VA-hh-RRR

C 2.049914 -2.828819 -0.975900
 C 2.395709 -1.359557 -0.940759
 O 2.047483 -0.811916 0.255213
 C 2.176891 0.633458 0.384098
 C 3.592288 0.977144 0.837952
 O 2.885893 -0.729077 -1.850973
 C 1.112260 1.105999 1.376086
 C -0.352482 0.843005 0.991481
 C -0.802495 -0.629126 1.085808
 C -0.624143 -1.219827 2.439629
 O -0.587928 1.244731 -0.380101
 C -0.952550 2.534606 -0.596597
 C -1.207120 2.772798 -2.065892
 O -1.051073 3.364524 0.280019
 O -2.219043 -0.635863 0.751181
 C -2.622815 -1.515247 -0.198999
 C -4.111569 -1.394326 -0.426572
 O -1.891318 -2.290984 -0.775061
 H 2.534139 -3.295260 -1.834860
 H 0.962514 -2.940987 -1.069792
 H 2.356942 -3.324516 -0.050434
 H -0.996586 1.448274 1.635176
 H 1.228784 2.190172 1.486726
 H 4.318734 0.635530 0.095860
 H 3.703289 2.061230 0.952427
 H 3.817979 0.503371 1.799945
 H 1.299397 0.664094 2.362520
 H -2.010067 2.117378 -2.418835
 H -0.311972 2.530396 -2.647914
 H -1.482508 3.816180 -2.222486
 H 1.992272 1.063381 -0.602897
 H -4.412876 -2.068128 -1.229210
 H -4.373295 -0.362726 -0.682280
 H -4.650496 -1.648679 0.492340
 H -0.276740 -1.216394 0.337022
 H -1.359454 -1.033251 3.215066
 H 0.264504 -1.792036 2.677400

3VA-hh-RRS

C 2.958141 1.827799 -1.508345
 C 2.969265 0.790356 -0.415387
 O 3.501352 0.910781 0.666721
 O 2.258809 -0.309828 -0.785986
 C 2.081790 -1.351659 0.210322
 C 0.663289 -1.898996 0.036351
 C -0.431755 -0.828243 0.038300
 O -1.694490 -1.533220 -0.084424
 C -2.630504 -1.029683 -0.928528
 O -2.477421 -0.046657 -1.619522
 C 3.156622 -2.416975 0.022481
 C -0.474374 0.041537 1.304683
 O -1.527037 1.051908 1.122485
 C -1.192760 2.144203 0.391012
 O -0.072986 2.365882 -0.020125
 C -0.781120 -0.699584 2.555686
 C -3.883873 -1.871691 -0.880733

C	-2.401719	3.008794	0.138085	C	3.436310	-1.171155	1.859128
H	3.776977	2.531433	-1.350274	C	3.149326	-0.571110	0.506141
H	2.005116	2.365587	-1.452528	O	3.375513	-1.110255	-0.557052
H	3.033383	1.363596	-2.495110	O	2.558184	0.644685	0.631263
H	-0.317490	-0.174507	-0.825783	C	2.116717	1.308813	-0.585393
H	0.472630	-2.624539	0.836632	C	0.678025	1.779120	-0.359293
H	4.148658	-1.982478	0.176179	C	-0.285259	0.662468	0.057478
H	3.021896	-3.228095	0.747109	O	-0.185154	-0.408331	-0.908828
H	3.109826	-2.841625	-0.986305	C	0.094742	-1.658201	-0.448445
H	0.593645	-2.443134	-0.913519	O	0.240340	-1.937173	0.721342
H	-4.357061	-1.769730	0.102171	C	3.076484	2.454141	-0.886574
H	-3.641532	-2.929577	-1.019710	C	-1.740447	1.140589	0.078176
H	-4.575994	-1.537922	-1.654502	O	-2.531976	-0.035140	0.469305
H	2.202226	-0.890940	1.193949	C	-3.820183	-0.057574	0.049851
H	-2.082212	3.998024	-0.192762	O	-4.338622	0.827053	-0.595785
H	-3.026667	3.084192	1.031855	C	-1.984917	2.252903	1.034861
H	-2.994936	2.535351	-0.652500	C	0.263012	-2.621932	-1.595379
H	0.470345	0.585658	1.388760	C	-4.503140	-1.326630	0.505183
H	-0.538361	-0.260942	3.517323	H	4.242527	-1.901390	1.770940
H	-1.404275	-1.586424	2.532252	H	2.528682	-1.686234	2.194322
				H	3.689116	-0.402243	2.592955
				H	-0.014231	0.261533	1.035957
3VA-hh-RSR				H	0.325591	2.241837	-1.290552
C	-2.511963	-2.005113	-1.747701	H	4.086167	2.068718	-1.058682
C	-2.638331	-1.005830	-0.625293	H	2.758961	2.992891	-1.786505
O	-3.007686	-1.269440	0.500444	H	3.111877	3.163907	-0.052703
O	-2.236926	0.226560	-1.027127	H	0.659171	2.557497	0.413116
C	-2.174628	1.283440	-0.028393	H	1.306901	-2.566679	-1.926202
C	-0.766127	1.883774	-0.075203	H	-0.382466	-2.363081	-2.437697
C	0.343882	0.844631	0.086844	H	0.061516	-3.637462	-1.250096
O	0.103066	0.115293	1.316363	H	2.146872	0.573636	-1.390612
C	0.185162	-1.240605	1.276398	H	-5.524376	-1.346111	0.123210
O	0.498759	-1.875657	0.291459	H	-4.514484	-1.370709	1.599348
C	-3.267311	2.299023	-0.338824	H	-3.951469	-2.203138	0.151175
C	1.745787	1.467394	0.139711	H	-2.058685	1.419876	-0.929682
O	2.725377	0.375826	0.181009	H	-2.781942	2.963077	0.848894
C	3.048916	-0.186310	-1.013390	H	-1.520046	2.238783	2.016442
O	2.661259	0.232004	-2.082662				
C	1.996982	2.332748	1.321749				
C	-0.226906	-1.838749	2.596768				
C	3.913930	-1.404486	-0.808301				
H	-3.211342	-2.827073	-1.584872				
H	-1.491254	-2.405138	-1.726794				
H	-2.679801	-1.539307	-2.721234				
H	0.312700	0.135880	-0.740445				
H	-0.692123	2.642738	0.713783				
H	-4.254140	1.830057	-0.274782				
H	-3.234656	3.125861	0.379647				
H	-3.143240	2.711013	-1.346364				
H	-0.613547	2.395996	-1.034087				
H	-1.320936	-1.908491	2.603582				
H	0.084656	-1.210941	3.434894				
H	0.191161	-2.842344	2.689771				
H	-2.349826	0.823590	0.945161				
H	4.376915	-1.688862	-1.754232				
H	3.271679	-2.220283	-0.457390				
H	4.675532	-1.222952	-0.045135				
H	1.910627	2.010962	-0.796144				
H	1.505262	2.128616	2.266169				
H	2.815183	3.044479	1.306404				
3VA-hh-RSS							
3VA-th-RRR							
C	-4.005171	-1.720013	-0.451955				
C	-2.585721	-1.613761	0.057021				
O	-1.789541	-2.529342	0.087673				
O	-2.328370	-0.355777	0.478419				
C	-1.041777	-0.079508	1.102934				
C	-0.123178	0.652652	0.120543				
C	0.201384	-0.105206	-1.174218				
C	1.066827	-1.376182	-1.006978				
C	1.169493	-2.154078	-2.271005				
C	-1.328328	0.723890	2.365190				
O	-0.778728	1.898758	-0.240701				
C	0.017119	2.976998	-0.445779				
O	1.224257	2.961043	-0.341043				
C	-0.811384	4.183037	-0.823127				
O	2.424680	-0.979363	-0.643905				
C	2.769583	-0.992170	0.660649				
C	4.218526	-0.600107	0.831207				
O	2.010598	-1.263474	1.569644				
H	-4.169510	-2.714131	-0.868925				
H	-4.195069	-0.955139	-1.211418				
H	-4.707723	-1.543937	0.369693				
H	0.799782	0.901352	0.646812				

H	0.737991	0.576131	-1.842832
H	-1.965064	0.147039	3.042565
H	-0.390358	0.947485	2.884231
H	-1.833434	1.663338	2.124382
H	-0.733739	-0.380443	-1.673035
H	-1.553087	4.391769	-0.045441
H	-1.359341	3.984980	-1.750360
H	-0.157755	5.045608	-0.956650
H	-0.568363	-1.028309	1.358605
H	4.503906	-0.708595	1.878107
H	4.354177	0.441012	0.518451
H	4.859814	-1.219772	0.197178
H	0.660309	-2.003140	-0.210086
H	1.962444	-1.944804	-2.980231
H	0.367622	-2.828514	-2.548621

O	-4.430791	0.187525	-0.748902
C	-0.380384	0.252318	-0.139608
O	0.442388	1.211867	-0.848442
C	1.331019	1.948280	-0.123695
C	2.222585	2.755758	-1.031033
C	-0.192233	-1.116368	-0.802442
C	1.280619	-1.557086	-0.914915
O	1.841434	-1.516971	0.431282
C	3.028625	-0.879402	0.595465
O	3.658844	-0.370254	-0.307480
C	1.436208	-2.930501	-1.466173
O	1.408988	1.917810	1.085223
C	3.420133	-0.841060	2.051257
H	-5.585563	-1.615571	0.684570
H	-4.533058	-1.168161	2.059948
H	-4.007686	-2.421662	0.935780
H	-0.050589	0.220765	0.900060
H	-0.613583	-1.100654	-1.815757
H	-1.717135	2.128649	1.470189
H	-1.487861	2.884749	-0.121017
H	-3.108784	2.384341	0.382444
H	-0.755726	-1.856011	-0.225325
H	1.706982	3.045569	-1.949295
H	3.080963	2.127095	-1.295651
H	2.586627	3.634901	-0.496476
H	-2.179446	0.758726	-1.242178
H	4.501758	-0.721972	2.134539
H	3.087253	-1.737111	2.580040
H	2.934308	0.030596	2.505123
H	1.829226	-0.837561	-1.526102
H	1.543462	-3.088785	-2.533478
H	1.318945	-3.791288	-0.816236

3VA-th-RRS

C	-4.660907	0.818008	1.193659
C	-3.885366	0.433420	-0.044743
O	-2.636873	0.018503	0.284243
C	-1.773758	-0.403143	-0.806019
C	-2.018004	-1.877528	-1.107345
O	-4.306447	0.482419	-1.179608
C	-0.330502	-0.079603	-0.415221
O	0.074331	-0.884628	0.720979
C	0.996465	-1.861309	0.505750
C	1.438275	-2.479195	1.807257
C	-0.119249	1.394262	-0.055042
C	1.312687	1.718312	0.411845
O	2.218154	1.267834	-0.639991
C	3.285365	0.516296	-0.264968
O	3.542560	0.225624	0.884161
C	1.532618	3.169714	0.655475
O	1.427354	-2.158919	-0.588345
C	4.062879	0.050007	-1.469936
H	-5.654942	1.162648	0.907066
H	-4.135142	1.607407	1.740695
H	-4.744465	-0.042891	1.865112
H	0.306363	-0.353236	-1.258972
H	-0.809518	1.681782	0.744374
H	-3.037548	-2.016559	-1.476686
H	-1.316549	-2.232650	-1.869027
H	-1.882441	-2.480264	-0.204601
H	-0.363984	2.001744	-0.935251
H	0.634869	-2.474868	2.547219
H	2.271521	-1.880012	2.192942
H	1.794402	-3.494917	1.626650
H	-2.028014	0.199803	-1.683772
H	5.088246	-0.179725	-1.175262
H	4.047374	0.794051	-2.269671
H	3.589038	-0.866903	-1.839485
H	1.536346	1.142977	1.312691
H	1.357208	3.597969	1.636046
H	1.751595	3.831544	-0.175853

3VA-th-RSS

C	2.847081	-2.554335	-1.050734
C	1.661588	-2.141087	-0.217727
O	0.530024	-2.560315	-0.345987
O	2.017674	-1.201799	0.695425
C	0.942754	-0.601052	1.459386
C	0.212741	0.426541	0.579808
C	-1.061512	0.965294	1.236165
C	-2.136017	1.409689	0.221556
C	-1.773379	2.599054	-0.590599
C	1.573399	-0.034687	2.722997
O	1.088908	1.550192	0.300586
C	1.762476	1.557668	-0.877898
O	1.698991	0.684259	-1.714337
C	2.587569	2.817692	-0.999418
O	-2.398003	0.322864	-0.708691
C	-3.170951	-0.701189	-0.261324
C	-3.188938	-1.827403	-1.264032
O	-3.727354	-0.702142	0.815888
H	2.622201	-3.485134	-1.573244
H	3.743466	-2.664878	-0.434571
H	3.035227	-1.762033	-1.784146
H	-0.032066	-0.052873	-0.367785
H	-0.818819	1.807170	1.894934
H	2.298447	0.746393	2.478782
H	0.805533	0.395736	3.374266
H	2.085450	-0.828239	3.275056
H	-1.508762	0.183856	1.858909

3VA=th=BSB

```

C -4.554049 -1.475660  1.009203
C -3.895176 -0.422497  0.149280
O -2.601862 -0.244934  0.522048
C -1.832760  0.751535 -0.204469
C -2.048270  2.121856  0.426961

```

H 3.270739 2.906929 -0.148707
 H 1.932274 3.695047 -0.986877
 H 3.153358 2.793410 -1.931256
 H 0.222964 -1.389136 1.700858
 H -3.982851 -2.530887 -1.009890
 H -2.220111 -2.340456 -1.226638
 H -3.323318 -1.445182 -2.279667
 H -3.066429 1.581466 0.785801
 H -2.161221 2.705756 -1.596891
 H -1.278862 3.441466 -0.121092

3VA-tt-RR

C 3.798706 -2.488481 -0.578557
 C 3.394992 -1.038972 -0.712715
 O 3.875615 -0.243082 -1.487728
 O 2.402484 -0.737887 0.164133
 C 1.880475 0.616880 0.130702
 C 0.408547 0.483081 0.561899
 C 0.189677 0.026700 2.001553
 C -1.304252 -0.155304 2.389579
 C -2.062409 -1.147110 1.581813
 O -2.590710 -0.663480 0.403241
 C -3.056063 -1.560231 -0.533561
 C -3.593844 -0.824843 -1.731701
 C 2.739591 1.535815 0.990996
 O -0.218798 1.785758 0.417409
 C -0.822138 2.064349 -0.764762
 O -0.823743 1.318222 -1.720199
 C -1.493536 3.416056 -0.712789
 O -3.014293 -2.756834 -0.373838
 H 4.611906 -2.704085 -1.272197
 H 2.943598 -3.137464 -0.794685
 H 4.117129 -2.698601 0.447710
 H -0.075064 -0.203016 -0.135351
 H 0.638868 0.749708 2.693639
 H 3.729164 1.644381 0.539385
 H 2.277916 2.526263 1.057665
 H 2.859146 1.137857 2.003615
 H 0.723663 -0.921470 2.131305
 H -0.799998 4.175601 -0.339872
 H -2.342069 3.377920 -0.020745
 H -1.847511 3.685195 -1.708520
 H 1.899692 0.957294 -0.907885
 H -3.909786 -1.546758 -2.485498
 H -2.824702 -0.158970 -2.136531
 H -4.447244 -0.203434 -1.437532
 H -1.934159 -2.221473 1.636670
 H -1.805902 0.817918 2.328168
 H -1.337574 -0.466072 3.441770

3VA-tt-RS

C -4.654921 -0.213920 -0.857601
 C -3.495117 0.140976 0.043526
 O -3.295208 1.236429 0.521531
 O -2.706792 -0.944221 0.244152
 C -1.516020 -0.785440 1.060548
 C -0.292802 -0.601503 0.147045
 C -0.057032 -1.724980 -0.860428
 C 1.164943 -1.493041 -1.792106
 C 2.478296 -1.375533 -1.104222
 O 2.770829 -0.122881 -0.608284

C 3.804595 0.013359 0.291378
 C 3.953723 1.456554 0.692226
 C -1.430199 -1.997786 1.979525
 O -0.481523 0.616866 -0.614874
 C -0.105579 1.780331 -0.027263
 O 0.455230 1.843898 1.046699
 C -0.515224 2.959870 -0.871086
 O 4.465781 -0.920963 0.678247
 H -5.344447 0.629142 -0.912127
 H -5.172368 -1.102914 -0.484529
 H -4.282991 -0.448375 -1.861111
 H 0.579418 -0.465957 0.791107
 H -0.955920 -1.851585 -1.475181
 H -0.515726 -1.954688 2.581092
 H -2.286076 -2.011125 2.661001
 H -1.432058 -2.934433 1.413854
 H 0.088614 -2.659849 -0.306484
 H -1.597783 3.093315 -0.764475
 H -0.299335 2.781711 -1.928180
 H -0.003370 3.857269 -0.521161
 H -1.631805 0.127434 1.648395
 H 4.733700 1.541696 1.449621
 H 3.001680 1.837827 1.075951
 H 4.222436 2.061317 -0.181298
 H 3.020602 -2.199621 -0.655998
 H 0.986271 -0.590389 -2.387754
 H 1.214644 -2.337113 -2.491733

3VAMe-m-RR

C 1.279635 1.761750 2.648016
 C 1.511658 1.912922 1.167852
 O 2.499548 2.367592 0.639101
 O 0.435800 1.421277 0.472758
 C 0.482634 1.254121 -0.904275
 C 1.669411 0.613561 -1.557255
 C 2.290024 -0.582601 -0.817184
 C 3.453911 -1.195246 -1.589065
 C -0.816300 1.517186 -1.592266
 C -1.930057 0.473662 -1.359107
 O -2.399049 0.680333 0.002272
 C -2.835584 -0.394167 0.688921
 C -3.222717 -0.008729 2.097205
 O 1.279215 -1.615458 -0.649860
 C 1.028685 -2.063999 0.606802
 O 1.526541 -1.595759 1.610411
 C 0.044501 -3.207161 0.582626
 C -3.106442 0.634165 -2.316426
 O -2.889753 -1.519929 0.234268
 H 2.033386 2.329630 3.194760
 H 1.359763 0.698622 2.902269
 H 0.275441 2.099642 2.920671
 H 1.367082 0.289165 -2.561135
 H 2.480148 1.345980 -1.686497
 H -1.214205 2.497356 -1.293024
 H -0.629239 1.562752 -2.671841
 H 0.277182 -3.899118 -0.231524
 H -0.967251 -2.820256 0.415674
 H 0.073975 -3.725377 1.542481
 H 2.622549 -0.281160 0.175764
 H -1.523493 -0.538431 -1.425988
 H -2.780617 0.475951 -3.350571

H -3.537737	1.638509	-2.238633	C 1.771789	-1.592464	-0.993325
H -3.883086	-0.101528	-2.088060	O 1.964996	-1.472194	0.446883
H -3.881995	0.864249	2.090180	C 3.126917	-0.923007	0.862861
H -2.321569	0.264022	2.657596	C 3.150786	-0.732035	2.359255
H -3.714032	-0.851311	2.585001	C -0.223976	0.804040	-1.322716
H 4.239497	-0.448309	-1.746552	C 0.787109	1.473052	-0.464214
H 3.885331	-2.032184	-1.030913	O 1.987843	1.802235	-1.047604
H 3.124293	-1.565428	-2.566326	C 2.973087	2.332507	-0.246660
3VAMe-m-RS					
C -1.435328	4.658329	-0.527889	O 2.812890	2.545554	0.934024
C -0.771101	3.403248	-0.017692	C 4.236974	2.552812	-1.029747
O -0.076251	3.317654	0.967455	O -3.254265	1.055163	-0.639631
O -1.064745	2.347184	-0.836860	C -3.490491	1.588139	0.583906
C -0.450059	1.107977	-0.629578	O -3.802370	0.945632	1.563890
C 1.036707	1.019766	-0.804036	C -3.291447	3.085499	0.558316
C 1.724985	0.049388	0.172344	C 2.538369	-2.809022	-1.512664
C 1.767855	0.548959	1.611422	O 4.023409	-0.586159	0.113875
C -1.377125	-0.043049	-0.857816	H -1.417775	-1.930147	3.467188
C -2.035170	-0.590865	0.430286	H -2.018021	-0.317834	2.983216
O -2.890271	-1.713846	0.078110	H -0.272859	-0.598105	3.101461
C -2.285629	-2.911574	-0.110362	H 0.700326	1.632807	0.599011
C -3.305951	-3.981647	-0.422674	H -1.119908	1.433734	-1.388959
O 3.081414	-0.083439	-0.344047	H -2.066960	-0.552715	-2.519556
C 3.763589	-1.206890	-0.018183	H -2.214917	-2.009255	-1.538937
O 3.320484	-2.098138	0.671806	H 0.167550	0.711896	-2.342546
C 5.144868	-1.184731	-0.634095	H 4.024475	2.824624	-2.066439
C -2.922916	0.411754	1.151187	H 4.802550	1.614013	-1.023493
O -1.088615	-3.087600	-0.031807	H 4.833835	3.326732	-0.543766
H -1.326456	5.451534	0.212425	H -0.080003	-2.666385	-0.793064
H -2.493766	4.475447	-0.736195	H 0.160424	-1.866031	-2.337802
H -0.966119	4.970282	-1.467792	H -3.774947	3.527345	-0.317464
H 1.268301	0.671913	-1.826036	H -2.219962	3.308393	0.492962
H 1.488853	2.009585	-0.694544	H -3.691305	3.521378	1.474640
H -2.178406	0.260666	-1.546057	H -3.423335	-0.815797	0.216621
H -0.827556	-0.868371	-1.323270	H 2.174951	-0.686554	-1.451082
H 5.710390	-0.326933	-0.254857	H 2.392613	-2.915066	-2.593676
H 5.073964	-1.073843	-1.720966	H 2.183298	-3.724372	-1.026355
H 5.666838	-2.109762	-0.386953	H 3.607489	-2.694097	-1.321479
H 1.258818	-0.940532	0.130781	H 2.457360	-1.405118	2.867324
H -1.255307	-0.967033	1.098201	H 2.864228	0.305846	2.566774
H -3.705930	0.792591	0.486145	H 4.168397	-0.879539	2.727511
H -2.323873	1.255784	1.506536	H -4.721146	-1.787350	-1.703454
H -3.402497	-0.058386	2.015364	H -5.492363	-0.339719	-1.030471
H -3.891837	-3.699646	-1.303536	H -4.589677	-0.233334	-2.558023
H -4.005303	-4.088398	0.413242	4VAMe-mT-RRS		
H -2.795576	-4.928556	-0.601319	C -1.666175	-3.952861	-1.388128
H 0.754925	0.744195	1.975388	C -1.153984	-3.040764	-0.295159
H 2.239819	-0.197634	2.255223	O -0.959549	-3.381534	0.852448
H 2.326240	1.488577	1.673474	O -0.941623	-1.798361	-0.790078
4VAMe-mt-RRR					
C -1.227329	-1.061570	2.835505	C -0.449034	-0.683567	0.038504
C -1.227451	-1.486267	1.387370	C 0.959255	-0.973771	0.603132
O -1.586719	-2.570655	0.977665	C 2.138208	-1.108208	-0.372700
O -0.810661	-0.465690	0.600785	C 2.079438	-2.282709	-1.342546
C -0.704528	-0.606539	-0.849869	C -1.407760	-0.437355	1.227509
C -2.088304	-0.923872	-1.485741	C -2.894997	-0.267872	0.906489
C -3.342743	-0.392856	-0.783616	O -3.086645	1.115274	0.475729
C -4.612938	-0.705585	-1.569605	C -4.151406	1.377049	-0.322504
C 0.271626	-1.738903	-1.252264	C -4.218644	2.850196	-0.653240
			C -0.462075	0.487227	-0.992136
			C -0.063647	1.818840	-0.472328
			O 1.252103	2.168220	-0.661969

C	1.728450	3.316164	-0.065199
O	1.051343	4.001484	0.664199
C	3.153619	3.563798	-0.478703
O	3.299549	-1.324330	0.491648
C	4.383441	-0.536860	0.328358
O	4.471332	0.358874	-0.486837
C	5.472179	-0.927421	1.301957
C	-3.781618	-0.538601	2.119039
O	-4.930103	0.533909	-0.711434
H	-1.910437	-4.926165	-0.961139
H	-0.901031	-4.073174	-2.162791
H	-2.549508	-3.518171	-1.866118
H	-0.647617	2.443379	0.188329
H	-1.478999	0.543917	-1.393059
H	1.200818	-0.143845	1.278071
H	0.905663	-1.875576	1.219046
H	0.188952	0.215833	-1.830213
H	3.174682	3.911173	-1.518875
H	3.739795	2.641540	-0.430875
H	3.583988	4.335480	0.161172
H	-1.305037	-1.280179	1.914325
H	-1.065724	0.456936	1.761079
H	5.754587	-1.974122	1.149093
H	5.107294	-0.836317	2.330266
H	6.339894	-0.283220	1.156432
H	2.307607	-0.175914	-0.912253
H	-3.201018	-0.911469	0.077949
H	-3.505930	0.113653	2.955345
H	-3.668723	-1.579723	2.440047
H	-4.831958	-0.369157	1.867553
H	-3.288273	3.175574	-1.130308
H	-4.333890	3.435333	0.265236
H	-5.063180	3.034967	-1.317875
H	1.245371	-2.165480	-2.039935
H	3.007105	-2.335653	-1.921631
H	1.952808	-3.227622	-0.802582

C -3.739660 1.644873 -0.872337
O -3.825677 -1.079892 1.228113
H -0.730068 5.356759 1.380449
H 0.260365 5.167283 -0.100689
H 0.930285 4.707396 1.465992
H -1.145555 -1.529733 1.293448
H -0.612641 0.829457 1.700766
H 1.115415 -0.279835 -1.498719
H 0.993034 1.298286 -2.254218
H 1.104815 0.515287 1.431322
H 2.055863 -4.508530 0.598779
H 2.326028 -3.398044 -0.759630
H 1.241043 -4.822609 -0.937585
H -1.365595 1.916533 -1.745700
H -1.120338 0.191074 -1.854833
H 3.181999 -1.765675 1.922555
H 4.549257 -0.647336 2.023814
H 4.757082 -2.251191 1.246564
H 3.233317 0.644667 -1.826806
H -2.534082 0.728201 0.645068
H -3.881660 1.607088 -1.958813
H -3.502200 2.670949 -0.577942
H -4.677488 1.358045 -0.386882
H -3.018960 -3.404098 -0.426182
H -4.229535 -2.717589 -1.529432
H -4.706535 -3.254488 0.116811
H 2.716859 2.966615 0.100270
H 4.198351 2.600480 -0.810063
H 2.735391 3.138683 -1.661270

4VAMe-mT-RSS

C -1.454930 -4.197470 -1.263040
C -1.583751 -2.692283 -1.154201
O -2.334463 -2.022636 -1.830526
O -0.744819 -2.229355 -0.200133
C -0.509335 -0.805703 0.110330
C 0.800572 -0.845667 0.931733
C 2.122136 -1.181827 0.225363
C 2.267213 -2.596280 -0.322982
C -1.605062 -0.262170 1.061374
C -3.084252 -0.311857 0.621203
O -3.780174 0.847184 1.178339
C -3.699846 2.004178 0.486556
C -4.498356 3.093765 1.163789
C -0.377578 0.049171 -1.191520
C 0.076194 1.447573 -0.970456
O 1.414043 1.691080 -1.184035
C 1.902339 2.961853 -0.978275
O 1.221650 3.865549 -0.554393
C 3.352929 3.031599 -1.376796
O 3.126324 -1.009680 1.278694
C 4.305558 -0.445145 0.944041
O 4.592825 -0.059746 -0.171115
C 5.215422 -0.360203 2.148834
C -3.840500 -1.515841 1.167998
O -3.066086 2.140631 -0.540150
H -2.228631 -4.578327 -1.930656
H -1.541346 -4.664032 -0.277052
H -0.468505 -4.459314 -1.661545
H -0.569471 2.301453 -0.824966
H -1.348117 0.071909 -1.688320

H 0.928925 0.142469 1.386645
H 0.655775 -1.556387 1.754265
H 0.318670 -0.461048 -1.868643
H 3.429823 3.028079 -2.470910
H 3.904453 2.162125 -1.007442
H 3.785396 3.957958 -0.995766
H -1.508400 -0.772385 2.028161
H -1.339562 0.785276 1.234834
H 5.398836 -1.361530 2.552068
H 4.738591 0.227083 2.940400
H 6.159900 0.102099 1.860116
H 2.344184 -0.452668 -0.553352
H -3.171240 -0.260157 -0.462711
H -3.855516 -1.490085 2.263392
H -3.360728 -2.447178 0.856177
H -4.873369 -1.521990 0.807148
H -4.108538 3.272395 2.171494
H -5.543976 2.786663 1.268324
H -4.434670 4.009616 0.575488
H 1.570330 -2.764292 -1.147841
H 3.284692 -2.741988 -0.699569
H 2.065574 -3.342115 0.453118

S22 Cartesian coordinates and imaginary frequencies of all

transition	state	structure
TS3VA-ht-RR		
C -2.416693 1.883694 1.762499	O 0.972443 -1.407808 -0.153461	
C -1.751974 1.900866 0.407946	C 1.094042 -1.390733 2.264649	
O -0.421049 2.117645 0.504233	O -3.171870 -0.010048 -0.710529	
C 0.350274 2.101510 -0.733188	C -3.023045 -1.328191 -0.418914	
C 1.595217 2.934120 -0.467821	O -2.737293 -1.760669 0.676129	
O -2.330208 1.716998 -0.646313	C -3.235422 -2.171381 -1.654239	
C 0.623203 0.639573 -1.145473	H -2.774630 0.396817 1.275290	
C 1.422248 -0.162145 -0.162458	H -0.342240 0.266583 -1.052668	
O 2.769722 -0.257964 -0.517642	H -1.488748 2.476237 0.806626	
C 3.649231 -0.753465 0.403851	H -4.027126 2.599361 1.229738	
C 5.049853 -0.764283 -0.156800	H -4.356892 2.353732 -0.499224	
C 0.543046 -2.285309 -0.216810	H -5.048084 1.246208 0.704684	
C -0.724432 -2.234975 0.265725	H -1.818899 2.307907 -0.924260	
O -1.768074 -1.949927 -0.600646	H 0.428075 -1.024083 3.047781	
C -2.972587 -1.581917 -0.059977	H 2.112012 -1.033510 2.459928	
O -3.168033 -1.506650 1.133039	H 1.111740 -2.482719 2.259098	
C -3.963844 -1.244140 -1.139307	H 1.080568 2.236608 -1.734693	
O 3.321450 -1.118885 1.510143	H 0.879075 3.153352 -0.137948	
H -3.355920 2.440341 1.706797	H 2.803678 1.859751 0.832474	
H -1.771965 2.300489 2.537947	H 4.715979 -0.659337 -2.206170	
H -2.662551 0.844699 2.010634	H 3.620548 -1.846679 -1.478699	
H 1.263353 -0.029572 0.902166	H 5.264074 -1.655402 -0.814918	
H 1.139828 0.640154 -2.113105	H -3.437900 -3.201907 -1.359060	
H 2.189827 2.508856 0.346812	H -4.051148 -1.777551 -2.265894	
H 2.219735 2.969937 -1.366983	H -2.321522 -2.152899 -2.259524	
H 1.321629 3.957915 -0.194415		
H -0.350505 0.165934 -1.306001		
H 5.384315 0.260120 -0.354699		
H 5.076204 -1.305282 -1.108076		
H 5.722232 -1.235762 0.560618		
H -0.267414 2.563681 -1.509066		
H 0.720494 -2.338233 -1.286461		
H 1.329185 -2.638716 0.440169		
H -1.002404 -2.298279 1.310087		
H -3.788058 -1.830067 -2.044074		
H -3.843479 -0.180971 -1.379521		
H -4.976228 -1.406165 -0.764464		
Imaginary Frequency: 378i		
TS3VA-ht-RS		
C 4.420925 -1.128866 -1.264271		
C 3.884805 -0.113175 -0.292624		
O 3.097876 0.799669 -0.941112		
C 2.432196 1.738705 -0.177207		
C 1.310876 2.317197 -0.677244		
C -0.437955 0.889202 -0.169521		
C -1.651909 1.745235 0.002941		
C -2.931377 0.954592 0.350090		
C -4.165416 1.841608 0.450389		
O 4.076414 -0.098429 0.902649		
O -0.062689 0.251990 1.001328		
C 0.677679 -0.897544 0.905519		
Imaginary Frequency: 360i		
TS3VA-hh-RRR		
C -1.841266 -0.336084 2.747054		
C -2.371678 0.309285 1.489361		
O -2.119436 -0.470257 0.404261		
C -2.418879 0.100600 -0.900224		
C -3.832277 -0.295366 -1.312177		
O -2.922571 1.386298 1.432490		
C -1.350078 -0.396157 -1.880330		
C 0.073836 -0.144666 -1.462785		
C 0.711468 -1.750234 -0.080679		
C 0.305868 -2.940810 -0.621106		
O 0.209370 1.068633 -0.792133		
C 1.391220 1.756978 -0.856201		
C 1.359156 2.938780 0.074503		
O 2.324420 1.413439 -1.546844		
O 2.094937 -1.514633 -0.072855		
C 2.599082 -0.660613 0.856760		
C 4.082155 -0.486679 0.662640		
O 1.926956 -0.100542 1.698313		
H -2.269488 0.160401 3.618960		
H -0.749853 -0.226875 2.770405		
H -2.070608 -1.405276 2.766288		
H 0.861686 -0.323710 -2.189283		
H -1.544910 0.109103 -2.840883		
H -4.558669 0.108888 -0.601584		
H -4.067164 0.103876 -2.305438		

H -3.938568 -1.385493 -1.344335
 H -1.468191 -1.469814 -2.068180
 H 1.557518 2.574857 1.089734
 H 0.376617 3.417170 0.075907
 H 2.135783 3.650132 -0.210423
 H -2.354129 1.185267 -0.798229
 H 4.519318 -0.048619 1.561038
 H 4.237103 0.190346 -0.185310
 H 4.561869 -1.439898 0.426142
 H 0.163749 -1.243566 0.700898
 H 0.980380 -3.554448 -1.208304
 H -0.733496 -3.236043 -0.544147

Imaginary Frequency: 515i

TS3VA-hh-RS

C 2.900770 1.897299 -1.516012
 C 2.877552 0.882179 -0.402225
 O 3.257026 1.077108 0.732591
 O 2.330322 -0.290052 -0.822953
 C 2.146928 -1.332364 0.172458
 C 0.785506 -1.977675 -0.094016
 C -0.347007 -0.999112 -0.198803
 O -1.577204 -1.655614 -0.214285
 C -2.617970 -1.108374 -0.905749
 O -2.528591 -0.110601 -1.586416
 C 3.305177 -2.319149 0.078033
 C -0.453122 0.289174 1.623375
 O -1.536566 1.074008 1.205280
 C -1.284077 2.090052 0.328005
 O -0.179798 2.345761 -0.098279
 C -0.671829 -0.542824 2.684790
 C -3.872609 -1.917062 -0.691037
 C -2.556855 2.804012 -0.037379
 H 3.673815 2.640591 -1.313404
 H 1.925885 2.397315 -1.533747
 H 3.065694 1.422157 -2.486030
 H -0.272726 -0.193470 -0.921441
 H 0.576006 -2.696273 0.708686
 H 4.250080 -1.815345 0.302199
 H 3.172490 -3.134459 0.798412
 H 3.366938 -2.751206 -0.926785
 H 0.839687 -2.561936 -1.028444
 H -3.667726 -2.986890 -0.789415
 H -4.631882 -1.607404 -1.410136
 H -4.246576 -1.745517 0.324961
 H 2.157866 -0.854876 1.154340
 H -2.316030 3.769638 -0.484064
 H -3.199934 2.934016 0.837083
 H -3.092214 2.189308 -0.769649
 H 0.515700 0.722941 1.404789
 H 0.161645 -1.066614 3.138278
 H -1.675013 -0.783800 3.018231

Imaginary Frequency: 500i

TS3VA-hh-RSR

C -2.728330 -1.935113 -1.773551
 C -2.728017 -1.015413 -0.577120
 O -2.853481 -1.379934 0.573779
 O -2.526179 0.270583 -0.956566

C -2.359561 1.274144 0.084184
 C -0.914204 1.807324 0.007985
 C 0.122142 0.729034 0.075485
 O 0.043135 -0.005997 1.253559
 C 0.324943 -1.343497 1.217180
 O 0.683514 -1.924605 0.216135
 C -3.405482 2.356930 -0.143411
 C 2.138823 1.686340 0.111395
 O 2.884347 0.503489 0.126103
 C 3.069587 -0.142154 -1.067003
 O 2.653283 0.277392 -2.122475
 C 2.197079 2.470235 1.226776
 C 0.067334 -1.972517 2.559115
 C 3.820758 -1.429032 -0.859139
 H -3.325058 -2.821635 -1.551400
 H -1.694873 -2.251874 -1.958745
 H -3.099470 -1.431354 -2.668632
 H 0.298151 0.119512 -0.804844
 H -0.777740 2.516665 0.835359
 H -4.414722 1.940293 -0.065285
 H -3.302163 3.148046 0.607725
 H -3.292840 2.806218 -1.136289
 H -0.777798 2.361162 -0.929382
 H -1.014682 -2.115158 2.663170
 H 0.404930 -1.323336 3.371033
 H 0.562744 -2.943143 2.610224
 H -2.515375 0.779174 1.044316
 H 4.227883 -1.769618 -1.812215
 H 3.114249 -2.176126 -0.479984
 H 4.617930 -1.305955 -0.121270
 H 1.950018 2.078432 -0.881799
 H 2.594573 2.092200 2.162004
 H 1.736857 3.451384 1.220355

Imaginary Frequency: 471i

TS3VA-hh-RSS

C 2.940420 -1.690190 1.918463
 C 2.836814 -1.015497 0.572620
 O 2.832540 -1.596502 -0.492022
 O 2.701972 0.327779 0.714276
 C 2.444834 1.116099 -0.481477
 C 1.050572 1.757488 -0.338371
 C -0.032388 0.767380 -0.033128
 O -0.133528 -0.216848 -1.012356
 C -0.444097 -1.498577 -0.636314
 O -0.602342 -1.829367 0.518563
 C 3.560367 2.144267 -0.613573
 C -1.991284 1.816878 -0.040378
 O -2.691885 0.918836 0.776458
 C -3.317610 -0.139253 0.183524
 O -3.353089 -0.315012 -1.014133
 C -1.803113 3.075519 0.458537
 C -0.563927 -2.383291 -1.844120
 C -3.903363 -1.055733 1.224225
 H 3.510196 -2.615920 1.818899
 H 1.925035 -1.943919 2.245970
 H 3.392911 -1.034586 2.665544
 H -0.111745 0.378300 0.976825
 H 0.834018 2.287346 -1.276558
 H 4.529125 1.648583 -0.732174

H 3.390573 2.778253 -1.491115
 H 3.606328 2.786417 0.272954
 H 1.063168 2.505741 0.462491
 H 0.342571 -2.309391 -2.452016
 H -1.414069 -2.049298 -2.448573
 H -0.718868 -3.414294 -1.524782
 H 2.447704 0.431179 -1.331003
 H -4.285995 -0.494606 2.080036
 H -3.103350 -1.717881 1.575992
 H -4.692051 -1.660653 0.774153
 H -2.060419 1.599523 -1.100645
 H -1.363910 3.844098 -0.166536
 H -1.983903 3.299479 1.504200

Imaginary Frequency: 478i

TS3VA-th-RRR

C -4.054768 -1.577882 -0.555438
 C -2.688901 -1.466125 0.082292
 O -1.949054 -2.402508 0.304693
 O -2.408665 -0.176365 0.373714
 C -1.160162 0.121664 1.059645
 C -0.152491 0.737926 0.087728
 C 0.103290 -0.041965 -1.166840
 C 1.147927 -2.015269 -0.769137
 C 0.934813 -2.722332 -1.914824
 C -1.501180 1.021978 2.240215
 O -0.662965 2.071861 -0.287404
 C 0.267819 3.016995 -0.551354
 O 1.465649 2.832677 -0.490684
 C -0.391510 4.321946 -0.937235
 O 2.445075 -1.536988 -0.553325
 C 2.765103 -1.081955 0.689489
 C 4.162710 -0.518990 0.702465
 O 2.004973 -1.102280 1.632913
 H -4.252719 -2.618651 -0.813692
 H -4.105019 -0.952251 -1.452481
 H -4.821086 -1.214222 0.137055
 H 0.776109 0.902354 0.635625
 H 0.909851 0.338673 -1.786815
 H -2.175441 0.501548 2.927090
 H -0.588484 1.281607 2.787314
 H -1.983447 1.942727 1.902418
 H -0.774047 -0.367213 -1.718579
 H -1.084758 4.644761 -0.154033
 H -0.975807 4.186236 -1.853601
 H 0.373341 5.082825 -1.096611
 H -0.732999 -0.818178 1.412710
 H 4.840484 -1.130091 0.101125
 H 4.517014 -0.448775 1.731728
 H 4.138143 0.486650 0.265377
 H 0.547660 -2.152716 0.120441
 H 1.663839 -2.739160 -2.717699
 H -0.028628 -3.193259 -2.068656

Imaginary Frequency: 478i

TS3VA-th-RRS

C 4.754763 -0.844501 1.150552
 C 3.952486 -0.461517 -0.071281
 O 2.712596 -0.046090 0.285081

C 1.821855 0.364230 -0.785343
 C 2.025237 1.847824 -1.070912
 O 4.349174 -0.513028 -1.214991
 C 0.387407 -0.023339 -0.368993
 O -0.032019 0.768624 0.775334
 C -0.856821 1.820807 0.547099
 C -1.289993 2.460504 1.841240
 C 0.263376 -1.469877 -0.005862
 C -1.911551 -1.988054 0.478142
 O -2.548169 -1.347391 -0.591707
 C -3.342176 -0.273395 -0.291589
 O -3.540111 0.109979 0.839398
 C -1.912770 -3.348097 0.495912
 O -1.222988 2.170004 -0.556995
 C -3.884860 0.364222 -1.541858
 H 5.743494 -1.186796 0.843483
 H 4.241296 -1.635489 1.706870
 H 4.849971 0.015899 1.821075
 H -0.264075 0.225971 -1.212031
 H 0.706018 -1.771828 0.939300
 H 3.033361 2.009896 -1.462945
 H 1.297313 2.201361 -1.806961
 H 1.904710 2.435238 -0.155960
 H 0.413475 -2.169431 -0.824268
 H -0.525599 2.359764 2.614819
 H -2.199322 1.948750 2.176429
 H -1.527632 3.511332 1.665693
 H 2.075547 -0.220796 -1.674585
 H -4.861276 0.802904 -1.326881
 H -3.955313 -0.352120 -2.362848
 H -3.200597 1.171090 -1.828178
 H -1.805717 -1.376025 1.364870
 H -1.473326 -3.877093 1.333912
 H -2.241909 -3.922245 -0.363397

Imaginary Frequency: 453i

TS3VA-th-RSR

C -4.575813 -1.501696 1.056336
 C -3.939330 -0.455357 0.171276
 O -2.637864 -0.274863 0.509832
 C -1.884659 0.707953 -0.249629
 C -2.061824 2.081865 0.386639
 O -4.498655 0.146735 -0.717971
 C -0.430221 0.170325 -0.242224
 O 0.393894 1.127885 -0.959217
 C 1.189792 1.954128 -0.231528
 C 2.062863 2.791934 -1.129759
 C -0.309533 -1.152644 -0.929615
 C 1.844630 -1.912995 -0.869374
 O 2.160800 -1.630910 0.464699
 C 3.083891 -0.646882 0.693108
 O 3.650199 -0.048837 -0.194322
 C 1.721891 -3.219583 -1.229069
 O 1.211521 1.979936 0.981371
 C 3.257096 -0.399111 2.167137
 H -5.616874 -1.640353 0.763115
 H -4.522633 -1.189210 2.104453
 H -4.034374 -2.449565 0.971084
 H -0.083962 0.115098 0.793037
 H -0.432227 -1.147724 -2.011289

H -1.683395 2.093139 1.412836
 H -1.527363 2.842415 -0.189655
 H -3.123341 2.345917 0.387103
 H -0.783108 -1.985871 -0.421058
 H 1.578796 2.993621 -2.087839
 H 2.985318 2.229457 -1.313446
 H 2.319077 3.723347 -0.621491
 H -2.267012 0.715999 -1.273926
 H 3.012078 -1.284562 2.757027
 H 2.582352 0.417249 2.448985
 H 4.282723 -0.077916 2.359558
 H 2.095861 -1.121616 -1.564110
 H 1.530330 -3.478236 -2.264233
 H 1.695897 -4.008382 -0.485083

Imaginary Frequency: 458i

TS3VA-th-RSS

C 2.679681 -2.486519 -1.308670
 C 1.580315 -2.121791 -0.345104
 O 0.440107 -2.536606 -0.391177
 O 2.022185 -1.235610 0.579837
 C 1.029197 -0.664538 1.469837
 C 0.268641 0.450765 0.716553
 C -0.889030 1.000075 1.487283
 C -2.430672 1.532577 -0.074909
 C -1.938457 2.608872 -0.752237
 C 1.772134 -0.201800 2.713134
 O 1.181929 1.540699 0.426987
 C 1.719054 1.611056 -0.814293
 O 1.486092 0.832467 -1.713954
 C 2.643961 2.801780 -0.917226
 O -2.454586 0.317173 -0.758627
 C -3.113393 -0.738885 -0.184211
 C -2.961014 -1.972130 -1.032229
 O -3.699643 -0.659744 0.871166
 H 2.406737 -3.391833 -1.852606
 H 3.632103 -2.620843 -0.789018
 H 2.793827 -1.658092 -2.017272
 H -0.065361 0.027705 -0.235303
 H -0.733447 1.936963 2.014123
 H 2.508009 0.566860 2.461877
 H 1.066298 0.217160 3.437587
 H 2.290063 -1.044943 3.179760
 H -1.529183 0.279381 1.989684
 H 3.022589 2.881590 -1.936726
 H 3.480804 2.684517 -0.220444
 H 2.113783 3.718266 -0.639817
 H 0.302762 -1.445555 1.712243
 H -3.656960 -2.737211 -0.685766
 H -1.932522 -2.341927 -0.941220
 H -3.139310 -1.740689 -2.086235
 H -3.146896 1.605645 0.734736
 H -1.395081 2.484754 -1.682544
 H -1.989380 3.594442 -0.304490

Imaginary Frequency: 498i

TS3VA-tt-RR

C 4.125920 -2.401221 -0.474402
 C 3.617258 -0.993363 -0.680210

O 4.017848 -0.216816 -1.518203
 O 2.635076 -0.707226 0.211634
 C 2.020058 0.604008 0.116232
 C 0.576713 0.393920 0.639122
 C 0.462438 0.030498 2.080920
 C -1.842256 -0.255353 2.490684
 C -2.396939 -1.058850 1.553535
 O -2.852359 -0.504248 0.372698
 C -3.286247 -1.359014 -0.618263
 C -3.707924 -0.575051 -1.830646
 C 2.839461 1.631803 0.884868
 O -0.146633 1.642761 0.442596
 C -0.774063 1.819489 -0.743196
 O -0.709552 1.039536 -1.670481
 C -1.585209 3.093163 -0.735764
 O -3.301970 -2.559478 -0.492582
 H 4.927362 -2.604806 -1.185187
 H 3.311378 -3.119107 -0.616588
 H 4.494385 -2.523616 0.549354
 H 0.118081 -0.371851 0.007956
 H 0.617290 0.815136 2.817297
 H 3.810431 1.769342 0.401921
 H 2.317873 2.594393 0.895674
 H 2.999826 1.310974 1.919148
 H 0.823461 -0.955695 2.354613
 H -1.804317 3.392666 -1.761735
 H -1.060718 3.892909 -0.206841
 H -2.529366 2.906139 -0.210890
 H 1.966151 0.874913 -0.941359
 H -4.087777 -1.260514 -2.588783
 H -2.849071 -0.016453 -2.218238
 H -4.483018 0.150348 -1.561153
 H -2.457772 -2.139045 1.602406
 H -1.935971 0.821732 2.416358
 H -1.612765 -0.673881 3.463473

Imaginary Frequency: 341i

TS3VA-tt-RS

C -4.726022 0.071123 -0.917611
 C -3.543148 0.325426 -0.012071
 O -3.228758 1.408288 0.432958
 O -2.883797 -0.832251 0.234486
 C -1.697031 -0.783170 1.067902
 C -0.441997 -0.770234 0.161485
 C -0.322245 -1.918154 -0.784062
 C 1.683625 -1.546510 -1.971194
 C 2.695710 -1.335728 -1.097727
 O 2.917745 -0.058988 -0.621700
 C 3.832072 0.106203 0.395182
 C 3.906768 1.555291 0.791070
 C -1.752067 -1.978649 2.008779
 O -0.487629 0.444341 -0.634907
 C -0.031200 1.579738 -0.054009
 O 0.488326 1.615773 1.042688
 C -0.292616 2.773814 -0.935798
 O 4.455464 -0.809016 0.876961
 H -5.305643 0.988484 -1.025559
 H -5.354275 -0.727249 -0.510901
 H -4.373662 -0.258972 -1.900961
 H 0.428014 -0.715875 0.823237

H -1.002429 -1.942620 -1.631168
 H -0.856543 -2.006926 2.639237
 H -2.626728 -1.902532 2.661740
 H -1.818301 -2.918965 1.452925
 H -0.066088 -2.882029 -0.355431
 H -1.359377 3.015831 -0.869408
 H -0.059664 2.551243 -1.980693
 H 0.293335 3.624689 -0.585652
 H -1.715473 0.152140 1.631380
 H 4.656282 1.677682 1.573549
 H 2.924824 1.885926 1.146623
 H 4.168407 2.170318 -0.076628
 H 3.324181 -2.102000 -0.660424
 H 1.185357 -0.709998 -2.446599
 H 1.595884 -2.519242 -2.440821

Imaginary Frequency: 341i

TS-BB3VA-ht-RR

C -4.583981 -2.173121 0.028556
 C -3.532168 -1.164688 -0.368152
 O -2.284751 -1.689482 -0.214942
 C -1.195713 -0.874758 -0.604373
 C 0.106572 -1.628900 -0.448412
 C 1.276342 -0.674937 -0.170026
 C 1.057571 0.175790 1.098754
 C -0.294096 0.891451 1.153171
 C -1.028665 0.829561 2.472919
 O -3.740221 -0.045065 -0.776348
 O 2.434565 -1.531131 0.024131
 C 3.653612 -0.979983 -0.189473
 O 3.832851 0.178904 -0.494007
 C 4.742812 -2.010688 0.003179
 O -0.254945 2.266612 0.759146
 C -0.068816 2.608885 -0.538623
 O 0.069534 1.815434 -1.444270
 C -0.061003 4.111120 -0.690794
 H -1.010384 0.152878 0.264599
 H 1.466777 -0.026409 -1.024067
 H 1.128784 -0.501816 1.959526
 H -1.197823 -0.213257 2.761309
 H -0.453775 1.314650 3.275185
 H -1.998429 1.331322 2.398561
 H 1.873553 0.901874 1.186751
 H 4.613436 -2.831517 -0.710074
 H 4.683268 -2.440435 1.008425
 H 5.716320 -1.542111 -0.144537
 H 0.338277 -2.231921 -1.337355
 H 0.010952 -2.326218 0.393750
 H -1.372557 -0.362952 -1.548714
 H -4.367191 -2.585885 1.018629
 H -4.585428 -3.008441 -0.680641
 H -5.563629 -1.694000 0.026336
 H 0.040834 4.367002 -1.745727
 H -0.985875 4.536290 -0.288319
 H 0.771815 4.540381 -0.123685

Imaginary Frequency: 1759i

TS-BB3VA-ht-RS

C -4.859965 -0.552681 -0.344320

C -3.437272 -0.457820 -0.843048
 O -2.566433 -0.797542 0.152325
 C -1.178522 -0.729247 -0.118329
 C -0.423231 -1.704132 0.767218
 C 0.876548 -1.108259 1.334726
 C 0.635459 0.225501 2.056053
 C -0.032811 1.281283 1.176493
 C -1.077193 2.155134 1.833033
 O -3.097997 -0.132755 -1.956081
 O 1.819296 -0.828950 0.268139
 C 2.509060 -1.874444 -0.250207
 O 2.414373 -3.012616 0.155031
 C 3.401379 -1.409185 -1.376474
 O 0.953812 2.111517 0.553908
 C 1.208850 2.053893 -0.779603
 O 0.632163 1.346014 -1.570719
 C 2.331335 3.007587 -1.123297
 H -0.707774 0.456459 0.302727
 H 1.337729 -1.833528 2.010958
 H -0.005382 0.016899 2.921860
 H -1.882772 1.537790 2.245150
 H -0.648077 2.750016 2.652923
 H -1.512934 2.848763 1.106379
 H 1.587470 0.612028 2.441255
 H 4.220421 -0.802993 -0.972644
 H 2.833961 -0.779580 -2.068325
 H 3.816071 -2.274650 -1.894537
 H -0.185784 -2.637075 0.242638
 H -1.064386 -1.970008 1.616775
 H -0.964544 -0.725970 -1.183955
 H -5.019567 0.156836 0.474882
 H -5.060441 -1.554807 0.048359
 H -5.545098 -0.328979 -1.162622
 H 2.454841 3.047068 -2.206128
 H 2.120499 4.006998 -0.730851
 H 3.262241 2.663605 -0.659146

Imaginary Frequency: 1776i

TS-BB3VA-hh-RRR

C -4.571955 1.567604 -0.440164
 C -3.755466 0.299697 -0.348811
 O -3.974695 -0.723854 -0.956052
 O -2.721697 0.466106 0.520697
 C -1.834961 -0.635129 0.766420
 C -0.537301 -0.059759 1.307348
 C 0.296254 0.576769 0.188508
 O 1.495167 1.095795 0.792690
 C 2.112592 2.119709 0.138744
 O 1.648982 2.666070 -0.836766
 C -2.473792 -1.754206 1.557082
 C 0.657122 -0.439980 -0.916338
 O 1.404942 -1.534564 -0.320263
 C 2.758205 -1.496690 -0.394428
 O 3.393660 -0.622308 -0.942151
 C -0.591761 -1.022290 -1.529583
 C 3.438671 2.436493 0.779798
 C 3.355326 -2.699334 0.298566
 H -5.373012 1.430538 -1.167164
 H -3.936024 2.407847 -0.737082
 H -4.997652 1.811462 0.539024

H	-0.248557	1.401521	-0.279720	C	-3.985986	0.262569	-1.497892
H	0.046903	-0.861209	1.770312	C	-3.000828	-0.744279	-0.950821
H	-3.361381	-2.134121	1.046619	O	-2.740220	-1.814147	-1.452467
H	-1.762078	-2.578048	1.675065	O	-2.434539	-0.277323	0.194155
H	-2.763808	-1.409064	2.560342	C	-1.486491	-1.102017	0.879534
H	-0.741752	0.693290	2.079540	C	-0.621085	-0.203461	1.754838
H	4.156892	1.670626	0.465543	C	0.571361	0.418881	1.004593
H	3.367770	2.407736	1.870497	O	0.114131	1.315540	-0.034663
H	3.784152	3.414592	0.442414	C	-0.167539	2.587535	0.335471
H	-1.443402	-1.063775	-0.427044	O	-0.077488	2.996981	1.472324
H	4.433043	-2.715990	0.133097	C	-2.123976	-2.298251	1.552532
H	2.900999	-3.621756	-0.075661	C	1.410677	-0.666254	0.325609
H	3.150450	-2.645316	1.373453	O	2.558857	0.003696	-0.273499
H	1.302963	0.050727	-1.651369	C	3.691461	-0.732570	-0.388137
H	-1.113031	-0.356058	-2.217438	O	3.795672	-1.879842	-0.012990
H	-0.490959	-2.038280	-1.908515	C	0.617660	-1.452340	-0.686551

Imaginary Frequency: 1717i

TS-BB3VA-hh-RS

C	-4.016726	0.382446	-2.104366	H	-3.471252	1.198108	-1.741717
C	-3.461051	-0.305708	-0.880353	H	-4.747872	0.495748	-0.747153
O	-3.694623	-1.443630	-0.542491	H	1.186074	0.992414	1.702347
O	-2.643902	0.541406	-0.194023	H	-0.217597	-0.797920	2.583942
C	-2.032278	0.088108	1.018020	H	-2.670398	-2.906654	0.828571
C	-0.816508	0.963586	1.267984	H	-1.352735	-2.923249	2.015399
C	0.342048	0.616486	0.318476	H	-2.819592	-1.977845	2.341688
O	1.469081	1.452593	0.653960	H	-1.220725	0.599361	2.198255
C	1.867095	2.381300	-0.255199	H	-1.517851	2.980849	-1.285131
O	1.311122	2.588550	-1.309536	H	0.165527	3.376212	-1.636859
C	-3.008559	-0.082062	2.159838	H	-0.784188	4.434082	-0.547039
C	0.783191	-0.842842	0.487176	H	-0.604220	-1.517026	-0.017156
O	1.849989	-1.053861	-0.483431	H	5.707021	-0.507672	-1.064298
C	2.786524	-1.981089	-0.165767	H	4.944545	1.013907	-0.505198
O	2.783899	-2.625450	0.859802	H	4.492207	0.334080	-2.069199
C	-0.359181	-1.802351	0.258965	H	1.791067	-1.335940	1.102950
C	3.090922	3.110449	0.247368	H	0.363179	-0.904551	-1.592977
C	3.812643	-2.096899	-1.269549	H	0.952214	-2.472443	-0.866557
H	-4.623131	-0.323633	-2.672465				
H	-3.202145	0.766023	-2.726902				
H	-4.629360	1.239915	-1.805844				
H	0.061563	0.811944	-0.718812				
H	-0.480433	0.824634	2.302843				
H	-3.801363	-0.783613	1.891750				
H	-2.487992	-0.467997	3.042650				
H	-3.465310	0.881379	2.429176				
H	-1.074533	2.023315	1.146024				
H	3.914297	2.403041	0.391394				
H	2.884417	3.571097	1.218818				
H	3.380442	3.875061	-0.474108				
H	-1.441924	-1.059197	0.730395				
H	4.604123	-2.779848	-0.959100				
H	4.232050	-1.114468	-1.507293				
H	3.335574	-2.475894	-2.179896				
H	1.210093	-0.978809	1.484427				
H	-0.625339	-1.947171	-0.788787				
H	-0.324278	-2.731174	0.825913				

Imaginary Frequency: 1693i

TS-BB3VA-hh-RSR

Imaginary Frequency: 1697i

TS-BB3VA-hh-RSS

C	-4.332868	-0.431801	-0.330032
C	-3.023984	-1.187785	-0.350155
O	-2.775535	-2.137124	-1.059191
O	-2.155231	-0.652474	0.546218
C	-0.865289	-1.259649	0.704165
C	0.077529	-0.223522	1.297450
C	0.710426	0.711690	0.253667
O	-0.283602	1.538374	-0.397769
C	-0.684901	2.651417	0.267046
O	-0.271984	2.969827	1.359516
C	-0.930134	-2.598868	1.406114
C	1.387825	-0.063638	-0.898293
O	2.467154	-0.851880	-0.329974
C	3.681611	-0.250563	-0.220083
O	3.899566	0.896640	-0.538941
C	0.440173	-1.018804	-1.576992
C	-1.700700	3.418577	-0.545687
C	4.699660	-1.213469	0.343736
H	-5.008212	-0.857414	-1.072893
H	-4.163067	0.628367	-0.544730

H -4.787954 -0.493243 0.664155
 H 1.437861 1.366985 0.737782
 H 0.899344 -0.745650 1.799431
 H -1.589799 -3.286865 0.872499
 H 0.069716 -3.043708 1.449518
 H -1.297380 -2.485140 2.436530
 H -0.433708 0.381799 2.054979
 H -2.577876 2.791233 -0.735980
 H -1.278138 3.693020 -1.517616
 H -1.998035 4.315627 -0.001817
 H -0.352765 -1.414270 -0.504677
 H 5.665018 -0.713231 0.425588
 H 4.787259 -2.090891 -0.305297
 H 4.379302 -1.567503 1.329150
 H 1.825191 0.664955 -1.589825
 H -0.278106 -0.542330 -2.242412
 H 0.902317 -1.910147 -1.998869

Imaginary Frequency: 1690i

TS-4VAMe-mT-RRR

C -0.633820 -1.194438 2.680117
 C -0.752091 -1.624892 1.240516
 O -1.035618 -2.734596 0.849917
 O -0.545356 -0.558227 0.408981
 C -0.667747 -0.730206 -0.986120
 C -2.055275 -1.070771 -1.501654
 C -3.254769 -0.701378 -0.625319
 C -4.580575 -1.111030 -1.260488
 C 0.453514 -1.496847 -1.652618
 C 1.890862 -1.172128 -1.234591
 O 2.115183 -1.854075 0.038202
 C 3.091031 -1.381921 0.838519
 C 3.248742 -2.246514 2.068724
 C -0.384346 1.420493 -1.664037
 C 0.316237 2.163575 -0.761305
 O 1.689348 2.251691 -0.868950
 C 2.376509 2.927489 0.117318
 O 1.828852 3.463339 1.050695
 C 3.855171 2.868306 -0.146381
 O -3.285585 0.742342 -0.427528
 C -3.445723 1.206087 0.835570
 O -3.550163 0.500482 1.816499
 C -3.482713 2.716462 0.848700
 C 2.912933 -1.679047 -2.249648
 O 3.774580 -0.409247 0.588283
 H -0.586345 -2.075409 3.321899
 H -1.520187 -0.603110 2.936291
 H 0.244575 -0.560090 2.827837
 H -0.098106 2.630019 0.123267
 H -1.460104 1.536548 -1.671418
 H -2.179457 -0.622048 -2.498040
 H -2.116426 -2.160071 -1.648826
 H 0.089267 1.128133 -2.597155
 H 4.071527 3.120011 -1.189020
 H 4.202270 1.844977 0.033734
 H 4.368919 3.557575 0.524870
 H 0.295308 -2.575998 -1.497254
 H 0.366262 -1.328620 -2.734268
 H -4.256466 3.082333 0.166348
 H -2.525462 3.121118 0.503314

H -3.681398 3.065496 1.862404
 H -3.163958 -1.165274 0.356096
 H 2.029149 -0.103833 -1.067580
 H 2.783085 -1.161748 -3.206828
 H 2.793517 -2.755159 -2.419138
 H 3.929200 -1.486279 -1.895881
 H 3.868837 -3.114995 1.816614
 H 2.283790 -2.620195 2.419141
 H 3.750882 -1.676138 2.851811
 H -4.606701 -2.193909 -1.422918
 H -5.414504 -0.845522 -0.603255
 H -4.725059 -0.610935 -2.224651

Imaginary Frequency: 421i

TS-4VAMe-mT-RRS

C -2.978043 -2.737161 -1.345070
 C -2.051324 -2.259832 -0.256517
 O -1.887982 -2.789558 0.819131
 O -1.426583 -1.098924 -0.631595
 C -0.549125 -0.442588 0.271088
 C 0.761628 -1.144648 0.545615
 C 1.724698 -1.429726 -0.619555
 C 1.174519 -2.283433 -1.753569
 C -1.203766 0.160409 1.501765
 C -2.712144 0.417089 1.464456
 O -3.019872 1.360074 0.393802
 C -4.052147 1.067256 -0.431085
 C -4.227627 2.147396 -1.473267
 C -0.121868 1.344064 -1.070174
 C 0.783741 2.222581 -0.556547
 O 2.119556 2.089224 -0.874512
 C 3.021317 2.911196 -0.235319
 O 2.694083 3.736470 0.583595
 C 4.420482 2.612919 -0.697424
 O 2.838762 -2.208831 -0.073527
 C 3.851483 -1.547960 0.519446
 O 3.901629 -0.340772 0.647121
 C 4.909733 -2.512981 1.004068
 C -3.226504 1.015361 2.770860
 O -4.732955 0.065864 -0.351060
 H -3.850810 -2.075178 -1.371544
 H -3.299546 -3.756066 -1.125503
 H -2.489400 -2.692758 -2.322586
 H 0.561892 3.005836 0.157816
 H -1.169629 1.589216 -0.963653
 H 1.308229 -0.528913 1.268563
 H 0.538861 -2.101577 1.042474
 H 0.154935 0.706923 -1.903590
 H 5.090493 3.398964 -0.346769
 H 4.459717 2.537119 -1.788216
 H 4.726167 1.647627 -0.280323
 H -1.039849 -0.517767 2.353487
 H -0.675998 1.092395 1.747208
 H 5.280194 -3.118375 0.170564
 H 4.479028 -3.200760 1.739330
 H 5.731351 -1.956327 1.456044
 H 2.135741 -0.491531 -0.997197
 H -3.251060 -0.505717 1.252108
 H -2.743062 1.976049 2.979283
 H -3.024257 0.336124 3.605938

H -4.308020 1.173970 2.715856
 H -3.417678 2.082321 -2.209086
 H -4.178299 3.139603 -1.016175
 H -5.182770 2.009250 -1.981497
 H 0.371871 -1.758297 -2.276659
 H 1.970878 -2.509395 -2.469967
 H 0.777604 -3.230770 -1.372180

Imaginary Frequency: 404i

TS-4VAMe-mT-RSR

C 0.716316 -4.678980 0.580867
 C 0.847914 -3.177120 0.701403
 O 1.473682 -2.607463 1.566612
 O 0.159607 -2.573331 -0.301037
 C 0.056052 -1.161448 -0.482497
 C -1.179421 -0.891348 -1.329538
 C -2.589648 -1.390971 -0.955606
 C -2.754579 -2.876044 -0.657371
 C 1.275116 -0.483801 -1.092043
 C 2.651715 -0.549763 -0.398004
 O 3.350643 0.678005 -0.773415
 C 3.546707 1.619048 0.177704
 C 4.123883 2.878322 -0.420975
 C -0.289666 -0.058119 1.485982
 C -0.028414 1.263125 1.276960
 O -1.036646 2.091134 0.791266
 C -0.670990 3.147680 -0.001673
 O 0.466765 3.338372 -0.368439
 C -1.871606 3.990753 -0.342343
 O -3.142548 -0.694604 0.200291
 C -3.719196 0.511692 -0.008922
 O -3.763120 1.062538 -1.090697
 C -4.271259 1.078915 1.275954
 C 3.539654 -1.693077 -0.874227
 O 3.260726 1.482371 1.350162
 H 1.301550 -5.156208 1.367447
 H 1.065892 -5.013916 -0.401153
 H -0.334468 -4.974631 0.670071
 H 0.944953 1.724796 1.378158
 H 0.454784 -0.637289 2.016420
 H -1.253625 0.189258 -1.481285
 H -0.985961 -1.316674 -2.330948
 H -1.311875 -0.415314 1.512315
 H -2.277671 4.447342 0.567310
 H -2.656416 3.362819 -0.777362
 H -1.576754 4.772982 -1.042519
 H 1.391110 -0.847522 -2.128236
 H 1.014606 0.575677 -1.174302
 H -3.455139 1.572809 1.814468
 H -4.677691 0.291968 1.915715
 H -5.039064 1.819204 1.044169
 H -3.221750 -1.119435 -1.806402
 H 2.547216 -0.560439 0.684803
 H 3.739114 -1.598224 -1.947661
 H 3.063013 -2.660854 -0.697597
 H 4.495801 -1.684025 -0.341887
 H 4.757715 2.660691 -1.283572
 H 4.682244 3.422877 0.342670
 H 3.286335 3.503031 -0.753403
 H -2.268416 -3.151230 0.280926

H -3.818864 -3.120989 -0.580124
 H -2.314991 -3.476052 -1.459992

Imaginary Frequency: 391i

TS-4VAMe-mT-RSS

C 0.693722 -4.515521 -0.867732
 C 0.063118 -3.141261 -0.866698
 O -0.787216 -2.770361 -1.642612
 O 0.595600 -2.390226 0.134095
 C 0.259606 -1.026263 0.387969
 C 1.437147 -0.370757 1.094921
 C 2.838481 -0.805308 0.622261
 C 3.422340 -1.968837 1.413756
 C -1.051153 -0.783261 1.112477
 C -2.387350 -1.220512 0.477263
 O -3.388421 -0.261299 0.936930
 C -4.013468 0.502733 0.010217
 C -4.919588 1.513804 0.668635
 C 0.169652 0.204220 -1.523242
 C -0.579635 1.315825 -1.271251
 O 0.044733 2.451134 -0.764608
 C -0.719293 3.361396 -0.093449
 O -1.878705 3.178933 0.204457
 C 0.081121 4.604875 0.202664
 O 3.760779 0.308537 0.819875
 C 4.057189 1.081103 -0.249514
 O 3.594950 0.925138 -1.360356
 C 5.048719 2.156850 0.130601
 C -2.873242 -2.592312 0.931035
 O -3.839706 0.408571 -1.187556
 H 1.772961 -4.434784 -1.035274
 H 0.242289 -5.117899 -1.656533
 H 0.548490 -5.001898 0.102478
 H -1.656400 1.378843 -1.362434
 H -0.297492 -0.591001 -2.089792
 H 1.338078 0.710768 0.958707
 H 1.365085 -0.548671 2.181900
 H 1.251007 0.292031 -1.572103
 H 0.256694 5.158255 -0.726938
 H 1.059625 4.345570 0.617494
 H -0.471936 5.235754 0.899376
 H -0.976638 -1.223759 2.122140
 H -1.109344 0.299787 1.262139
 H 4.642923 2.774767 0.938356
 H 5.264585 2.776675 -0.740149
 H 5.972544 1.701897 0.502792
 H 2.823571 -1.031627 -0.445025
 H -2.341683 -1.165771 -0.608175
 H -3.035162 -2.600046 2.014996
 H -2.142647 -3.368100 0.686334
 H -3.815938 -2.847674 0.437247
 H -5.335380 1.132274 1.604034
 H -5.716247 1.792764 -0.023492
 H -4.319967 2.404239 0.889053
 H 2.759880 -2.835284 1.346366
 H 4.408213 -2.245212 1.025898
 H 3.532578 -1.695966 2.469320

Imaginary Frequency: 407i

